Shallow volcanic processes at persistently active volcanoes: multidisciplinary study at Poas volcano, Costa Rica

Thesis

UNRESTRICTED

Shallow volcanic processes at persistently active volcanoes: evidence from a multidisciplinary study at Poás volcano, Costa Rica

A thesis presented for the degree of

Doctor of Philosophy

By

Nicolas Fournier

B.Sc. (Hons), M.Sc.
Université Blaise Pascal, Clermont-Ferrand, France

Department of Earth Sciences
The Open University

October 2003

Submission date: 20 October 2003
Award date: 2 November 2004

Abstract

There is a discrepancy between the amount of gas emitted and the quantity of magma erupted at many persistently active volcanoes. The gas output suggests a larger magma supply than is observed to erupt. This is a major issue in contemporary volcanology but as yet it is poorly understood.

Calculations based on the micro-gravity data collected during the 1986-89 degassing crisis at Poas volcano, Costa Rica, and a new sulphur budget analysis suggest that approximately 28 x 10^9 kg of magma was intruded beneath the Poás summit crater during this period, but much of the magma (at least 16 x 10^9 kg) was recycled to depth. A new high-resolution Bouguer survey in the active crater also shows that a significant amount of magma has been intruded into the subsurface at Poás - probably during the last century (20% of it during the 1986-89 crisis) despite almost no magma being erupted in this period. This implies that the magma intruded had already degassed, otherwise major near surface exsolution of volatiles and eruptions would have followed intrusion. The magma reservoir at Poás must therefore be shallow enough in the edifice to allow volatile exsolution and segregation from the magma, and wide enough to allow magma convection. The stocky shape of the shallow intrusions at Poás and the apparent lack of ground deformation during their emplacement (both determined by geophysical studies) indicate that magma migrates mainly by assimilation of the surrounding material.

Hydrothermal systems seem to have a major role in controlling both the development of magma reservoirs high in the volcanic edifice and the subsurface intrusion of magma, facilitating assimilation by intruding magmas. Thus hydrothermal systems may have a much greater role in controlling the type of activity and the long-term evolution of stratovolcanoes than previously suggested.

Frontispiece

Artistic view of a volcano (presumably Stromboli…) by Rachel

Calvin and Hobbes "Homicidal Psycho Jungle Cat" - Bill Watterson.

Acknowledgments

My first thoughts are for my main supervisors Hazel Rymer and Glyn Williams-Jones for putting up with me for 3 years, despite my numerous adventures wherever I had to travel to. Many thanks for their inalterable optimism and confidence, and the opportunity they gave me to follow my ideas all along this project. I hope they improved their Franglais as much as they made me improve my English. Many thanks, too, to Dave Rothery for accepting to be my third supervisor, for insightful discussions and a good time in the field (as well as for taking compromising pictures).

Thanks also to my examiners, Harry Pinkerton (external) and Steve Self (internal) for helpful comments and a challenging but thoroughly enjoyable Viva.

Financial support for this project came from The Open University, NERC, the NASA/EOS-IDS programme and the Royal Society. Thanks to the Volcano and Magmatic Study Group (VMSG) too for financial support for the IUGG2003 conference in Sapporo, Japan. Big financial wizard John Holbrook and Liz Lomas are also to be thanked for their help on numerous occasions.

None of the fieldwork would have been possible without the enthusiasm and help of Jorge Brenes (OVSICORI, Costa Rica). From the active crater at Poás, braving pouring rain and scary landslides, to working our way through the jungle on Poás' western flank, he proved to be more than a great guide but a real friend. OVSICORI (Costa Rica) and INETER (Nicaragua, especially Martha Navarro and Felix, despite the US$ 50 he still owes me) are to be thanked for their logistical support when I was in the field. Equally, a big "thank you" goes to the people from the National Parks at Poás and Masaya. I hope they will miss the view of a crazy, bald volcanologist obviously enjoying running down craters and falling into crater lakes with a pH of less than 0.5. Thanks also to Don Francisco and Dona Yolanda at the Hotel Regis in Masaya and everybody at the

Pension Alajuela in Alajuela for coping with the mess I was bringing with me every time, and the late discussions at night growing louder thanks to the rum "Flor de Cana". Still on the field side of this project, I had some invaluable helpers to assist me on site, so a big round of applause to Raphaël Laugeois, Anna Ksienzyk, Stéphanie Markiewicz, Dan Croucher and Ben Kennedy. My first trip was greatly improved by Pierre Delmelle and colleagues from Louvain and John Stix (Canada) is also to be thanked for the use of his COSPEC. The last fieldtrip was another success due to the great collaboration with Brian Evans and Debbie Duffy from University of Exeter. A big thank you also to numerous lads in Costa Rica (Tex, etc) for helping me to play gigs in Costa Rican bars to get some money after having had everything of value stolen except the instruments, my passport and my guitar. Also, a big thank you to "Mula" for the physiological support at Poás and his almost legal beverages.

Thanks to Maurizio Ripepe (University of Florence, Italy), both from the scientific and culinary points of view, and to all the people who participated in the multidisciplinary experiment at Stromboli in 2002 ("H", John, Dave, Jo, Manu, Jeff, Tonio, Elske, etc). Back in the lab, many thanks to Emily Brodsky (UCLA, USA) for introducing me to time series analysis and seismic data processing and taking the time to teach me the basics of frequency analysis. In 2001, I had the opportunity to supervise 2 Honours degree research projects, so many thanks to Jean-Michel Bernardon and Stéphanie Markiewicz for having been great students and for the ticket to the unforgettable AC/DC concert in Milton Keynes.

Obviously, you cannot work properly if you are not surrounded by clever and enthusiastic people, so a standing ovation for the people of the Volcano Dynamics Group and, more generally, the Department of Earth Sciences at the Open University. Special mention to Joachim Gottsmann and Luke Wooller for insightful discussions and good time, Adam Maciejewski for DIY advices and lovely company while

reconstructing the OP-FTIR, Christian Lacasse and John Murray for drinkable coffee and good laughs, Dan Croucher for wild runs and stories, Mike Widdowson, Steve Blake and Steve Self for always being receptive to my questions, Kirti Sharma for indispensable "fag breaks", and Ashea Tambe for being a wonderful link between such a nice bunch of people.

A big thank you to my parents and grand-parents, the Moreau tribe -and associated brothers in-law, and continental friends (Rachel, Regis, Laure, Tonio, Mamour, etc) who were always there when I needed them in mighty England or on the continent.

Finally, all my love goes to Magali who not only came with me to England, graduated, and found a job there, but also always supported my decisions wherever I was, and had to put up for 3 years with a country where nobody has been able so far to pronounce her name correctly.

This work is dedicated to the smile of people in Central America (both "Nicas" and "Ticos"), especially the street kids of Masaya, and the Borucas tribe in Costa Rica who hosted me in the mountains for 3 days and nights during the "Diablitos" celebration. I learned a lot from them.

Pura vida

Table of contents

List of Figures

Chapter 1

Introduction

Poás volcano, Costa Rica

1.1. Introduction to this work

Processes controlling persistent degassing on volcanoes are unclear. The amount of gas emitted at a volcano can be measured, and this places constraints on the estimated mass of magma degassing. The main problem to be addressed in this thesis is that although many volcanoes degas continuously, the amount of magma actually erupted is much smaller than the estimated amount of magma degassing. This implies that the degassed magma is either intruded or otherwise "recycled" at depth. It seems unlikely that degassed magma accumulates within the shallow reservoir feeding activity, because the degassed magma would tend to stifle further activity. This is therefore not a viable mechanism to sustain long term degassing on volcanoes. Another possibility is that the degassed magma is intruded adjacent to the shallow plumbing system, within or below the edifice. In this case, the space available for new gas-rich magma in the plumbing system does not decrease significantly and persistent degassing is possible. The question raised here is: "How do we study these phenomena and what are the most appropriate tools to use?"

While seismology can provide insights into the progression of magma upwards, it cannot be used to assess the amount of magma involved. The mass of magma can be determined using gravimetry, of which there are 3 types; dynamic (i.e., micro-gravity, which is concerned with small changes in gravity through time measured with a frequency of days or weeks), continuous (i.e., tidal gravity where measurements are made typically once per second or minute) and static (i.e. Bouguer gravity, providing a picture of the time averaged gravity field).

This work involved installation of a high-resolution Bouguer survey on Poás crater floor – likely to be one of the highest resolution Bouguer surveys ever carried out at an active crater – to investigate volumes of magma intruded at Poás and the re-evaluation

of previously published micro-gravity data. It also involved studies of continuously recorded gravity at Stromboli volcano to investigate the rate of degassing proceeses.

Finally, because micro-gravity monitoring is a valuable tool for assessing subsurface mass changes, we developed an automated continuous gravity recording methodology by designing new logging software and data processing guidelines.

In summary, this work assesses the relationship between the amount of magma degassing and the amount of magma intruding a persistently active volcano, and uses new micro-gravity methodologies as a tool for monitoring subsurface mass changes. It finally assesses the role of shallow volcanic processes (i.e., subsurface intrusions, magma reservoirs and hydrothermal system) in controlling major phases in the evolution of a volcano.

This chapter guides the reader through the thesis by highlighting the issues raised in each of the following chapters. The scope extends from developing instrumental and analytical methods, to the collection of new data sets.

1.2. Gravity methods in Volcanology

Spatial variations of the gravitational field at the Earth's surface have been used for over 80 years in order to detect subsurface density contrasts (Telford et al., 1990). Logically, gravity surveys (i.e., Bouguer surveys) have been used more recently on volcanoes to investigate their internal structure (Thorpe et al., 1981, Brown et al., 1987). The main source of error for the Bouguer survey is the estimate of the effect of the surrounding topography on the gravity reading at the measurement points (i.e., terrain correction). This is due to a generally poor knowledge of the topography, especially close to the gravity stations. However, recent advances in producing Digital Elevation

Models now allow digital topographic data to be used to compute the terrain correction more accurately than using older methods.

In addition to static surveys, variations of micro-gravity through time (a.k.a. dynamic gravity) have also been recorded on many volcanoes as a monitoring tool for subsurface mass changes (Brown et al., 1987, Rymer et al., 1989). One of the major advantages of this method is that, in addition to investigating small gravity changes, there is no need for terrain correction unless there is a major change in topography (in the event of an eruption for example). Indeed, so long as the topography remains the same around the micro-gravity stations, its effect on the gravity readings will be constant through time. Micro-gravity changes through time can then be compared immediately, requiring only the processing of the Earth tide corrections.

Both static and dynamic gravity methods have usually been carried out using Lacoste & Romberg meters. Feedback systems on these instruments now provide the capability for continuously streaming data, thus allowing continuous recording with computers or PDAs via a serial communication protocol.

1.3. Poás volcano, Costa Rica

1.3.1. Background

Details of the geology and eruptive history at Poás volcano can be found in Barquero et al., (1985), Rowe et al. (1995), Rymer et al., (2000). An overview of the geology and eruptive history is given here:

Costa Rica is located on the western continental wedge of the Caribbean plate (**Fig 1.1**) in Central America. It features 6 active volcanoes linked with the subduction of the Cocos plate beneath the west side of the Caribbean plate (**Fig 1.2**), one of which is Poás volcano, a stratovolcano located in Costa Rican Cordillera Central (**Fig 1.3**). The edifice is limited to the south by the Central Valley (Valle central) and to the west by the steep

valley of Bajos del Toro. To the east lies the extinct stratovolcano Barva. Poás rises to 2708 m a.s.l. with a base at about 1000 m a.s.l. and is a composite edifice with a summit caldera of about 3 km diameter known as Von Frantzius within which are an old centre of activity (Botos) and the present active crater Laguna Caliente (**Fig 1.4**). Botos crater is filled with a fresh water lake whereas Laguna Caliente is partially filled by an acidic crater lake. Fumaroles are emitted from the crater bottom but the fumarolic field has migrated through time within the active crater. Between 2001 and 2003 fumaroles could be found in two distinct places: firstly on the eastern inner wall and secondly on the so-called "dome", an altered lava dome that presently delimits the southern side of the crater lake (**Fig 1.4**). Their emission temperature was around 100°C in January 2003 but they have varied significantly, reaching 900°C in 1981 when incandescence of the dome was observed.

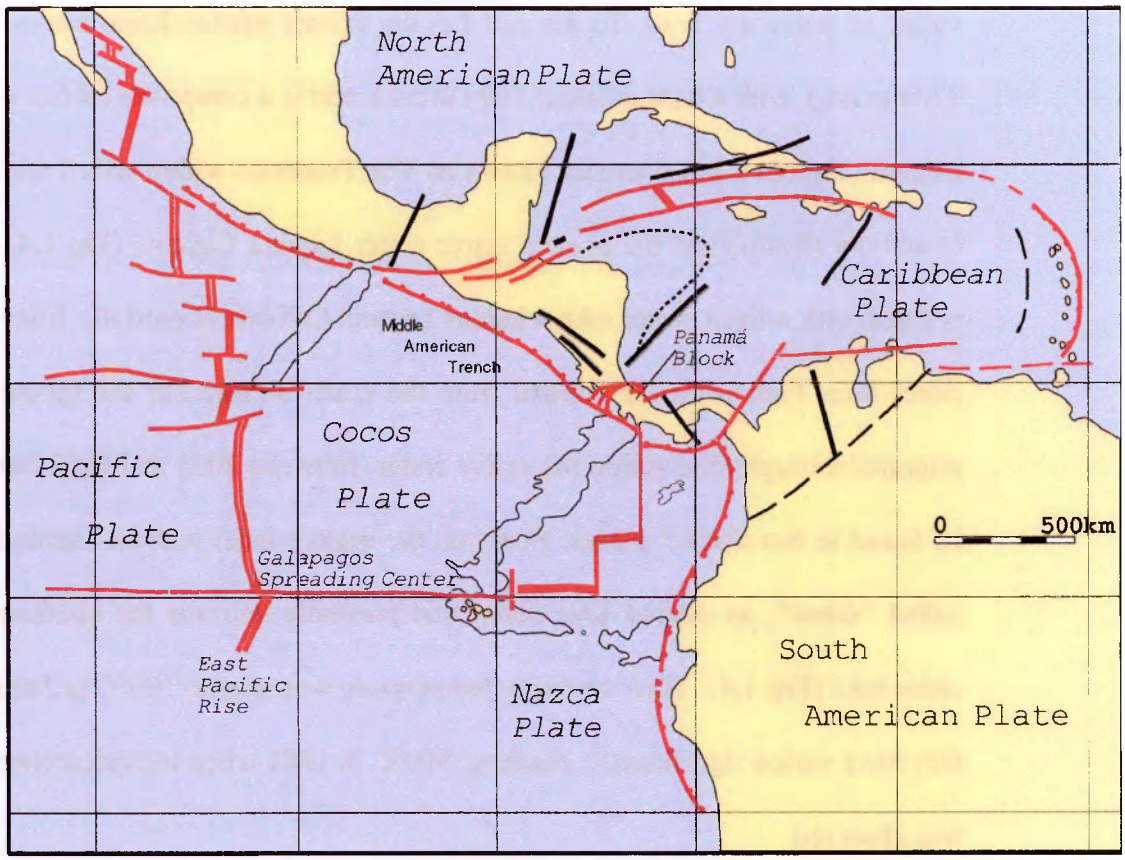

Fig 1.1. Tectonic sketch map of Central America.

Fig 1.2. Regional map of the active volcanoes of Costa Rica.

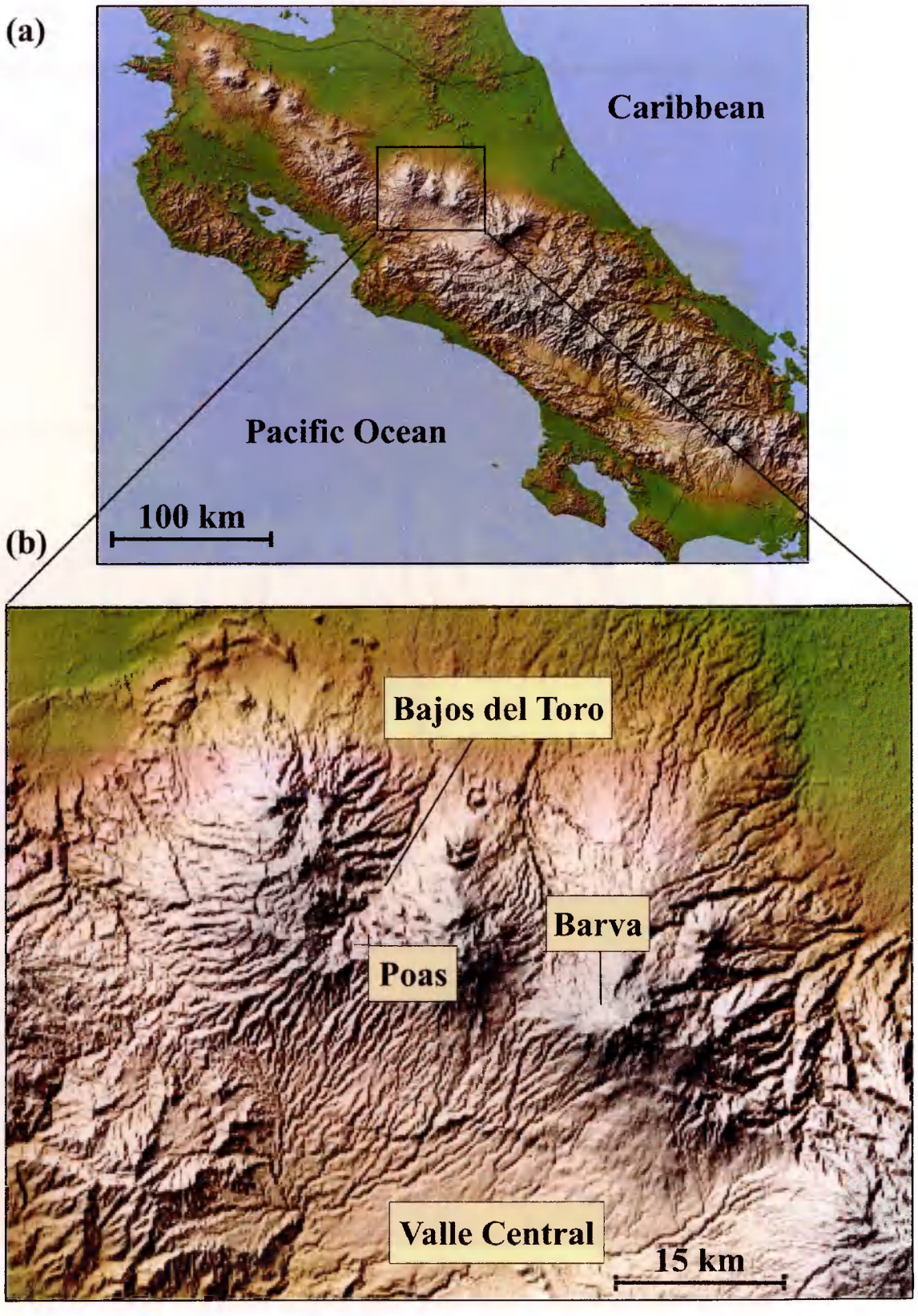

Fig 1.3. SRTM Radar Satellite data. *Top*: All of Costa Rica. *Bottom*: Valle Central, Costa Rica.

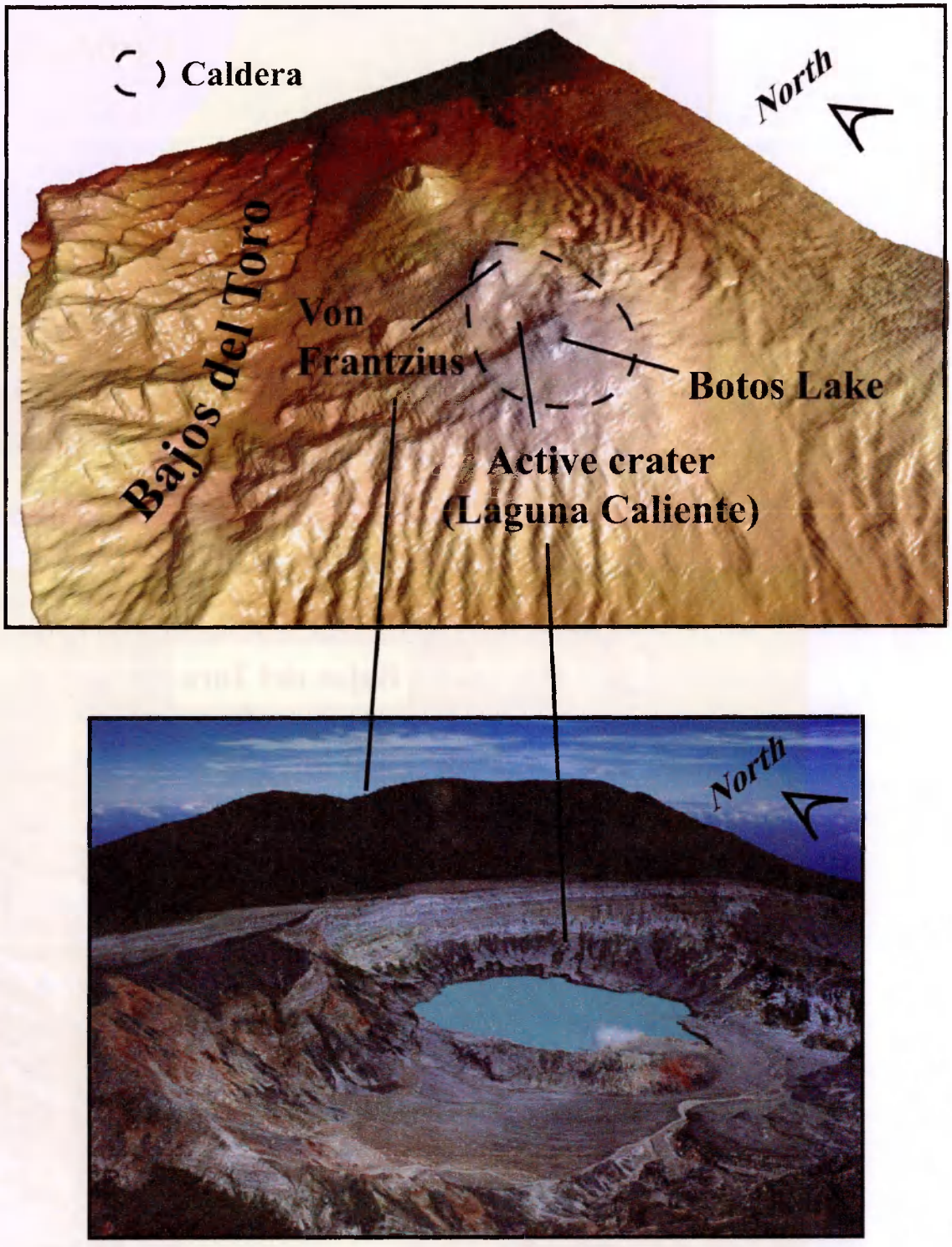

Fig 1.4. Poás volcano, Costa Rica. *Top*: Digital Elevation Model of the edifice derived from SRTM Radar Satellite data. *Bottom*: Picture of Poás' active crater, taken from the Mirador (view point). Relief in the background is Von Frantzius, remnants of an old caldera wall.

Lavas erupted at Poás range in composition from basalts to low-silica andesites. Lava flows are visible down the quebradas (steep valleys) on the western flank, as well as on the eastern inner walls of the active crater. The most recent lavas are believed to come from the Botos crater, which is topographically higher and erupted approximately 7500 years ago. Since then, the activity has been limited to the Laguna Caliente crater and makes Poás one of the most active historic Costa Rican volcanoes in historical time.

The earliest well-documented eruption occurred in 1834 with eruption of ash. Since then, the main type of activity has been phreatic and phreato-magmatic, with geyser-like activity, and eruption of mud, in the active crater and occasional ash emissions (1834, 1880, 1907, 1910, 1953, 1954, 1965), alternating with periods of quiescence and passive degassing (Rymer, 1985 and references therein). The crater has been partially filled by an acid lake since 1834, but this disappeared occasionally in 1953 and during the last crisis in 1986-1989 which culminated in steam and ash eruptions. The lake gradually recovered its previous depth of approximately 50 metres by 1997. Since then, gases have risen through the lake and partially mixed with water. Convection cells within the lake are outlined at its surface by spherules of native sulphur as well as water movement. The lake colour varies slightly through time between light blue and lagoon-like light green. Its temperature has been relatively steady for the last 10 years and is presently ~35°C. The lake water pH has been relatively constant since 1979, remaining below 1.

1.3.2. Previous works and Monitoring

Structural information at Poás has been inferred mainly from gravity surveys (Thorpe et al., 1981, Rymer, 1985), revealing the Von Frantzius caldera and an older 9 km-diameter caldera at about 2000 m a.s.l. A shallow magma reservoir has also been identified approximately 500 m below the floor of the active crater (Thorpe et al., 1981). Additionally, micro-gravity near the summit has been monitored once or twice a

year by Hazel Rymer and colleagues from The Open University for about 20 years (Brown et al., 1987, Rymer et al., 1987, 1989, 2000) and now represents one of the longest micro-gravity data sets available at any active volcano. The main objective of this micro-gravity monitoring is to detect and quantify amounts of magma intruding in subsurface of the summit area, such as during the 1986-1989 crisis (Rymer et al., 2000). Previous works by Brantley et al. (1987), Rowe et al. (1992a, 1992b, 1994, 1995), Sanford et al. (1995) and Martinez et al. (2000) investigated the summit hydrothermal system by modelling the chemical interaction of rainwater with magmatic fluids. Rowe et al. (1992) proposed that an unusually low level of precipitation was responsible for the 1986-1989 crisis. An alternative hypothesis was proposed by Rymer et al. (1989) who suggested that the crisis was due to the intrusion of magma close to the crater floor. This last work was achieved by coupling micro-gravity data with energy balance considerations (i.e., calculation of the energy output at the crater and retrieval of the amount of magma necessary to account for this energy release).

A seismic station, run by the OVSICORI, is now continuously recording seismic signals approximately 2 km from the active crater.

1.4. Environmental impact of persistently active volcanoes

Persistently active volcanoes release significant amounts of gas and aerosols in the atmosphere over long periods of time. While large eruptions allow the volatiles and aerosols to reach the stratosphere and travel around the globe with the strong stratospheric winds, passive volcanic degassing is likely to have a regional impact. For example, Masaya volcano, Nicaragua, releases 1000's of tonnes per day of SO_2 (Williams-Jones, 2001), and its volcanic plume has a huge impact on the surrounding environment downwind. Dry deposition literally burns the vegetation whereas

remobilisation by the rain into the soil of the acids thus deposited is likely to affect the soil chemistry (Delmelle et al., 1999). An example of the multidisciplinary methodology needed to study the impact of volcanoes on the surrounding environment is illustrated in **Fig 1.5**. We investigated this environmental question at the beginning of this project but instrumental and analytical problems prevented this work from being viable at that stage and thus was not pursued during this project.

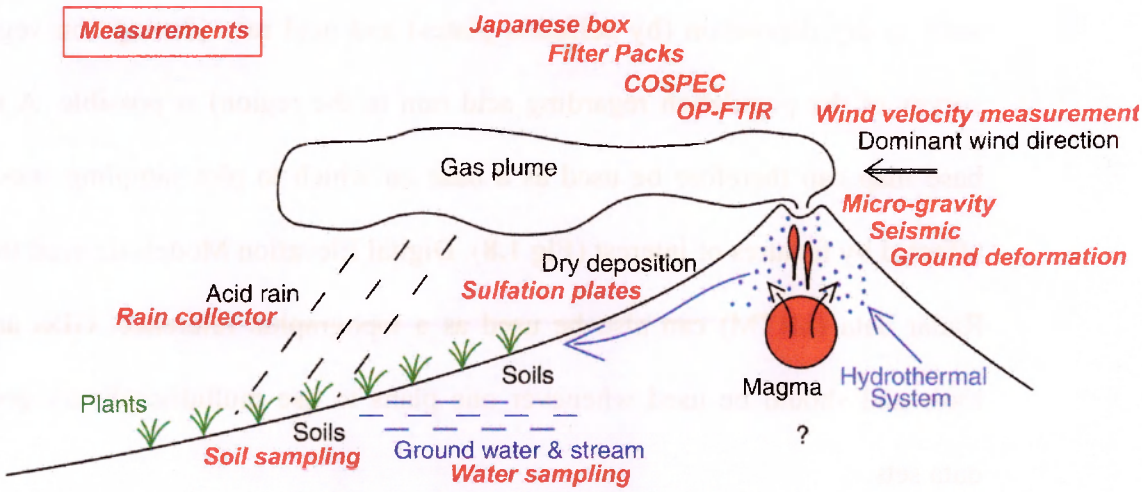

Fig 1.5. Schematic methodology for multidisciplinary studies of environmental impact of volcanoes. Methods used are mentioned in italics.

A soil sampling campaign was carried out around Masaya and Poás volcanoes in 2001. Soil analyses at Masaya clearly show that the pH of soils to a depth of o.3 m increases with distance from the active vent. Soil acidity distribution correlates well with levels of dry deposition downwind at Masaya with a maximum 8 times greater than the maximum sulfation rate for industrial sulphur point sources (**Fig 1.6**, Delmelle et al., 1999). At Poás, a network of sulfation plates was installed for 3 weeks (**Fig 1.7**) and soils were sampled at the same locations. Although results of the plate and soil analyses were not yet available for the end of this project, the importance of integrating all available information into a Geographical Information System (GIS) is clear. Indeed, by georeferencing several types of information, comparison of several different sets of data such as dry deposition (by sulfation plates) and acid rain (damage on vegetation and survey of the population regarding acid rain in the region) is possible. A topographic base map can therefore be used as a base on which to plot sampling sites or regions affected by features of interest (**Fig 1.8**). Digital Elevation Models derived from satellite Radar data (SRTM) can also be used as a topographic reference. GISs are powerful tools and should be used whenever one plans to use multidisciplinary georeferenced data sets.

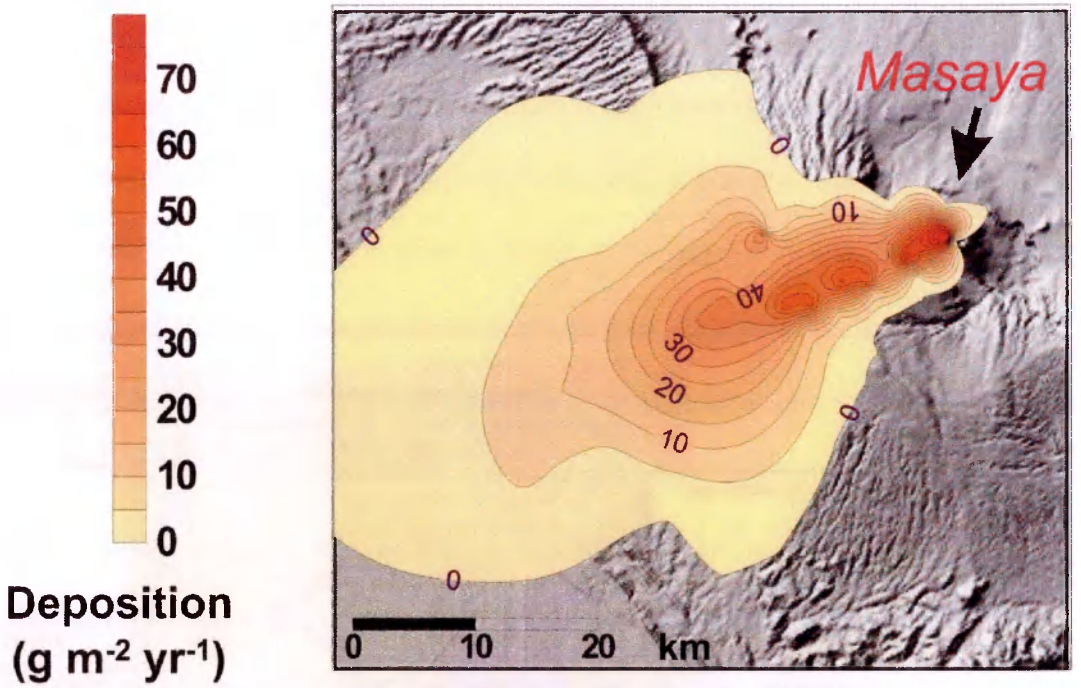

Fig 1.6. Map of dry sulphur deposition at Masaya volcano by Delmelle et al. (1999)

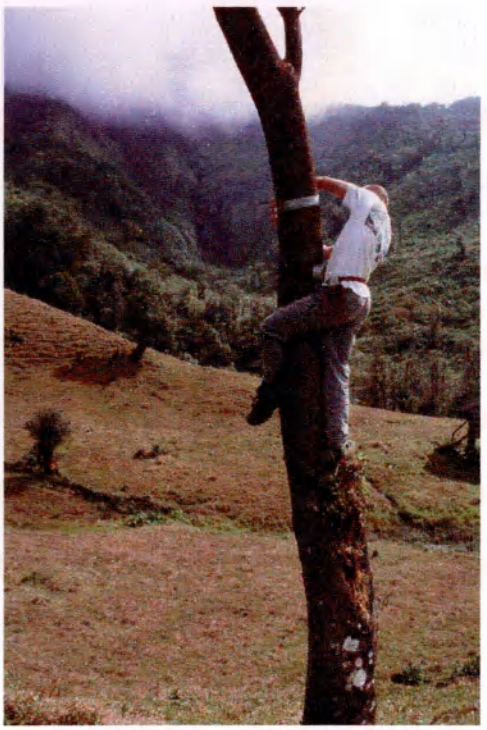

Fig 1.7. Installation of sulfation plates on the flank of Poás volcano, Costa Rica. The plates must be placed in relatively open places and at least 2-3 m above the ground. They are left approximately 3 weeks before collection.

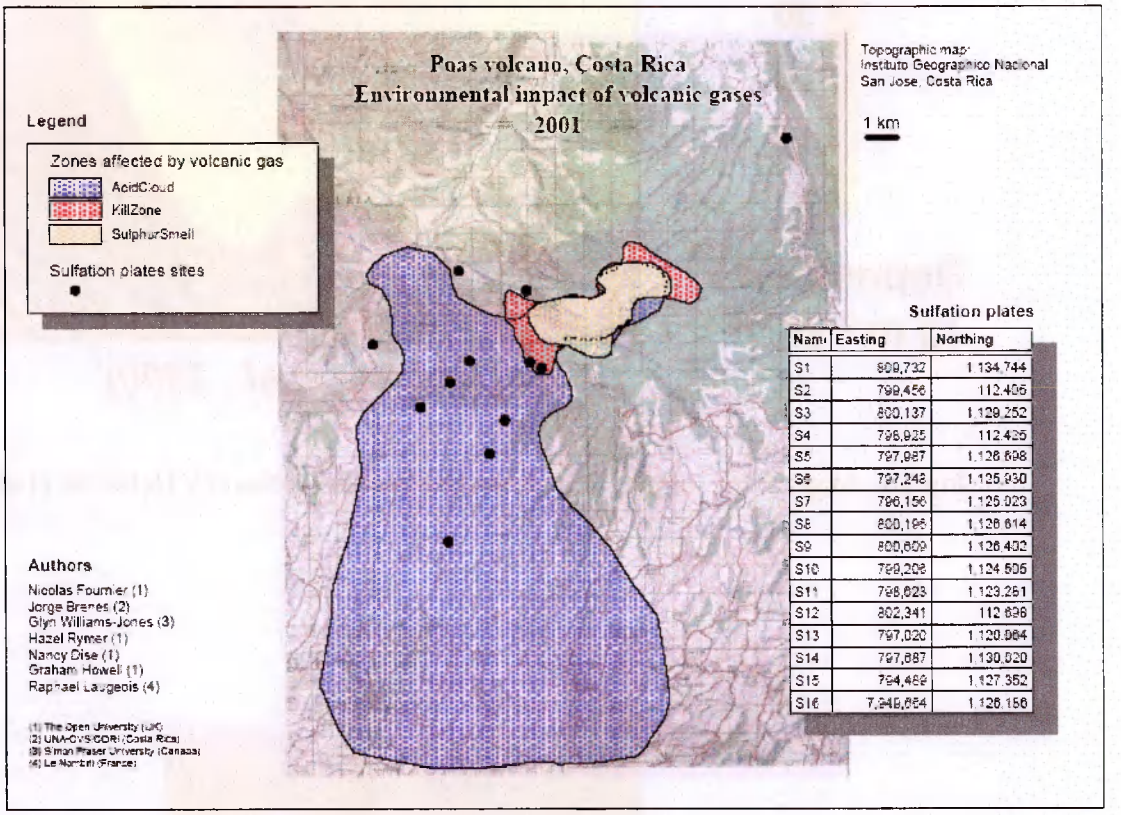

Fig 1.8. Example of the use of Geographical Information System (using MAPINFO®) for the integration of results from georeferenced multidisciplinary studies. The background topographic map has been georeferenced as a raster image and zones of environmental damage can be drawn into polygons. Sampling sites for dry deposition (i.e., sulfation plate sites) are indicated with black dots.

1.5. Outline of the present work

The principal objective of this work was to investigate subsurface processes and phenomena controlling the degassing at persistently active volcanoes. During the project it became clear to the author that the methodology involved, especially the use of gravity studies on active volcanoes, could be improved. The development of new methodologies therefore became an important part of this work and is illustrated in this thesis.

During three field seasons (January-March 2001, February-March 2002 and November 2002-January 2003) the author collected multidisciplinary sets of data including:

Geophysics

- Repeating measurements of previously installed micro-gravity networks at Poás (Costa Rica) and Masaya (Nicaragua), as well as GPS measurement of gravity stations coordinates
- New High-resolution Bouguer surveys at both the Poás and Masaya crater zones
- Topographic survey at Poás and Masaya summit areas using real-time kinematic GPS
- New continuous (i.e., automated) micro-gravity recording, as well as broadband seismic recording, at Poás and Masaya
- SO_2 flux measurements using COSPEC at Poás (carrying the instrument across the floor of the active crater) and Masaya (plume transect using a car)

Geochemistry

- Establishment of a network of sulfation plates at Poás to study the dry deposition
- Gas sampling at Poás and Masaya with Japanese boxes and filter packs
- Water sampling of the main rivers on the flanks of Poás
- Soil degassing at Poás and Masaya (Radon, H_2S, CO_2, CO)

- Soil sampling and onsite soil pH measurements at Poás and Masaya

Geology

- Sampling of pyroclastic deposits in the active crater for density and effective porosity study at Poás and Masaya
- Sampling of lava flows in the active crater and on the west flank of Poás. Sampling of summit lavas at Masaya; both for density studies
- Survey of erupted products at the top and on the west flank at Poás.

Additional continuous gravity and seismic measurements were performed at Stromboli volcano (Italy) in May 2002, as well as at The Open University (July 2002, May 2003), to assess the gravity meter response to seismicity.

Although the fieldwork has obviously been a team effort, with other researchers involved, more than 90 % of the project has been the author's own work, both in the definition of new methodologies and in the interpretation of the results from this study.

The next chapter of the thesis investigates the use of a sulphur budget for Poás volcano in order to monitor the amount of magma degassing between 1998 and 2001. It also reassesses previously published gravity data by Rymer et al. (2000) on the last eruptive crisis at Poás (1986-89) and compares this crisis with the present state of activity at Poás. A newly developed dynamic gravity correction for the local water table is proposed and gives new estimates of mass, volume and location of magmatic intrusions in near surface suspected during the 1986-1989 crisis. This has been published in *Earth and Planetary Science Letters*.

Chapter 3 explores a new type of high-resolution Bouguer survey at Poás volcano and investigates structural features in the near surface below the crater floor. It also illustrates the development of automated routines leading to high-resolution Digital Elevation Models by coupling digitised topographic maps with a Real-time kinematic Ground Positioning System. This chapter constitutes a paper pulished in *Geophysical*

Research Letters, and it describes a methodology for the new high-resolution Bouguer survey.

Continuous gravity recording is detailed in Chapter 4 with the development of logging software as well as preliminary conclusions from promising tests in diverse settings (lab as well as several volcanoes). Suggestions, for instance about in-depth data processing, are also given in order to optimise gravity work on other volcanoes. Part of this chapter (g_log4PDA) has been published in *Computers and* Geosciences.

Finally, overall conclusions about this work are given in chapter 5 as well as a discussion of the insights coming out of this project, first about general gravity methods in volcanology, then about the volcanic processes and monitoring at Poás volcano. The chapter ends by highlighting new contributions from this work on our general understanding of volcanoes.

This project involved substantial programming in MATLAB® 6.1 and MICROSOFT VISUAL BASIC® 6.0 Pro languages; the code is given in the Appendixes C and D. All software developed during this work are the property of The Open University but are freely available to all researchers in the field of Earth Sciences by contacting the author.

Chapter 2

Degassing at Poás

and the 1986-89 crisis

This chapter is a paper submitted to Journal of Volcanology and Geothermal Research **"Persistent volcanic degassing: evidence from multidisciplinary study of hydrothermal and shallow magmatic processes at Poás volcano, Costa Rica".**

Nicolas Fournier [a], Hazel Rymer [a], Glyn Williams-Jones [b!], Jorge Brenes [c],
[a] Volcano Dynamics Group, Dept of Earth Sciences The Open University, UK
[b] Dept of Earth Sciences, Simon Fraser University, British Columbia, Canada
[c] OVSICORI, San Jose, Costa Rica

Poás crater lake

2.1 Abstract

Poás volcano, Costa Rica, experienced its last eruptive crisis in the late 1980s. It usually hosts an acidic crater lake that acts as a buffer for the heat output from the shallow magma chamber and intrusions. During such a crisis, the dramatic drop of the summit water table influences micro-gravity measurements that are used as one of the main monitoring techniques. This partially hides the signal due to possible magmatic intrusion for which inferred volumes can be underestimated. We therefore use the 1986-1989 data to calculate the variations of micro-gravity due to hydrothermal/hydrogeological processes in order to extract the magmatic signal. Taking into account this "aquifer effect", the corresponding modelled mass for the intrusion is almost 30 times bigger than the one previously calculated when not considering the effect of the drop of the water table. Micro-gravity monitoring is therefore greatly improved and allows not only a better estimate of the mass of magma intruded but also a better detection limit of possible intrusions. Retrieval of the amount of magma intruded during the last crisis shows that not all the magma degassing at that period was intruded at shallow level but rather, some must have been recycled in the magma chamber or intruded cryptically. Present analysis of the system using sulphur budget shows that about 7-21 x 10^9 kg yr^{-1} of magma degassed between 1998 and 2001, which is similar to the estimate after the 1986-89 crisis, revealing a relatively stable magmatic activity as Poás since then, with no shallow magma intrusion detected. We propose a two-step monitoring system at Poás, which may be applied to all volcanoes with crater lakes, integrating both sulphur budget analysis and micro-gravity. At Poás, the sulphur budget allows one to estimate the annual amount of magma degassing at depth greater than 500 m below the crater bottom, which corresponds to the top of the upper magma reservoir, while micro-gravity allows the detection of potentially hazardous intrusions at

shallow levels. Finally, the upper reservoir at Poás volcano is clearly shallow enough to allow major volatile exsolution from the andesitic magma and wide enough to allow magma convection and thus the magma/volatile segregation necessary for the sustained persistent degassing at this volcano. This structural characteristic may be a key parameter for persistent degassing on volcanoes without associated eruptions.

Keywords: crater lake; magma degassing; geophysics; sulphur budget; Poás volcano

2.2. Introduction

Poás volcano, Costa Rica rises to 2500 m above sea level (a.s.l.) and forms part of the Central American Volcanic Belt. Poás has been persistently active since historical times. Its active crater is partially filled by an acid lake (pH <1 since 1979) and shows significant and persistent fumarolic activity (**Fig 2.1a**). A lake of meteoric water fills the other inactive crater Botos. Much of the active crater is hydrothermally altered and fumaroles are presently located on the inner walls of the crater and close to the lake, on the eroded remains of the 1953 lava extrusion usually called "the Dome". They have relatively low temperatures (<100°C) and tend to migrate along the inner walls over time. Additionally, gas permanently bubbles through the crater lake forming a mist at the surface of the water.

The most recent eruptive crisis started in 1986 when lake level began to drop dramatically, with complete desiccation of the lake in 1989, followed by phreatic eruptions and sulphur flows on the crater floor (Smithonian, 1989, Oppenheimer, 1992). The crisis has been attributed to shallow magmatic intrusions (Rymer et al., 2000) and to a period of unusually low rain fall (Rowe et al., 1992) The lake was re-established by 1994 and its level gradually again rose, finally reaching its pre-crisis level in 1998. The acid lake level has remained fairly constant since then with a current apparently stable lake depth of approximately 52 metres (Rymer et al., 2000).

Here we present a new combination of micro-gravity and SO_2 flux data to assess the present state of activity at Poás volcano and analyse the previously published work to refine the models for ongoing persistent activity and the causes of the last crisis.

2.3. System approach

The aim is to use a holistic approach to study the Poás system, utilising an array of data sets not usually considered together. Micro-gravity and ground deformation measurements can provide information on any change in subsurface. SO_2 flux measurements and sulphur budget can be used to estimate the amount of magma degassing between 1998 and 2001. As the system seems currently in relative steady state both in terms of fluids composition and lake level, this is expected to reflect the present state of activity at Poás.

2.3.1. Sulphur budget

In terms of magma emission, Poás volcano can currently be considered to be a closed-system since there is no open vent at the summit and no juvenile material has been erupted since 1953. Therefore, part of the sulphur exsolved from the magma cannot exit the volcano in a gaseous form (i.e., mainly SO_2 and H_2S) via an open vent but, rather, is trapped at different stages within the hydrothermal system in the shallow parts of the edifice. Estimates of the amount of sulphur exsolving from the magma will thus be significantly underestimated if based solely on SO_2 flux measured at fumaroles, for instance by correlation spectrometry (COSPEC; Stoiber et al., 1986, Andres et al., 1992).

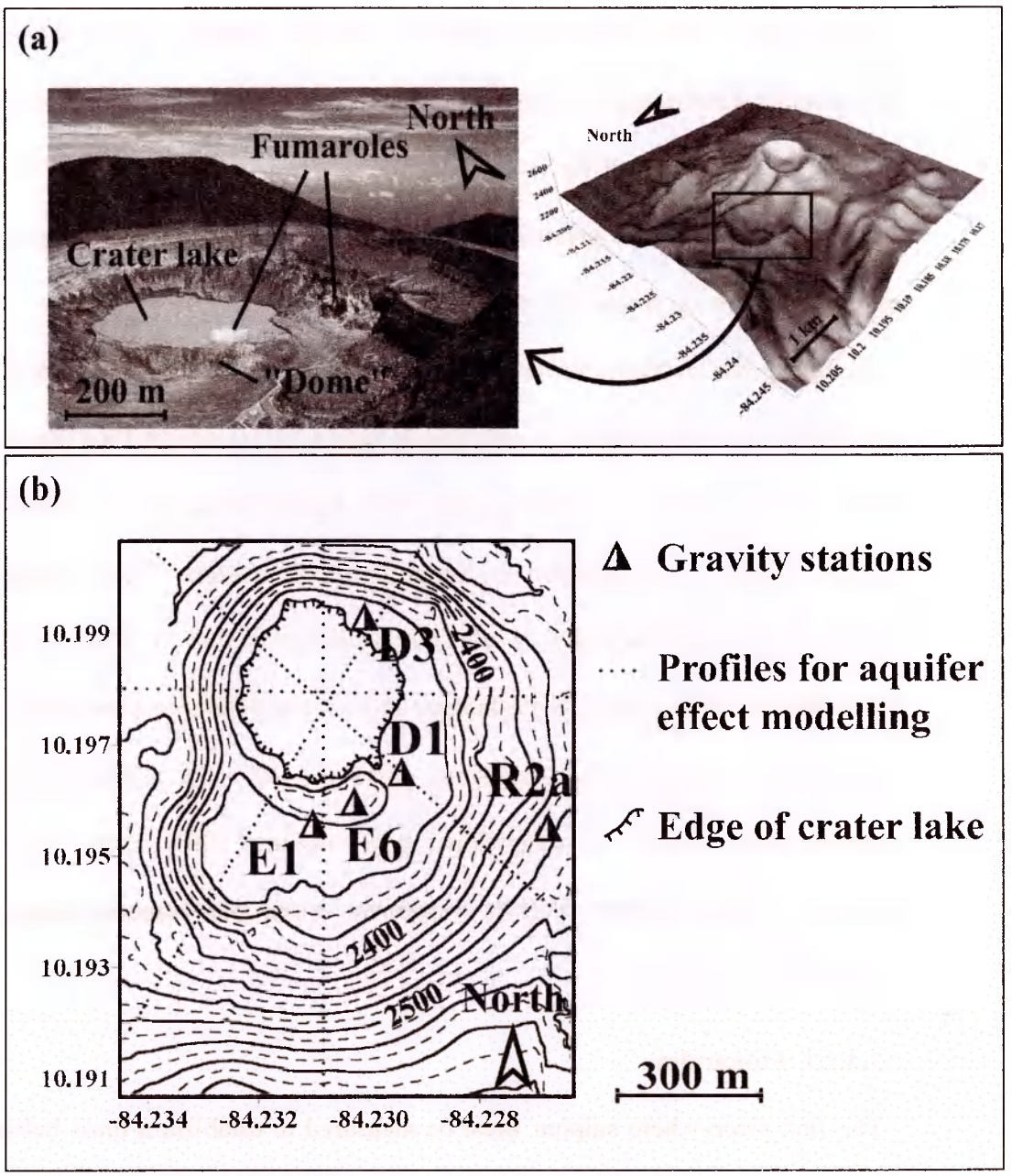

Fig 2.1. (a) Picture of the active crater. Note the crater lake and the fumarolic activity on both the "dome" (south side of the lake) and the inner eastern crater wall. Digital Elevation Model of Poás volcano is given for location of the active crater. (b) Contour map of Poás crater derived from Real-Time Kinematic GPS measurements. Elevation contours in metres above sea level. 5 micro-gravity stations used by Rymer et al. (2000) are marked with bi-colour triangles. Aligned points indicate the 4 profiles used for modelling the effect of the water table variation on the gravity field at the crater.

The fate of degassed volatiles at Poás is complex. Here we consider only SO_2 and H_2S for simplicity. Once sulphur has exsolved from the magma, it rises through the well-developed hydrothermal system. It can then be scrubbed by the hydrothermal system (e.g., ultimately entering the crater lake and/or descending the flanks via acid streams like the Rio Agrio), can precipitate within the porous substratum at shallow depths, or exit the volcano via fumaroles as a dispersed gas plume.

Assuming the sulphur leaves the magma reservoir in a gaseous form in thermal equilibrium with the magma, it will rapidly mix with the surrounding fluids and several processes can then occur. Boiling only of the hydrothermal system cannot account for the observed gas composition at fumaroles (pers. comm. Tassi). Indeed, the high SO_2/H_2S ratio (Montegrossi et al., 2001) indicates that if boiling occurs in the hydrothermal system under the influence of rising high temperature gases, the physical and chemical interaction between these gases and the water is incomplete. Therefore, the fumaroles release low temperature gases (around 100°C) and their composition reflects a mix between juvenile magmatic gases and vapour from the boiling hydrothermal system.

2.3.1.1. Fumaroles

The first place where sulphur must be measured to establish a mass balance is at the fumaroles. COSPEC measurements (8 transects through the plume) were made in 2001. As the plume was not high enough to allow traditional COSPEC measurements outside the crater (e.g., by car or airborne; Casadevall et al., 1982, Andres et al., 1992), the instrument was carried down to the crater floor and transported on a backpack frame beneath the plume (**Fig 2.2**). Simultaneous GPS tracking was used to correct for the difference in perpendicularity between the traverses and plume direction. Wind speed (5 m s^{-1}) was measured simultaneously on the dome crest using a hand-held anemometer approximately at plume height.

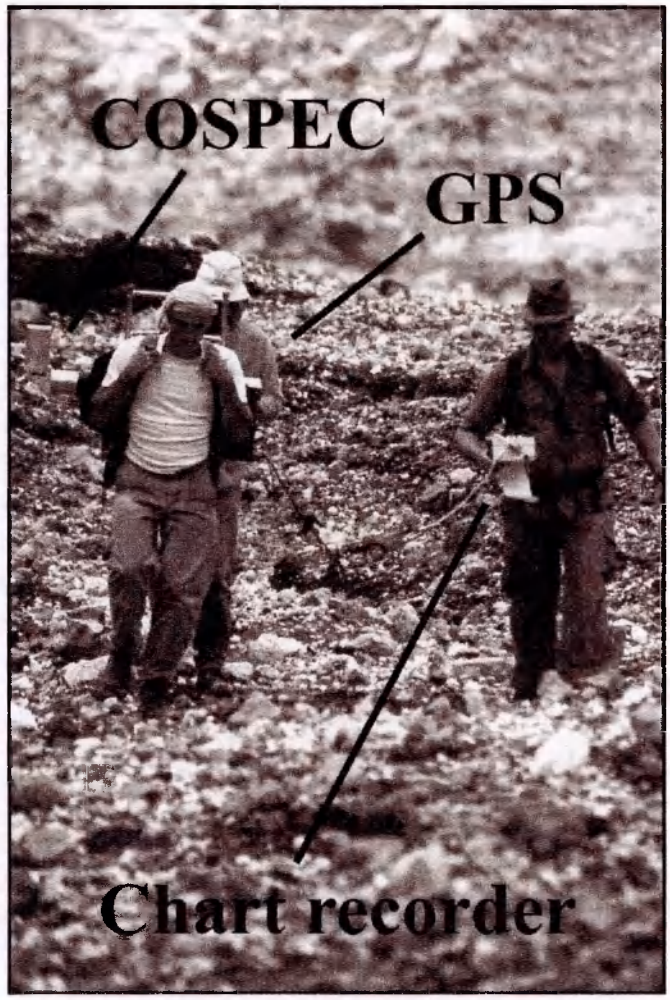

Fig 2.2. COSPEC measurements on the floor of Poás crater with hand-held GPS tracking (for speed and direction of the transects) and chart recorder.

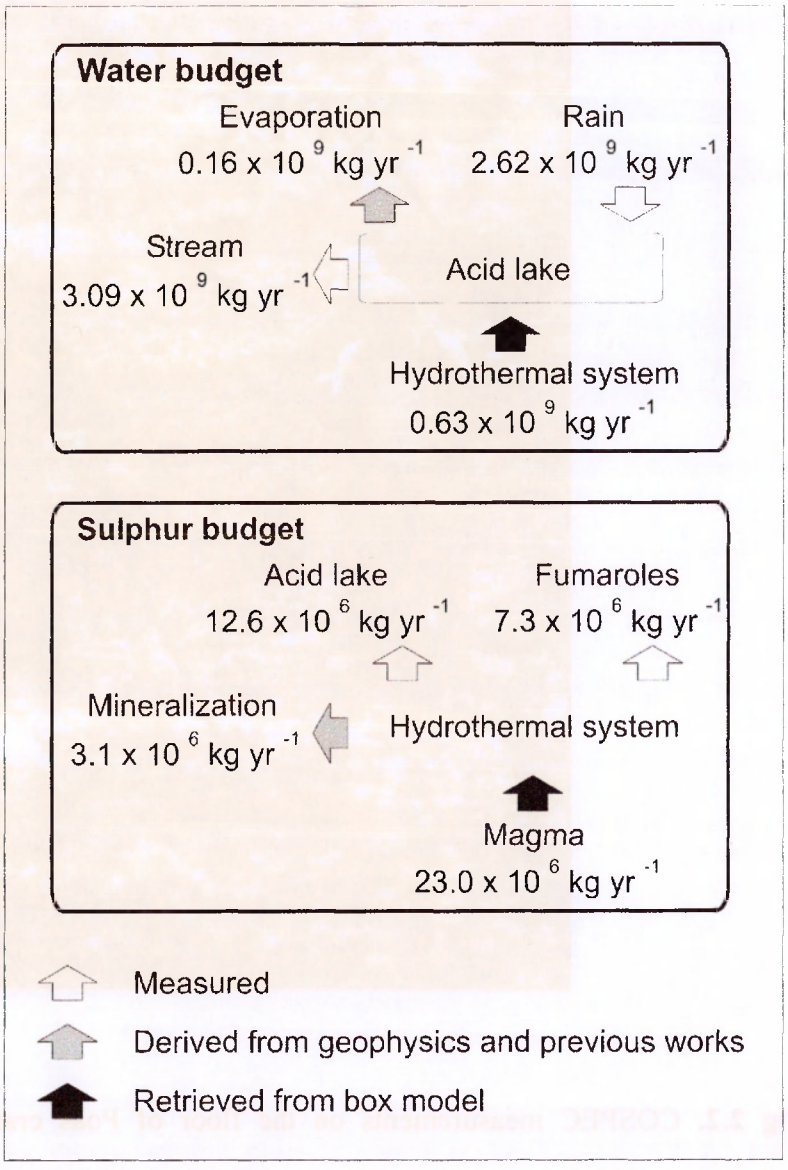

Fig 2.3. Box model for fluid circulation at the summit of Poás volcano. *Top*: annual water budget for physical and chemical equilibrium of the lake (i.e., constant lake level and water composition). *Bottom*: annual sulphur budget for physical and chemical equilibrium of the lake.

Due to the limitations of the COSPEC technique, we assume that the gaseous form of sulphur was essentially SO_2. This does not take into account the sulphur released as H_2S. However, the high SO_2/H_2S ratio observed by Montegrossi et al. (2001) at Poás fumaroles implies an uncertainty within that of the COSPEC flux measurements, the largest component of which is due to wind speed measurement imprecision (Doukas, 2002, Williams-Jones et al., submitted). At Poás, this uncertainty is small (~10%) as measurements are made virtually at plume height. It should also be noted that apart from combustion at the surface (Harris et al., 2000), scrubbed sulphur is extremely difficult to remove as SO_2 (Symonds et al., 2001). One can therefore assume that the sulphur emitted at the fumaroles as SO_2 comes directly from the magma.

Finally, it gives an average S flux of approximately 7.3 x 10^6 tonnes per year (40 ± 4 tonnes per day, t d^{-1}, SO_2 flux). Fumarole composition has been relatively constant between 1998 and 2001 (pers. comm. Tassi) so we take this sulphur degassing rate for this mass balance calculation.

2.3.1.2. Crater lake

The second place where sulphur accumulates is within the crater lake. In order to estimate sulphur flux into the lake, a water balance for the lake (**Fig 2.3**) based on work from Rowe et al. (1992) has been established for the 1998-2001 period. The amount of water coming from the hydrothermal system and entering the crater lake can be estimated as follows:

$$\Delta M_{lake} = M_{hydro.syst} + M_{rain} - M_{evap} - M_{stream} \qquad (2.1)$$

where the variation of the mass of water in the lake (ΔM_{lake}) is derived from the balance between the mass of water coming from the hydrothermal system ($M_{hydro.syst}$), rain (M_{rain}), and the mass of water leaving the lake as evaporation (M_{evap}) and draining towards the west flank via the Rio Agrio (M_{stream}). New values for rain, evaporation and

drainage are averaged for the 4 years considered here (**Fig 2.3**; average from 1998 to 2001, courtesy of the Parque Nacional del Volcan Poás and OVSICORI) and calculations are derived from Rowe et al. (1992, 1995). As the average lake level for this period can be considered as constant (error is within ± 2 m of seasonal variations due to changes of rainwater runoff available), ΔM_{lake} equals zero. Rearranging the Equation (2.1):

$$M_{hydro.syst} = M_{rain} - M_{evap} - M_{stream} \qquad (2.2)$$

we find that the average amount of water entering the lake from the hydrothermal system is 20 kg s^{-1}.

As the acid lake can be considered as the exposed part of the liquid dominant zone of the hydrothermal system, we can assume here that sulphur content of the hydrothermal system is close to that of the lake. We measured in 2001 an average concentration in SO_4 of approximately 60,000 ppm which is comparable to that measured by Rowe et al. (1995). This gives a H_2O/S ratio of 50. Therefore, based on previously calculated 6.3 x 10^8 kg yr^{-1} of water entering the lake from the hydrothermal system, it gives an associated flux of 12.6 x 10^6 kg yr^{-1} of sulphur coming from the hydrothermal system and being dissolved in the lake. Lake composition having been relatively constant between 1998 and 2001 (courtesy of OVSICORI) we kept this flux for this period. Isotopic studies on sulphur from the lake (Rowe er al., 1994, Kusakabe et al., 2000, pers. comm. Vaselli) indicate that the proportion of sulphur coming from bacterial activity is negligible compared to the magmatic input. Therefore, this validates the use of the sulphur at Poás crater lake as a magma-derived tracer.

2.3.1.3. Mineralization

Another fate of sulphur leaving the magmatic system is precipitation within the porous volcanic media at shallow depths. Rowe et al. (1992) estimated that the acidity of the hydrothermal system is sufficient to dissolve the substratum and the Rio Agrio removes

approximately 1650 m^3 yr^{-1} of material from the upper part of the active cone. Measurements of flux and water composition at Rio Agrio before 2001 (courtesy of OVSICORI) show a relatively constant chemical composition and behaviour of this river apart from the seasonal variations due to heavy rain (i.e., flux increase and dilution). We assume here that the dissolution rate of the upper part of the volcano suggested by Rowe et al. (1992) remained approximately the same for the 1998-2001 period. It implies a significant amount of material removal in the upper part of the edifice and it suggests that over time, the yield strength of the material will dramatically decrease and lead to significant ground deformation. This will be further exacerbated by the high seasonal precipitation in the region and the formation of clays by the hydrothermal alteration. However, our GPS ground deformation monitoring does not currently show any significant deformation of the upper edifice (maximum deformation is less than 6 centimetres and very localised). Therefore, while some gaps due to material removal may be locally supported when present at the surface, the majority must be filled to maintain the stability of the substratum and mineral deposition is the most likely mechanism for this. The presence of subaqueous accumulation of sulphur was suggested following observation in 1978 (Bennett et al., 1978) and sulphur flows and spatter cones were observed at the bottom of Poás crater shortly after the lake disappeared in early 1989 (Oppenheimer, 1992). This liquid sulphur erupted in 1989 can be interpreted as a remobilisation of previously precipitated solid sulphur, due to general overheating by a shallow magmatic intrusion (Rymer et al., 2000). This suggests that a significant amount of sulphur precipitates beneath the lake between periods of crisis. One possibility is that cavities created by substratum dissolution (the material being removed by the Rio Agrio), would be filled by solid sulphur (Rowe et al., 1992). Ground subsidence at the surface (Rymer et al., 2000) when molten sulphur was remobilised during the 1986-89 crises supports this hypothesis. The system thus

requires the subsurface precipitation of ~1650 m^3 of sulphur every year in order to fill the voids. With an average density of 1.9 x 10^3 kg m^{-3} (Bennett et al., 1978), a total mass of 31 x 10^5 kg yr^{-1} of sulphur may be deposited or a daily deposition rate of 8.5 t d^{-1} of sulphur accumulating in the substratum. It should be noted that the gaps need not necessarily to be entirely filled in order to maintain sufficient yield strength and prevent ground deformation. It is also possible that mineral deposition in the voids is not only confined to sulphur, so this may be an overestimate of the sulphur deposition, hence the slight difference with previous estimation (6.3 t d^{-1} of S in Andres et al., 1992)), although such a difference is not significant at the scale of the whole model. Summing these data (**Fig 2.3**), we estimate a total sulphur flux from the magmatic system of approximately 230 x 10^5 kg yr^{-1}.

2.3.2. Amount of magma presently degassing

Based on the estimated amount of sulphur released from the magmatic system over a fixed period, it is possible to assess the amount of magma degassing during the same period from pre-eruptive sulphur content. The main problem resides in the estimate of the original sulphur content of the magma before degassing at Poás. Due to the lack of glass inclusions data, we had to assume reasonable values derived from other studies in comparable geotectonic settings, bearing in mind that we are interested in orders of magnitude only. Average estimates of sulphur content in similar subduction-zone magmas suggest 3000 ppm by weight (Johnson et al., 1994 and references therein). As a first estimate, we assume here a 3000 ± 500 ppm by weight initial sulphur content for Poás magma. Andesite samples from Poás show remnant sulphur of up to 900 ppm (Rowe et al., 1995). This implies that degassing can remove at least 2100 ± 500 ppm, which represents 50-78% of the original dissolved sulphur in the magma. Assuming this average range of degassing, we may slightly overestimate the mass of magma degassing compared with the hypothesis where all the dissolved sulphur is degassed. As this study

is monitoring orientated, we choose the "worst case scenario", and find that approximately 7-21 x 10^9 kg yr^{-1} of magma may have degassed between 1998 and 2001. This estimate could be greatly improved by determining the exact initial sulphur content in glass inclusions in Poás lavas and values given here are a first approximation we used to obtain orders of magnitude of the amount of magma degassing. A fundamental question concerning the behaviour of the degassing magma remains: is it intruded into the upper edifice or recycled within the magma reservoir? Furthermore, was the 1986-89 crisis a significant event compared with the present degassing state of the volcano?

2.4. The 1986-1989 crisis and micro-gravity monitoring

Micro-gravity monitoring at active volcanoes requires careful procedures and an understanding of how relative gravity varies in response to volcanic and non-volcanic phenomena (Rymer et al., 1987). At Poás, which has a highly developed hydrothermal system, gravity variations may be due to ground deformation, magmatic processes and/or changes in the hydrothermal system.

During the last crisis at Poás (1986-1989) Rymer et al. (2000) reported a micro-gravity decrease at the most northerly crater bottom station (i.e., D3; **Fig 2.1b**) as the level of the active crater lake decreased between 1986 and 1989. In contrast, other crater stations (i.e., D1, E1, E6) were characterised by a gravity increase that has been interpreted in terms of a magmatic intrusion below these stations.

The net gravity increase observed at stations in the southern part of the crater bottom was used to calculate a minimum value for the mass of the intruded magma, without however quantifying the effect of the water table variation. The calculated mass of the intrusion (10^8 kg in Rymer et al., 2000) was a minimum estimate as the effect on gravity of a lake level fall and the associated disruption of the hydrothermal system would be to further decrease gravity.

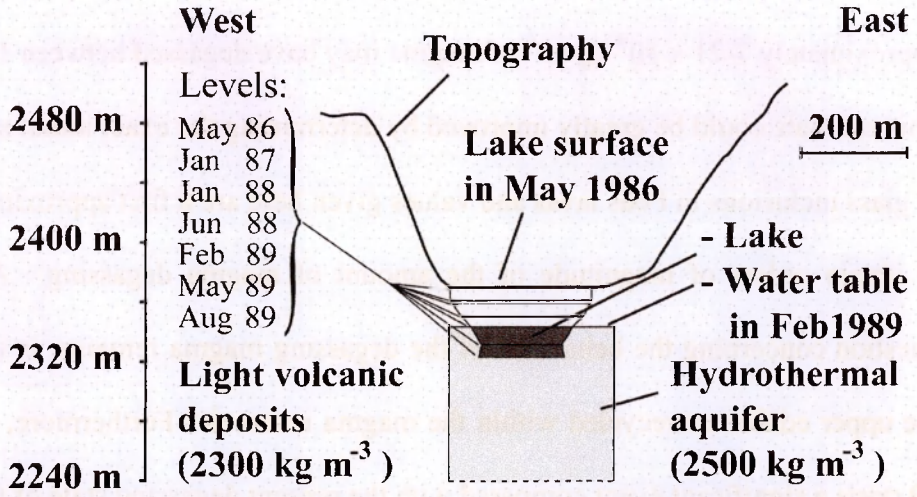

Fig 2.4. Example of 2.5D gravity modelling of the aquifer effect: profile #1 in February 1989.Variation of lake level through time is indicated (respectively, from top to bottom, May1986, January 1987, January 1988, June 1988, February 1989, May 1989 and August 1989). "Dry" deposits above the aquifer (white) have an average density of 2.3 x 10^3 kg m^{-3} while water saturated deposits (light grey) have an average density of 2.5 x 10^3 kg m^{-3} (light grey). In dark grey is the actual lake at the studied period (average density of 1000 kg m^{-3}). Width of the aquifer in the third dimension (not shown here) corresponds to the width of the crater bottom perpendicularly to the profile. Width of the lake in the third dimension (not shown here) corresponds to the width the lake perpendicularly to the profile.

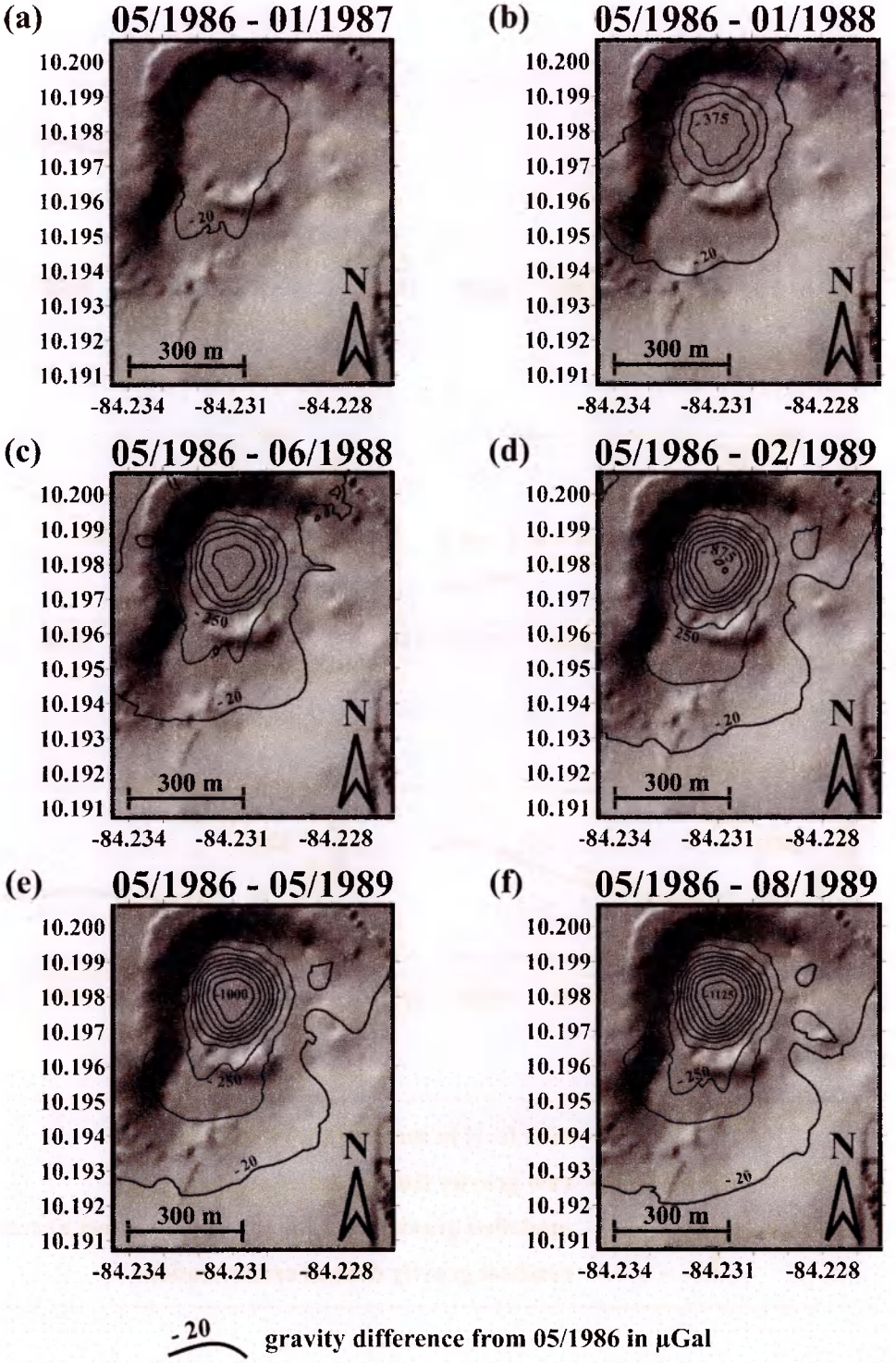

Fig 2.5. Modelled variation of gravity (in µGal), since May 1986, due to the drop of the water table at Poás active crater. Six periods have been modelled from May1986 to: (a) January 1987, (b) January 1988, (c) June 1988, (d) February 1989, (e) May 1989 and (f) August 1989. Only gravity change greater than 20 µGal is shown as this corresponds to the estimated maximum gravity noise during the measurements.

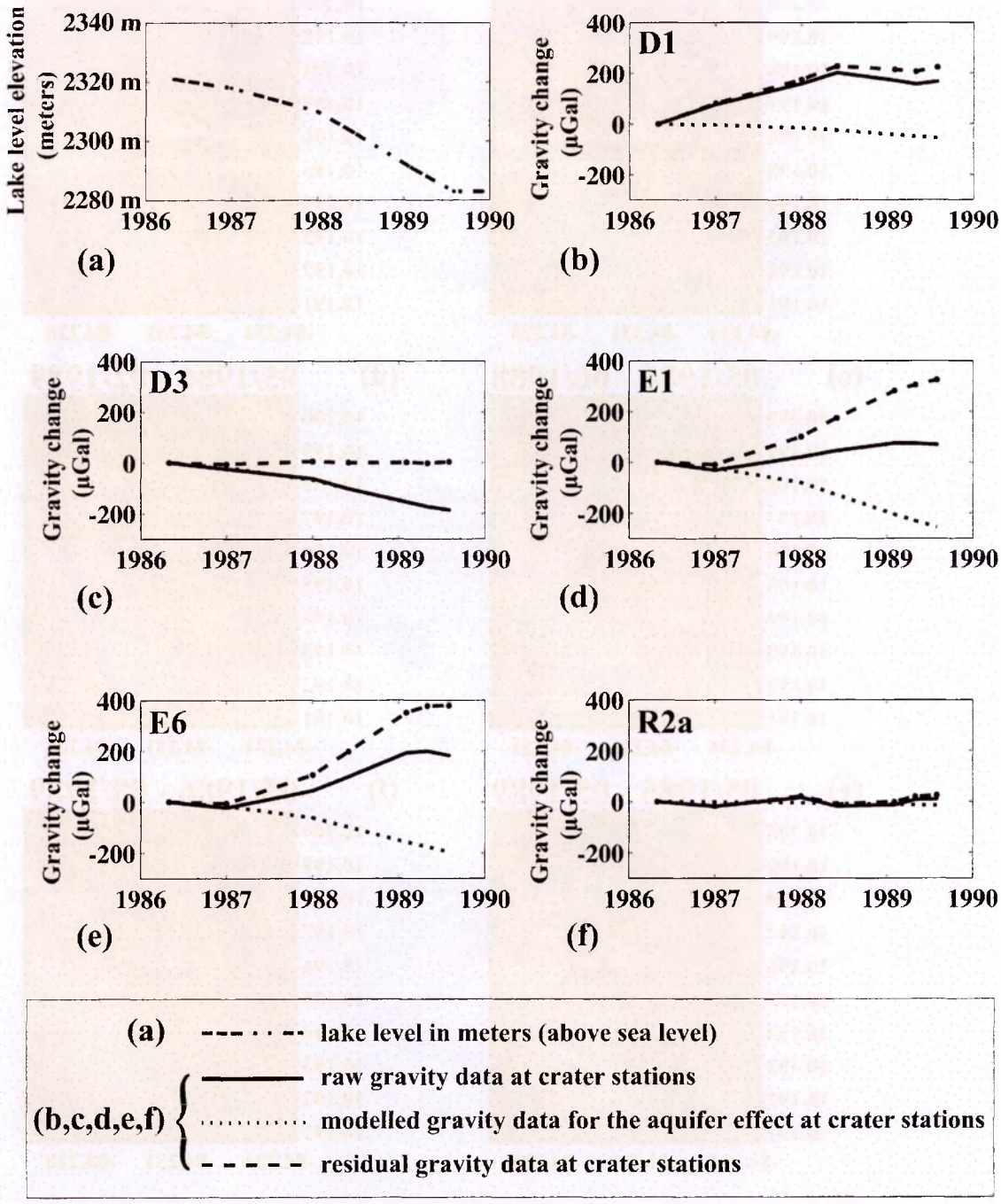

Fig 2.6. (a) Variation of lake level through the 1986-89 crisis. (b), (c), (d), (e) and (f) Raw gravity data (corrected for ground deformation and Earth Tide only), modelled data for the effect of the changes of water table on gravity and residual for each gravity station (respectively D1, D3, E1, E6, R2a), through time during the crisis. All gravity data are given with respect to May 1986.

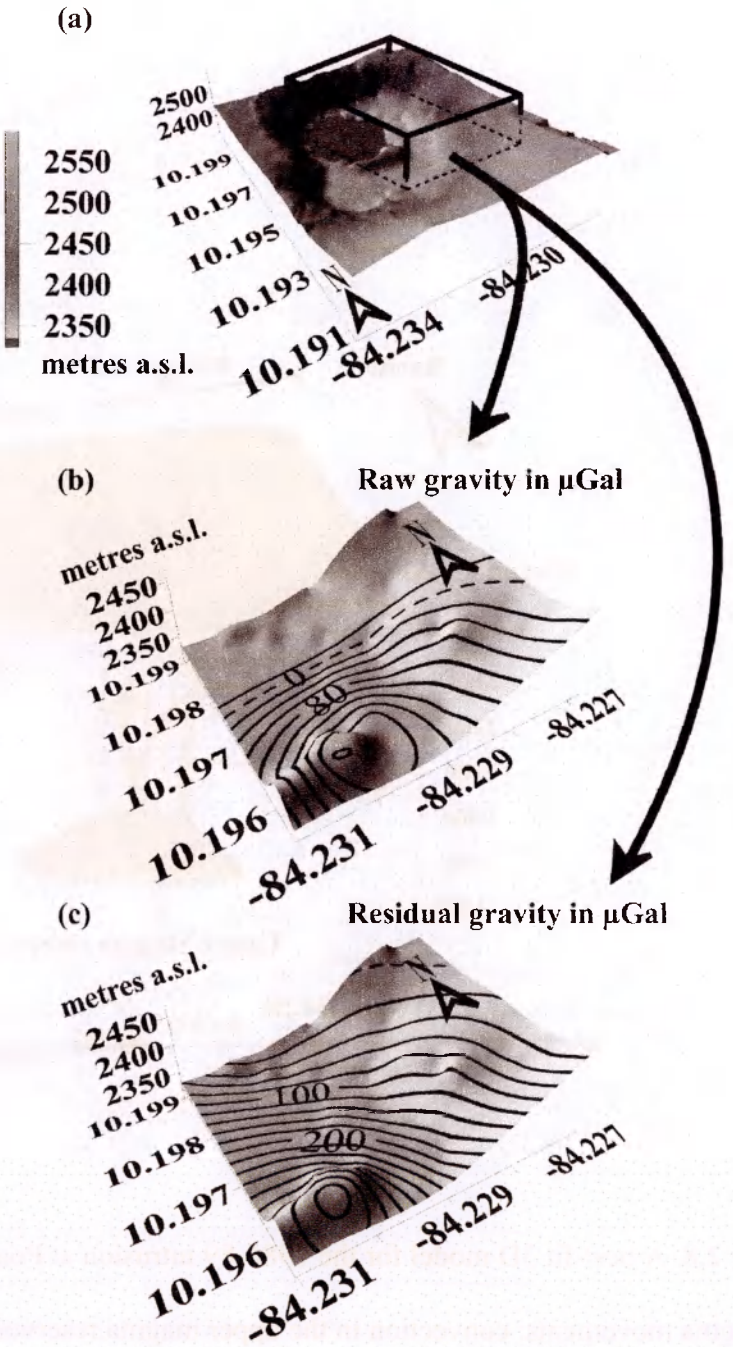

Fig 2.7. (a) Zone of the crater delimited by the gravity network (3D frame). (b) Final map of raw gravity anomaly (anomaly in August 1989 with respect to May 1986). (c) Final map of residual gravity anomaly (anomaly in August 1989 with respect to May 1986). Only gravity change greater than 20 µGal is shown as this corresponds to the estimated maximum gravity noise during the measurements. Note the difference of the maximum anomaly and of the geographical extension of the anomaly between the raw gravity (b) and the residual gravity (c).

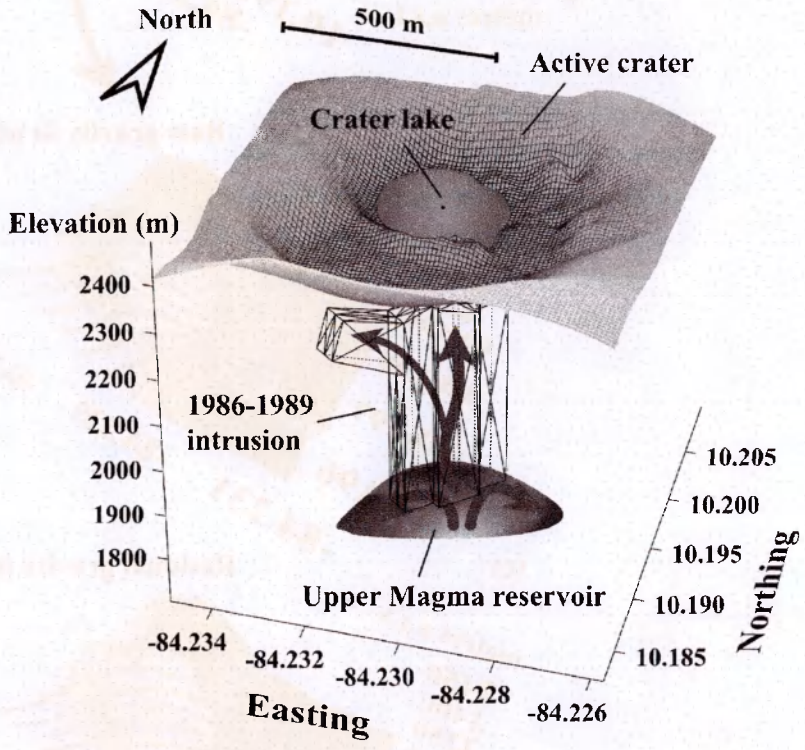

Fig 2.8. A best-fit 3D model for the 1986-89 intrusion at Poás. Grey arrows show magma movements: convection in the upper magma reservoir and magma rise as an intrusion during the 1986-1989 crisis.

Here, we quantify the response of gravity to hydrothermal phenomena at Poás by distinguishing between the magmatic and hydrothermal influences on gravity variations for the 1986-1989 lake level drop. We model the gravity effect of the lake level fall and assumed hydrothermal system level drop during the 1986 to 1989 crisis, in order to extract a more realistic estimate of the magmatic signature from the overall gravity signal.

2.4.1. Hydrothermal/Hydrogeological processes: the "aquifer effect"

Variations of lake level induce mass changes that are simple to quantify. A reasonably accurate geometry of the lake and crater can be deduced from records of lake depth and diameter, combined with our Real-Time Kinematic GPS measurements made in February 2002 (**Fig 2.1b**). Additionally, the fall of the local water table must be considered along with the mass loss due to the drop of the lake level. Aquifer parameters such as lateral extension and porosity must therefore be characterised in order to model mass changes. Acid springs due to the draining of the hydrothermal system exist only on the western flank of Poás (Rowe et al., 1995). This suggests that the system is mainly closed on the other sides. Fumaroles on the inner walls of the crater are characterised by higher SO_2/H_2S ratios than fumaroles on the dome (Montegrossi et al., 2001), which may indicate that magmatic gases are less mixed with lake water in the zone close to the crater wall. This suggests that the crater walls act as a barrier for the water and thus limit the aquifer on all sides. To a first approximation therefore, we assume that the horizontal extent of the summit aquifer and hydrothermal system is confined by the faults marked by the walls of the active crater. Previous works (Sanford et al., 1995) give porosities between 10% and 50% for the tuff and 1% for the lava flows within the crater at Poás. Higher values (50-60 %) have been reported (Foster et al., 1985) for laboratory measurements of porosity on other Costa Rican volcanic tuffs. However, the shallow fine tuff close to the lake is mixed with mud ejected from

the lake bottom during previous phreatic eruptions and clay formed by hydrothermal alteration and this would tend to decrease the porosity. In fact, we measured a mean effective porosity, for 8 samples taken close to the surface of the crater floor, of 20%, which is consistent with the standard modelling of Sanford et al. (1995).

The average density previously determined at the summit of Poás is 2.4 x 10^3 kg m^{-3}, but the scale of previous Bouguer survey (Brown et al., 1987) does not allow for discrimination between the water-saturated and unsaturated zones. We measured an average density of 2.3 x 10^3 kg m^{-3} and a porosity of 20% for the dry tuff at the summit. Consequently, taking a density of 1.0 x 10^3 kg m^{-3} for water within the pores, we derive a bulk density of 2.5 x 10^3 kg m^{-3} for water-saturated tuff.

From 1986, the lake level dropped gradually until its disappearance in 1989, followed by steam and ash eruptions. We assume for the purpose of this modelling that the level of the entire hydrothermal aquifer dropped by the same amount and at the same rate as the lake level. We modelled the effect of this drop from May 1986 on gravity at the stations from our network at top of Poás volcano. Four stations are located at the crater bottom (D1, D3, E1 and E6) and one at the crater rim (R2a) and their 3D coordinates have been measured by differential GPS (**Fig 2.1b**). Variations of the water table has been modelled along four profiles, each crossing the centre of the lake, using the 2.5D gravity modelling software GravMag (British Geological Survey; Pedley et al., 1997). While the modelling allows control of the third dimension, it is not strictly three-dimensional as the modelled bodies must be centred on the profile under consideration (**Fig 2.4**). Modelled data have been compiled and interpolated between the profiles for the entire crater area. The effect of the water table variation on any point of the crater zone is determined using an accurate Digital Elevation Model (DEM) of the area, derived from a Kinematic differential GPS survey in 2002 (Leica® system 500, **Fig 2.1b**). The modelled gravity decrease (**Fig 2.5**), normalized to May 1986 values (i.e.,

gravity changes from the start of the crisis), as the water table drops down, ranges from 0 to –1.2 mGal, the greatest negative gravity anomaly being observed when the lake level is at its minimum in August 1989 and at locations close to the lake. We can then extract modelled data at each of the stations for which we have actual micro-gravity data collected during the same period with G-meters from Lacoste & Romberg® (G-403 and G-513). All actual gravity data are corrected for height changes (i.e., ground deformation) and gravity changes due to Earth Tides (Rymer et al., 1996).

Comparison between the model and actual data through the 1986-1989 crisis shows that gravity data at the most northerly crater bottom station (D3) was only influenced by the water table variation (**Fig 2.6c**), supporting the hypothesis of Rymer et al. (2000). It also shows a discrepancy (positive gravity anomaly) with gravity data at other stations at the crater bottom (D1, E1, E6, **Fig 2.6b**, 6d, 6e, respectively). This suggests that gravity at these stations has been influenced by another phenomena in addition to the water table variation. Rymer et al. (2000) interpreted the observed gravity increase as a magmatic intrusion under the crater bottom, which is consistent with a thermal crisis leading to phreatic eruptions. Gravity increase due to mineral precipitation is not a viable hypothesis during this crisis as the temperature increase led to the remobilisation of previously deposited minerals and finally sulphur eruption (Oppenheimer, 1992), in contrast with the deposition expected between crisis when temperature is lower. Therefore, we favour magma intrusion as the most plausible cause for the gravity increase. Rymer et al. (2000) consequently derived the mass of the magma body directly from the observed gravity increase (minimum mass of 10^8 kg for a point source gravity model and a mass of 10^9 kg for a vertical cylinder of 100 m radius extending from the surface to 400 m depth). However, their mass estimate was a minimum since observed gravity data were a response to a combination of a gravity decrease due to the aquifer effect and a gravity increase due to the rise of a magma intrusion.

We thus subtracted the gravity variations due to the aquifer effect from the actual gravity data for the 1986-1989 crisis. The corresponding residual will reflect the gravity changes due to the magma intrusion (**Fig 2.7**). As expected, the immediate result is that the maximum positive gravity anomaly is much greater for the residuals than for the raw data (+378 μGal gravity change at station E6 from 1986 to August 1989 for the residual map, and only +202 μGal at station D1 August 1989-June 1988 for the raw data). Another consequence is that the area affected by the gravity change due to the magma intrusion is wider than observed with raw data. One can now model the residual gravity to determine the location, size, shape and finally volume of the magma intrusion.

2.4.2 Magma intrusion

One of the first parameters to define is the density of the ascending magma. The magma density changes with the amount of volatiles present in the melt, with the original content depending on the magma composition; previously erupted lava at Poás is andesitic in composition (Rowe et al., 1992). Assuming that water is the main volatile species, we can use the Burnham model (Burnham, 1994) to assess the solubility of volatiles in the melt for a given depth. We know that the top of the upper magma reservoir (i.e., roof of the upper magma chamber) is about 500 m below the crater bottom (i.e. top of the magma reservoir is ~1800 m a.s.l.; Thorpe et al., 1981); the water solubility for an andesitic magma at depths less than 500 m is almost nil. In other words, if the magma body is not subject to convection and hence refilled regularly by gas rich magma (as seems to be the case in the upper magma reservoir, considering that Poás is continuously degassing), a shallow magma intrusion less than 500 m deep must be almost entirely degassed when it is emplaced, especially if it rises slowly. We therefore assume a density of 2.7 x 10^3 kg m^{-3} for the degassed, but not yet solidified

intruded magma. This is consistent with previously published Bouguer anomaly (Thorpe et al., 1981, Brown et al., 1987).

For the modelling, we also consider that the magma intrusion was rooted to the upper magma reservoir, with a base at ~1800 m a.s.l. for the intrusion. The upper part of the edifice (i.e., surrounding rocks) is mainly composed of light volcaniclastic deposits with an average density of 2.4 x 10^3 kg m^{-3} (Brown et al., 1987). We used the 2.5D modelling software to model the gravity anomaly along profiles from the interpolated residual map, always validating model data with observed residuals at our stations. Forward modelling has been used to produce the first raw models while fine-tuning has been achieved with inverse modelling.

Our best-fit model for the magma intrusion is centred under the southern side of the crater lake. At its highest point, the top of intrusion is ~20 m beneath the "dome" surface (**Fig 2.8**), which is coherent with the ash and dry steam eruption (~450°C) in April 1989 (Smithonian, 1989). With an average horizontal cross-section of 100 m x 80 m and a shallower and more horizontal extension towards the southwest, we find a total volume for the intrusion of 1.0 x 10^7 m^3. With a density of 2.7 x 10^3 kg m^{-3}, this gives a total mass of about 27 x 10^9 kg intruded shallowly between 1986 and 1989. This is almost 30 times greater than the previous estimate from Rymer et al. (2000) which did not take into account the aquifer effect on gravity at the crater bottom.

For the 4 years of the crisis, an average of 7 x 10^9 kg yr^{-1} of magma was intruded, which is the lower limit of the range of the present estimated amount of magma degassing at Poás (i.e. 7-21 x 10^9 kg yr^{-1} of magma degassing). Due to the negligible volatile solubility in magma at the depth of emplacement (< 500 m below the surface), the intruded magma must have been almost entirely degassed when emplaced during the 1986-89 crisis. It is possible, however, that only part of the degassing magma during this period was intruded, with the rest of it being recycled in the magma reservoir as it is

at present. If this is the case, we cannot directly compare the two situations, but can nevertheless use the sulphur budget and SO_2 flux measurements through time to determine the significance of the 1986-89 crisis with respect to Poás' recent activity.

2.5. SO_2 flux and volcano behaviour

Pre-crisis airborne COSPEC measurements (Casadevall et al., 1984) measured an average daily SO_2 flux at the fumaroles of 760 ± 310 t d^{-1} in February 1982 and 500 t d^{-1} in December 1982 (Stoiber et al., 1986). Data on sulphur removal from the acid lake through the acid streams is unavailable for this crisis, thus it is difficult to draw a satisfying sulphur budget for the system and estimate the total amount of sulphur leaving the magma prior to the crisis. We therefore assume a minimum amount of 500 t d^{-1} of SO_2 leaving the magma before the crisis. As there was no evidence of any magma intrusion at that time, it implies that most of the degassing magma was not intruded to shallow levels but remained within the magma chamber and/or recycled at greater depth. This gives a minimum of 44 x 10^9 kg yr^{-1} of magma degassing prior to the crisis and re-circulating inside the magma reservoir, which is 2 to 6 times the amount of magma presently degassing at Poás.

After the crisis, there were no further eruptions until 1994 when a series of block and ash explosions occurred. This suggests that while the magma was no longer ascending (no increase of micro-gravity), it was still able to provide sufficient energy to provoke these eruptions. In February 1991, when there was still no significant lake at Poás active crater, measured SO_2 flux was 90 ± 30 t d^{-1} (Andres et al., 1992). At that time, sulphur scrubbing must have been small due to the limited gas-water interaction because of the close presence of the hot magma intruded during the 1986-89 crisis. This can be converted to an approximate volume of 8 x 10^9 kg yr^{-1} of magma degassing at that time which is within the range of current degassing rates.

2.6. Discussion

While we lack continuous long-term SO_2 flux data for Poás, it is still possible to extract some important information about the behaviour of the volcano. Firstly, the total amount of magma degassing at Poás dropped by more than 5 times after the 1986-89 crisis, perhaps indicating a significant decrease of the amount of magma rising into the edifice. Secondly, the amount of magma intruded during the crisis is much smaller than the average amount of magma degassing per year through the past 10 years. This suggests that part of the degassed magma has been recycled within the magma reservoir, which means that convection is occurring within this reservoir, supplying the system with gas and sustaining the persistent degassing at this volcano. As the magma intrusion had to be mainly degassed when emplaced, there was a need for an external driving force to push it up. Therefore, although the 1986-89 intrusion does not reflect directly the amount of magma degassing at the time, it may well be the consequence of a vigorous input of magma into the upper magma reservoir. The origin of the crisis was therefore much deeper as it involves changes in the amount of fresh magma circulating before and after 1986-89. In terms of monitoring at Poás, it implies that these changing phenomena, occurring deeper than 500 m below the crater bottom, may be responsible for long-term variations of the volcano behaviour. Using the sulphur budget in addition to more common techniques (e.g., seismic) is a valuable tool for the monitoring of deeper processes, as it allows us to quantify the amount of magma degassing, information that cannot be obtained from other geophysical techniques.

At a shallow level (i.e., above the top of the magma reservoir, less than 500 m below the crater bottom), the sulphur budget is no longer appropriate as the confining pressure does not exceed 1 kbar and is therefore not sufficient to prevent degassing of volatiles such as H_2O and SO_2 (Carroll et al., 1994). In other words, the observed and calculated amount of gas released by the magma reflects deeper degassing and not the shallower

intrusion. Micro-gravity is a valuable monitoring tool as it allows us not only to detect the intrusion but also to quantify the amount of magma rising from the magma reservoir towards the surface. This permits energy balance calculations between the rising magma and the water at the surface in order to assess likelihood of phreatic eruptions. This work shows that this can only be achieved by taking into account the "aquifer effect" (i.e., variation of the superficial part of the hydrothermal system). In fact, this model not only allows a better estimation of the amount of magma involved which would have otherwise been underestimated, but also increases the detection limits of the intrusions as the "aquifer effect" can largely exceed the signal due to small intrusions, even close to the surface.

In a broader context, it appears that when a volcano has a shallow magma reservoir, it allows a major degassing of the rising magma before this one reaches the surface, avoiding dramatic volatile exsolution in narrow conduits and hence acceleration of the magma when getting close to the surface. This would explain the relatively high amount of shallow intrusions at Poás and the noticeably small number of associated magmatic eruptions. So long as the upper magma reservoir is shallow enough to allow most of the volatiles to exsolve and wide enough to allow the dispersion of the associated energy released by convection, a volcano will show persistent passive degassing rather than repeated eruptions. This is even more important in the case of volcanoes with viscous magma (e.g., andesitic magma at Poás) where magma/volatile segregation is difficult to achieve even at shallow levels. This causes increased pressure in the bubbles and can lead to catastrophic eruptions if the energy released cannot be counter balanced by convection at relatively shallow depths.

Comment

This chapter shows that a significant amount of magma was intruded at shallow depth beneath Poás during the 1986-89 crisis. But was that event unusual or had other shallow magmatic intrusions previously been intruded? The next chapter investigates the total amount of magma intruded below the surface at Poás, with the help of a new high-resolution Bouguer survey.

Chapter 3

High-resolution gravity survey at Poás volcano

This chapter is based on a paper published in Geophysical Research Letters 31 L15602,doi:1 0.1 029/2004GL020563, 2004
"High-resolution gravity survey: investigation of subsurface structures at Poás volcano, Costa Rica".

Nicolas Fournier [a], Hazel Rymer [a], Glyn Williams-Jones [b!] and Jorge Brenes [c]
[a] Volcano Dynamics Group, Dept of Earth Sciences The Open University, UK
[b] Dept of Earth Sciences, Simon Fraser University, British Columbia, Canada
[c] OVSICORI, San Jose, Costa Rica

Micro-gravity training at Irazú volcano, Costa Rica

3.1. Abstract

Bouguer gravity surveys have long been used to investigate sub-surface density contrasts. The main sources of error in previous surveys have been the determination of relative elevations of stations and the effect of topography (removed via the terrain correction). The availability of high precision Kinematic GPS data now facilitates generation of high-resolution Digital Elevation Models that can help to improve the accuracy of relative elevation determination and the terrain correction. Here we report analysis of a high-resolution gravity survey at Poás volcano, Costa Rica. Our gravity modelling (i) identifies small pockets of magma at shallow depths which relate to successive magma intrusion through time and (ii) shows that the persistent degassing on the eastern part of the crater is related to local deformation at the top of the volcano and changes in the fractures network, rather than to a near surface magma intrusion.

3.2. Introduction

Structural studies on volcanoes using gravity surveys are typically carried out on a large, whole volcano scale, (e.g., Locke et al., 1993) with a view to determining the general plumbing system within and below the edifice. More detailed surveys would not only require a greater number of measurements but also the confidence that the various corrections needed for data processing are accurate enough to allow comparison of small gravity differences between close stations. The main source of errors in the corrections lies in the poor knowledge of topography within about 100 m of each measurement point (station). This "terrain effect" is especially significant in topographically severe place such as volcanoes. Improved accuracy of topographic models would reduce the errors in terrain corrections used for gravity surveys. Smaller gravity differences between stations could then be investigated with high precision topographic models and so surveys could become more accurate.

Development of new technology (e.g., real-time kinematic Global Positioning System) now allows 3D coordinates to be recorded in the field in a matter of seconds and therefore allows the generation of precise Digital Elevation Models that can be used to calculate terrain correction around the gravity stations.

Previous gravity surveys have been carried out at Poás volcano to investigate the structure of the whole edifice (Thorpe et al., 1981; Brown et al., 1987). However, while these studies provide information about the main features of the edifice, they do not have the resolution to detect small sub-surface bodies and it is these features which are important for micro-gravity monitoring.

Here we present the results of a new high-resolution gravity survey carried out at the top of Poás volcano, which provides new insights into the structure of the active crater at Poás.

3.3. Data collection and reduction

A 0.17 km^2 network of 33 stations was established on the crater floor of Poás in Ferbruary 2002. Stations coordinates were determined by differential GPS with a precision of 3 cm or better for most stations. Gravity data were collected at every station with a Lacoste & Romberg® G-meter (s.n. G-403) and measurements were repeated as often as possible (up to 4 times per day per station) to quantify the instrument drift.

Raw data were corrected for Earth Tides (Brouke et al., 1972) and then for instrumental drift, which was typically 80 $\mu Gal\ day^{-1}$. The standard latitude and elevation corrections were also made.

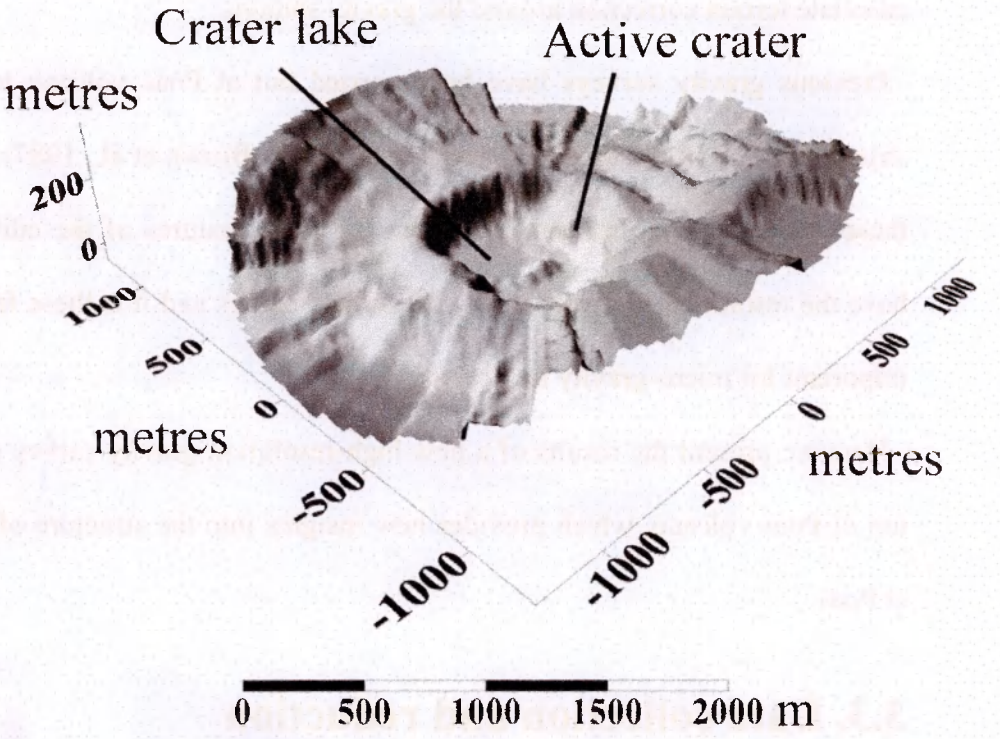

Fig 3.1. Topography estimate for Terrain Correction Hammer zones. Hammer zones are divided in 64 sectors where accuracy of the topography increases dramatically close to the station where the influence of surrounding topography is greater.

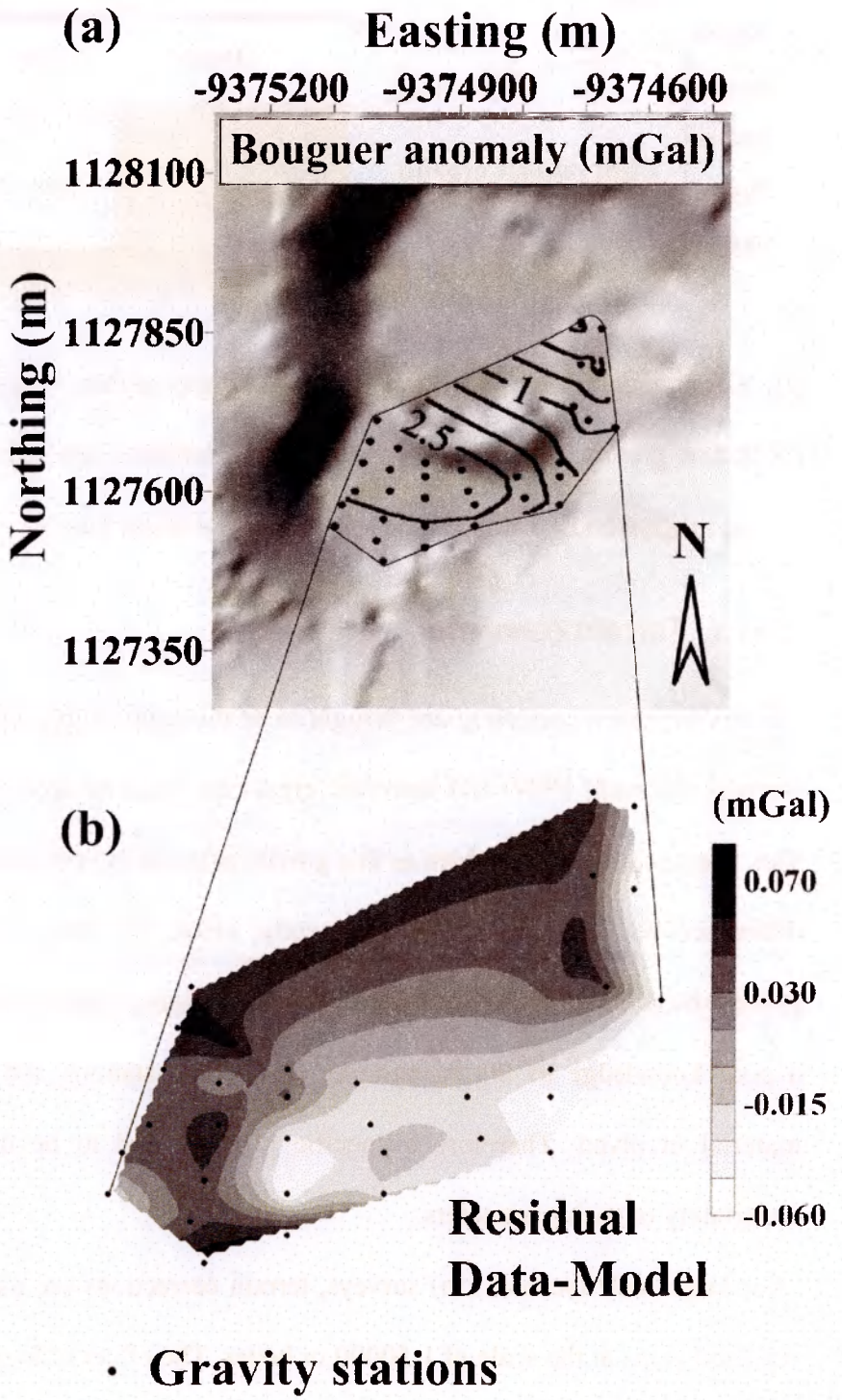

Fig 3.2. (a) Map of Bouguer anomaly in mGal. Contours are 0.50 mGal and points on the map indicate stations for the high-resolution gravity network. (b) Residual gravity anomaly in mGal between data and model. Mean residual gravity station is 15 μGal which is the estimated noise for the gravity meter.

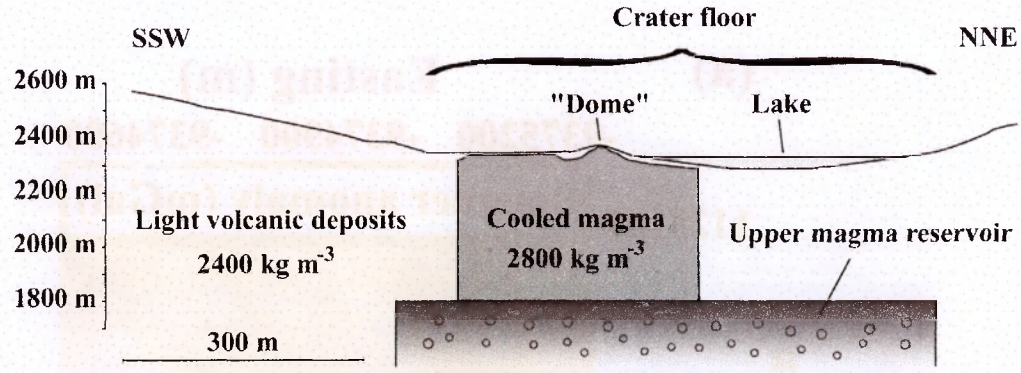

Fig 3.3. Schematic cross-section of the active crater at Poás volcano inferred from high-resolution gravity survey. Different material densities are indicated in kg m-3. The cooled magma body is off-centred with the actual crater lake.

3.3.1. Terrain correction

Errors in terrain correction are thought to be the main source of inaccuracy in Bouguer Surveys (Nowell, 1999) and therefore great care must be taken to minimize any error. This is especially the case here as this gravity network is very small and so is the gravity difference between stations. Consequently, errors in terrain correction could easily exceed the actual gravity differences between stations. Causes of these errors are mainly a poor knowledge of the topography around the stations and of the density of the material involved. Therefore a specific protocol had to be designed to reduce the uncertainty of such parameters.

For large scale (several km) surveys, terrain corrections are usually carried out using digitised maps at the scale of 1:50000 or better. The effect of local topography (within a few tens of metres) is sometimes ignored, sometimes estimated crudely. For this work, it was vital to obtain accurate corrections since the terrain effect was so large.

Obviously, the influence of topography is greatest close to the station and this influence decreases with distance from the station. There is therefore a threshold distance, beyond which the terrain correction for different stations will tend to be the same. We determined this maximum distance by comparing resulting terrain corrections

between stations and when the difference between stations becomes negligible compared to the instrument noise (i.e., 15 μGal), the zones taken into account for the terrain correction do not need to extend any further. Due to the limited extension of this high-resolution network, we found that terrain corrections converge for all stations from 1290 m thus we defined 1295 m as the outer radius of concern for this study.

The highest resolution maps available for the Poás crater are 1:50000 maps which are not sufficient for this study. Therefore, precise topographic campaign was carried out in February 2002 using RTK Leica® GPS receivers. The RTK GPS allows measurements of coordinates with a precision better than 3 cm in less than 10 seconds. An extensive survey was carried out at Poás with precise 3D coordinates measured for 2670 points along crests (i.e. crater rim, and 'dome' crest), bases of slopes (i.e. limits of the crater bottom) and around the edge of the acid lake. The static Base receiver was located at the 'mirador' viewpoint (on the southern rim of the crater) during the whole survey in order to keep direct sight with the mobile Rover. Elevation of the acid lake has also been measured (2330.41 m a.s.l.) and the elevation of the surface of the lake (area within the measured edge) has been fitted with this value. From these topographic data, we generated a high-resolution Digital Elevation Model (DEM) with resolution of less than 5 metres horizontally.

We designed an automated gravity terrain correction using this DEM based on 260 "Hammer" zones (Hammer, 1939). Each zone annulus was 5 m thick for zones inside the crater and 10 m for zones outside the crater where topographic effects are less. Each "Hammer" zone was divided in 64 equal sectors. Tests for each gravity station, using successively 8, 16, 32 and 64 sectors for each Hammer zone, show that the resulting terrain corrections tend to converge at 32 sectors per Hammer zone. The results shown here were achieved by using 64 sectors (**Fig. 3.1**).

3.3.2. Lake correction

As density of the lake water (1.0 x 10^3 kg m^{-3}) greatly differs from that of the substratum (2.4 x 10^3 kg m^{-3}), the effect of the lake on the gravity field on the crater floor must be taken into account. Lake bathymetry (Martinez et al., 2000) was combined with our RTK GPS survey to estimate the shape of the lake. To a first approximation, Poás lake geometry can be represented as an asymmetric inverted flat-bottomed cone. The lake bottom is a circular with a radius diameter of 80 m while the contours of the lake are ellipsoidal. Slope of the lake wall is assumed here to be constant from the surface to the bottom.

3.4. Gravity modelling

The reduced gravity data show a positive Bouguer anomaly inside the active crater, centred on the south side of the lake, with a relative maximum amplitude of 3.51 mGal **(Fig 3.2a)**.

We modelled this anomaly using 2.5D gravity modelling software GravMag (British Geological Survey; Pedley et al., 1997). The modelling is not strictly three-dimensional because although it allows control of the third dimension, the modelled bodies must be centred on the studied profile. As the extent of the gravity network is relatively small, the zone investigated by the Bouguer survey remains relatively shallow and we do not expect to investigate structures deeper than a kilometre below the crater floor.

We modelled two perpendicular profiles across the crater floor and compared model gravity anomalies with actual gravity data along the profiles. The final best-fit model was achieved when the mean residual between data and model fell below 15 μGal which is the estimated instrument noise (the maximum residual at gravity stations did not exceed 80 μGal; **Fig 3.2b**). The model comprises a quasi-vertical structure with a density contrast of + 0.4 x 10^3 kg m^{-3} with the surroundings, extending from 500 m

below the crater floor (i.e., ~1800 m a.s.l.), up to only a few metres below the crater floor. It is centred on the maximum gravity anomaly, south of the so-called "dome" on the south side of the lake, and has a horizontal cross-section of ~ 300 x 340 m (**Fig 3.3**).

The top of Poás volcano is mainly made of light vesiculated material, with a measured density of 2.4 x 10^3 kg m^{-3}. This is similar to the values used in previous studies (Brown et al., 1987; Rymer et al., 2000). If we take this as the background density for our models, it gives a density of 2.8 x 10^3 kg m^{-3} for the vertical structure responsible for the observed high-resolution Bouguer anomaly. Because of its vertical elongated shape and especially its density, this body is thought to be crystallised magma, rooted to the upper reservoir at ~1800 m a.s.l. (Thorpe et al., 1981; Rymer et al., 2000). The closest analogue to a magma body located at shallow depth under the crater floor is the degassed lava flows located on the inner eastern crater wall. Measurements on these lava flows give an average density of 2.8 x 10^3 kg m^{-3}, which fits well with the inferred density from the Bouguer survey for a cooled magma body under the crater floor. At such shallow depths, volatile solubility in magmas is almost nil (Burnham et al., 1994), therefore magma so close to the surface is expected to be almost entirely degassed (see **chapter 2**). High-temperature fumaroles (960°C) on the "dome" in 1981 (Casertano et al., 1987) indicated the presence of a hot magma body at the time, only a few metres below the surface. The presently low temperatures at the fumaroles on the "dome" (i.e., <100°C) are not compatible with hot magma just underneath the surface, so the shallow magma body has now to be mostly crystallised. It is this frozen magma that we have identified and modelled using the high-resolution gravity survey.

3.5. Discussion

The total mass of intruded magma responsible for the observed positive gravity anomaly is ~ 149 x 10^9 kg. This is a minimum estimate as part of the crater floor has not

been investigated for this Bouguer survey (i.e., crater lake). However, stations on the eastern side of the lake do not show the higher gravity values that would be expected if there was shallow magma close to the eastern fumarolic field. Thus the underestimate – if any- cannot be huge.

This overall mass of magma represents more than 5 times the total mass of magma intruded during the last crisis in 1986-89 (i.e., ~ 27 x 10^9 kg; see **Chapter 2**). At least two episodes of magma intrusions at the summit of Poás volcano are thus necessary to account for the observed Bouguer anomaly. While this high-resolution Bouguer survey cannot discriminate between the different intrusions, it clearly shows that the greatest part of the magma intruded at the top of Poás is localised on the southern side of the crater lake. The present degassing seen on the crater walls, especially on the eastern side, is therefore related to fractures going deep below the crater floor rather than the presence of magma immediately underneath.

The presence of a solidified, high level body below Poás active crater has two major consequences. Firstly, it may prevent magmatic gas rising up at this place and thus play a role in the location of fumaroles in the active crater. This would explain why so few fumaroles are now located on the eastern side of the crater and none at all on the south. Fumaroles at the south were present 20 years ago. This may indicate that, at the time, the magma was still hot enough to heat the hydrothermal system in its periphery. Secondly, frozen magma is much denser than the surrounding volcanoclastic deposits and therefore may strengthen the area below the crater floor. Fractures appearing due to its weight would then be localised around it, close to the crater walls, where gas would tend to escape. Hydrothermal alteration of the circular fractures on the crater walls combined to this dense amount of frozen magma below the crater floor could then well be important factors driving crater subsidence at the submit and formation of pit-craters.

3.6. High-resolution Bouguer surveys: the cook book

As specified earlier in this chapter, Bouguer surveys require a succession of corrections and data processing. Here is a summary of the methodology that has been followed for this work at Poás volcano. The main difference between high-resolution and conventional Bouguer surveys is the care taken for the terrain correction. Indeed, as the network is small, so are the gravity differences between the stations. Therefore, the usual correction can easily exceed the gravity signal, especially the terrain correction, which is the greatest source of inaccuracy in Bouguer surveys. The overall methodology presented here can be applied to all volcanoes where a precise survey of subsurface features is needed.

3.6.1. Network and Data collection

Establishment of a high-resolution gravity network has to comply with two conflicting constraints: how to maximize coverage of the surveyed area while permitting repeat measurements of gravity at the stations as often as possible (to precisely determine instrument drift). For this work, I set up profiles covering the flat area of Poás crater floor, trying to keep the distance between stations as close to constant as possible. This network represents a total of 33 stations distributed along 9 profiles (**Fig 3.4**). Not all profiles have the same number of stations. In each profile, stations were numbered starting at the station closest to the crater lake. (e.g., moving outwards, a1, a2, a3 and so on).

Precise positioning was measured for each station using Real-Time kinematic GPS (error <3 cm) and each station was marked with a coloured flag on site. Repeat measurements were made as often as possible during the three day survey.

Once the data were collected, Earth tide corrections were made using the Tide Calc software (Brouke et al., 1972).

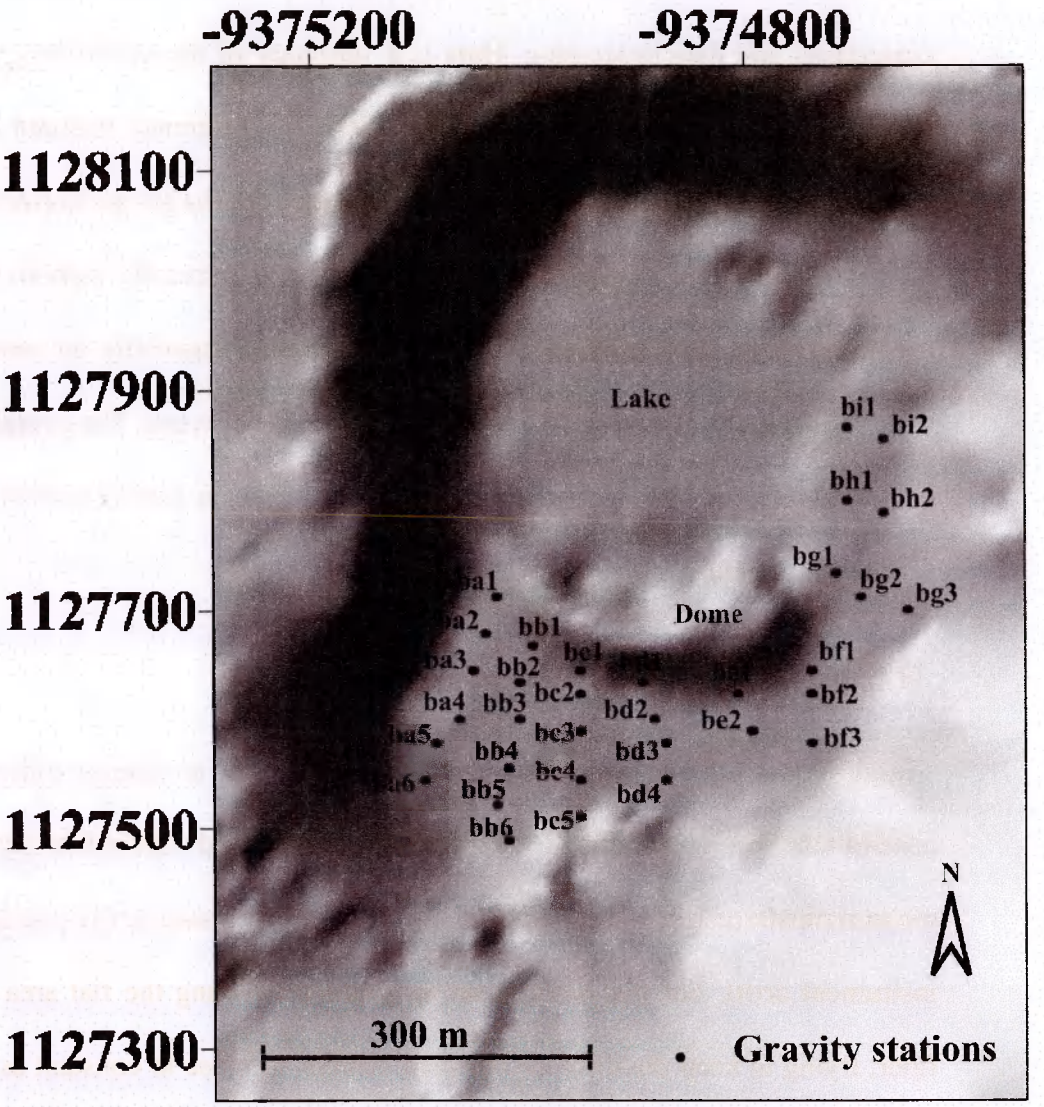

Fig 3.4. Map of the high-resolution gravity network. Easting and Northing are given in metres in an arbitrary system.

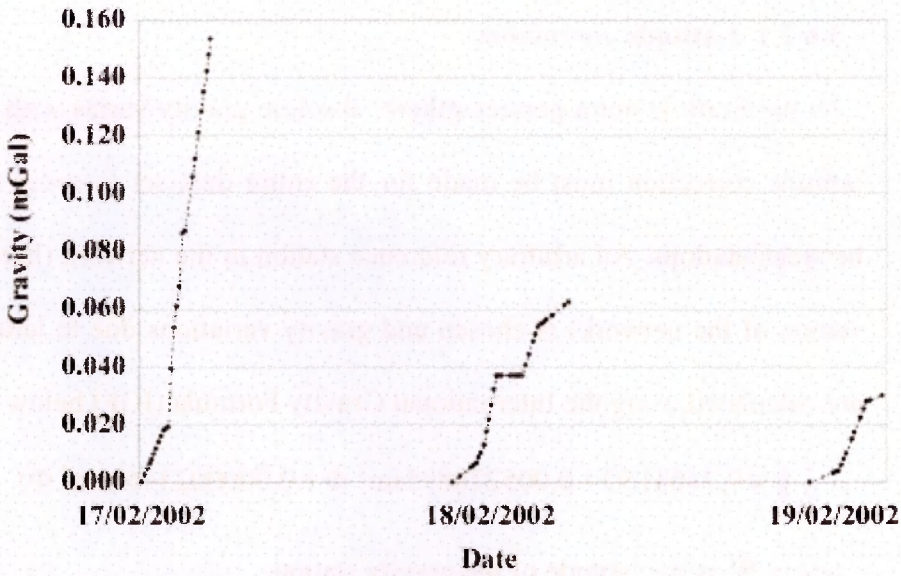

Fig 3.5. Drift function for the G403 G-meter during the 3 day gravity survey at Poás volcano. For each day, drift is normalized to the first data obtained during the survey. Instrumental drift is therefore relative to the first station measured.

A drift function was then determined for each of the three days by repeating measurements at the same stations. Indeed, gravity values – once corrected for the Earth tides- should be identical for repeated measurements at each station. The different values obtained throughout the survey will then reflect instrument drift. There are numerous phenomena affecting the instrument's stability and thus increasing the drift. During this survey, the walk down to the crater floor with the instrument (even though carefully clamped) has been the greatest source of instrument instability. The gravity meter (G403) was left to stabilise for an hour on the crater floor before starting the survey each day. Calculation of the Earth Tide induced gravity variation and determination of the instrument drift have to be done on site as they represent a valuable checking method for the validity of the data.

Once the instrument drift is determined (**Fig 3.5**), the following corrections can be made.

3.6.2. Corrections

3.6.2.1. Latitude correction

As the Earth is not a perfect sphere, absolute gravity varies with latitude and hence a latitude correction must be made for the entire data set in order to allow comparison between stations. An arbitrary reference station in the network (here, the most northerly station of the network) is chosen and gravity variations due to latitude at other stations are calculated using the International Gravity Formula (IGF) below:

$$g = 9.780315(1 + 0.005278895\sin^2\Phi + 0.0000023462\sin^4\Phi) \quad (3.1)$$

where Φ is the latitude of the gravity station.

The difference between this theoretical g between stations corresponds to the gravity difference due to different latitude at each station. Because of the small size of the gravity network (i.e., 0.17 km^2) at Poás, latitude corrections for all stations do not exceed the estimated noise for the instrument, which is 15 μGal.

3.6.2.2. Free-air and Bouguer corrections

The value of gravity varies with distance from the centre of the Earth. Therefore, where gravity stations have different elevations, they cannot be compared directly without taking this into account. Thus, gravity data at all the stations must be normalized to a same elevation using the 0.3086 mGal m^{-1} mean Free-Air gradient. If the original station elevation is higher than the elevation at which it will be normalized, then the Free-Air correction is negative (getting close to the centre of the Earth). It will be positive in the opposite case.

The Bouguer correction takes into account the material virtually added/subtracted when normalizing the gravity station at one same elevation and ignored during the Free-Air correction. Therefore, the density of the material involved must be determined.

In this study, the material involved is the same for all stations as the network is located on the same material (i.e., light volcano-clastic deposits) and shows little elevation

difference between stations. At Poás the average density (ρ) of this material above the upper magma reservoir has been estimated as 2.4 x 10^3 kg m^{-3} by Brown et al. (1987) during a previous larger scale Bouguer survey. The Bouguer correction gradient is therefore $0.0419\times\rho$ mGal m^{-1} (with ρ in g cm^{-3}).

Finally, it is possible to combine the free-air and Bouguer correction using the following formula:

$$\Delta g = \Delta h \times (0.3086 - 0.0419 \times \rho) \qquad (3.2)$$

with Δg the gravity correction in mGal to be added to all but the reference station, Δh the elevation difference in metres between the reference station and each station of the network, ρ the density of the material involved in the Bouguer correction, in g cm^{-3}.

3.6.2.3. Terrain correction

Principles of terrain corrections have been covered earlier in the chapter so here I will concentrate on the technical aspects of it. It covers the design of high-resolution Digital Elevation Model (DEM) and the programming involved in the automated terrain correction based on this DEM.

Terrain corrections have been based on the "Hammer zones" method but rather than using a topographic map on top of which is superposed transparency with the Hammer zones, I chose to design an automated terrain calculation using any available DEM. This has two major advantages: firstly, it is re-usable for any future study that the group may want to carry out and secondly, it greatly increases the accuracy of the terrain correction as far as the resolution of the DEM is satisfactory. Indeed, the usual method with the overlay requires a manual reading and estimate of the mean elevation in every sector of the Hammer zones whereas this programme precisely averages all points of topography in the corresponding zone. The main steps in the terrain correction are given here.

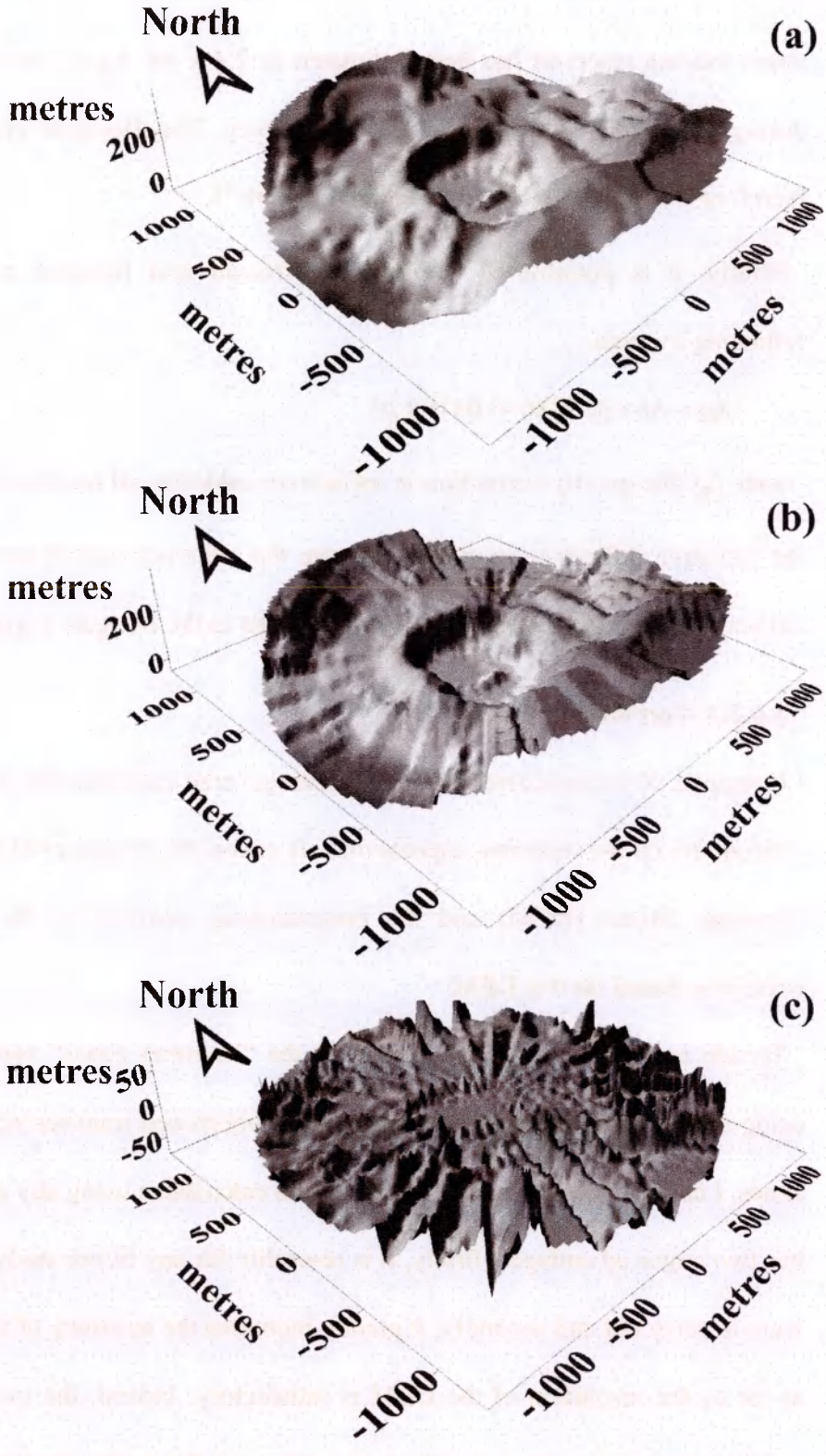

Fig 3.6. (a) Digital Elevation Model for Poás summit. (b) Hammer Digital Elevation model. (c) Difference between (a) and (b). Note that the maximum differences are far from the stations.

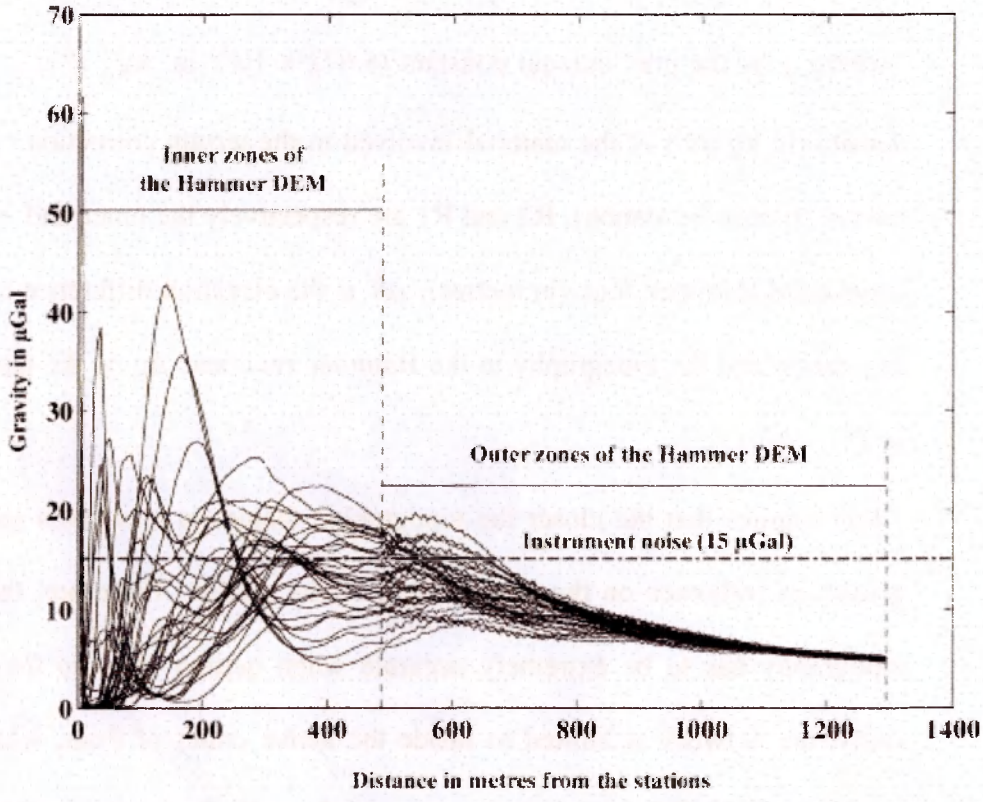

Fig 3.7. Terrain correction for each Hammer zone at every station. Each curve represents one station. Note that the terrain corrections tend to converge for all stations from about 1150 m from every station. Also note that the terrain correction becomes less smooth with distance in the outer Hammer DEM because there are fewer points per zone (i.e., lower resolution).

3.6.2.3.1. High-resolution Digital Elevation Model

The terrain correction is applied using the following formula

$$\Delta g = 2\pi\gamma\rho(R_2 - R_1 + \sqrt{R_1^2 + \Delta h^2} - \sqrt{R_2^2 + \Delta h^2}) \quad (3.3)$$

where γ is the gravitational constant (6.672 x 10^{-11} m^3 kg^{-1} s^{-2}), ρ is the estimated density (in kg m^{-3}) of the material involved in the terrain correction (i.e. density of the terrain around the station), R2 and R1 are respectively the outer and inner radius of the considered Hammer zone (in metres), Δh is the elevation difference in metres between the station and the topography in the Hammer zone and Δg is the terrain correction in m s^{-2}.

This implies that the closer the topographic feature is to a given gravity station, the greater its influence on the gravity field at that station. Therefore, the estimate of the topography has to be extremely accurate when getting close to the station. For this study, the network is limited to inside the active crater of Poás, where the only map available (1:50,000 scale) does not comply with these requirements. However, it appears accurate enough for zones outside the active crater. I therefore combined a digitised 1:50,000 topographic map with a precise DEM created using the 2670 points measured by RTK GPS during a topographic survey in February 2002. The main difficulty lies in the offset between the Costa Rican topographic map local Ocotepeque 1935 datum and the actual WGS84 (World Geodetic System 1984) datum I used for the GPS survey. Thus all digitised 1:50,000 topographic data have been corrected for this off-set by using the protocol developed by Kenneth Orvis at the Department of Geography, University of Tennesse, USA (GPS Locations and Costa Rican Topo Maps, downloadable at http://web.utk.edu/~shorn/).

For the zone under consideration (the top of Poás volcano, Costa Rica), it gives the following corrections to be added to the Ocotepeque datum data in order to obtain WGS84 type data.

- WGS84 Longitude (deg.min.sec) = Ocotepeque Longitude deg.min.(sec–7.035)
- WGS84 Latitude (deg.min.sec) = Ocotepeque Latitude deg.min.(sec – 5.410)
- WGS84 Elevation (metres) = Ocotepeque Elevation + 12.25 (metres)

As these numbers come from a manual reading of a chart, precise adjustment has been made comparing coordinates in both datum for known points both on the map and measured with GPS.

This result is a hybrid DEM with a high resolution (<3 metres) at its centre (i.e., inside the active crater, up to the rims) based only on GPS data and a lower resolution outside the active crater (20 m) based on the 1:50,000 topographic map and GPS data (**Fig 3.6a**). Both sets of X, Y, Z coordinates used for this DEM are compiled in **Appendix B**.

3.6.2.3.2. Automated terrain correction

The main idea here is to convert the topography around each station into a suitable "Hammer DEM"; in other words, we want to represent the actual topography by a series of hollow vertical cylinders (with the gravity station at the centre of their base), each divided into 64 sectors of different elevation.

The first step for each station is then the calculation of the horizontal distance and the difference in elevation between the station and every point of the topography (i.e., every point of the DEM grid). Therefore, coordinates must be represented in metres and not in decimal degrees or deg.min.sec. The following step is to sort the topographic points into Hammer cylinders and sectors and finally calculate the effect it has on gravity.

One way of checking whether the terrain correction has taken into account terrain sufficiently far away from the stations is to compare the terrain correction for every Hammer zone between stations. There must be a distance (from the stations) from which the terrain correction tends to be the same for all stations. There is thus no need to take into account terrain farther away from the stations for the terrain correction. This

is illustrated by the **Fig 3** where the terrain correction for all stations (in μGal) converges after a distance of 1200 m from the stations and thus becomes negligible (**Fig 3.7**). Another interesting point shown here is that the transition between using the inner DEM and the outer DEM for the terrain correction has a direct influence on the modelled gravity correction. Indeed, as the space between the outer DEM grid nodes is greater than that of the inner DEM grid nodes, estimates of topography will become less accurate. The code written in Matlab® for this automated terrain correction using DEMs is given in the **Appendix C** and its results are illustrated in **Fig 3.6b** and **3.6c**.

3.6.2.4. Lake correction

In order to make data reduction as simple and accurate as possible, the terrain correction does not take the lake into account. Instead, the effect of the low density of the lake (water density is only 1000 kg m^{-3}) on the gravity field at the crater floor can be assessed by modelling the gravity anomaly due to the lake with the 2.5D modelling software GravMag.

The first step is the modelling of the lake bathymetry in 3D. This was achieved using previous work from Martinez et al. (2000), as described in the first part of this chapter. From here, it is possible to draw precise polygons representing the lake for the gravity modelling. I thus drew 8 profiles through the middle of the lake and modelled the effect of a body with a 1000 kg m^{-3} density (i.e., the lake) surrounded by a substratum density of 2400 kg m^{-3} (i.e., the volcaniclastic deposits in the crater)

All modelled gravity profiles were then interpolated by krigging and the gravity anomaly due to the lake was determined for each station and added to the other corrections.

As the grid nodes of the interpolated gravity anomaly do not always coincide with the gravity station locations (the grid is produced by "krigging" and is therefore rectangular while the gravity network is not), one has to extract the data at each station from this

modelled 2D gravity field. To do this, I took the 3 closest nodes of the grid to the each station and assumed that within this small distance (a few metres), the plane (X, Y, G) passing through these 3 points and representing the interpolated gravity is linear. Then I calculated the equation of this surface and solved it for the corresponding station coordinates (i.e., X and Y). Once the gravity effect of the lake is extracted for every station, it is added to the previous corrections.

The final result is much more accurate than having to deal with a negative relief of low density to take into account in the terrain correction as the lake bottom is not a flat surface everywhere (i.e., slopes on the sides, not vertical walls).

3.6.3. Gravity modelling

The gravity modelling was carried out using the 2.5D GravMag package from the British Geological Survey. To be able to correctly localise a body responsible for a Bouguer anomaly, one needs to use data which have undergone all the corrections mentioned above. However, when it comes to model the residual gravity anomaly, the GravMag software already takes into account the free-air gradient and the Bouguer correction. This means that data for this modelling must not be corrected for these phenomena.

The first raw models were produced using conventional forward modelling, hand drawing and manually modifying the polygons shape, size (including the halfstrike), and density in the software. Once the general shape of the bodies was obtained, fine-tuning was achieved using inverse modelling over more than 450 iterations. During these iterations, the software repeatedly changed the model parameters (i.e., polygons size, shape, location and density). It then compares the modelled data with actual data and tries to achieve the best fit.

When the model was satisfactory, the modelled gravity was once again interpolated for the crater area and compared with actual data at the stations. I checked the accuracy

of the interpolation by comparing interpolated and non-interpolated data at the stations. Indeed, the "krigging" interpolation method does not keep the actual data points during the interpolation, unlike the "natural neighbourhood" method, but the latter is not the most appropriate for regularly spaced data (as for this network) Thus, I chose the "krigging" but had to check for possible inaccuracies. Finally one can produce a map of residuals between actual data and modelled gravity a shown in **Fig 3.2.**

Comment

This new high-resolution Bouguer survey and results in chapter 2 show that there were several episodes of magmatic intrusions at Poás volcano. Any future shallow intrusion will induce micro-gravity changes at the summit of Poás so continuous micro-gravity recording would be extremely useful as a monitoring tool. The next chapter investigates automated continuous gravity recording new methodologies with new logging software and data processing guidelines.

Chapter 4

Continuous micro-gravity recording

Part of this chapter has been published in Computers & Geosciences, Volume 30, Issue 5, June 2004, Pages 553-558
"g_log4PDA: an application for continuous monitoring of gravity using LaCoste&Romberg Aliod 100 systems and Palm OS® run hand-held computers"

Joachim Gottsmann, Nicolas Fournier, Hazel Rymer,
Volcano Dynamics Group, Dept of Earth Sciences The Open University, UK

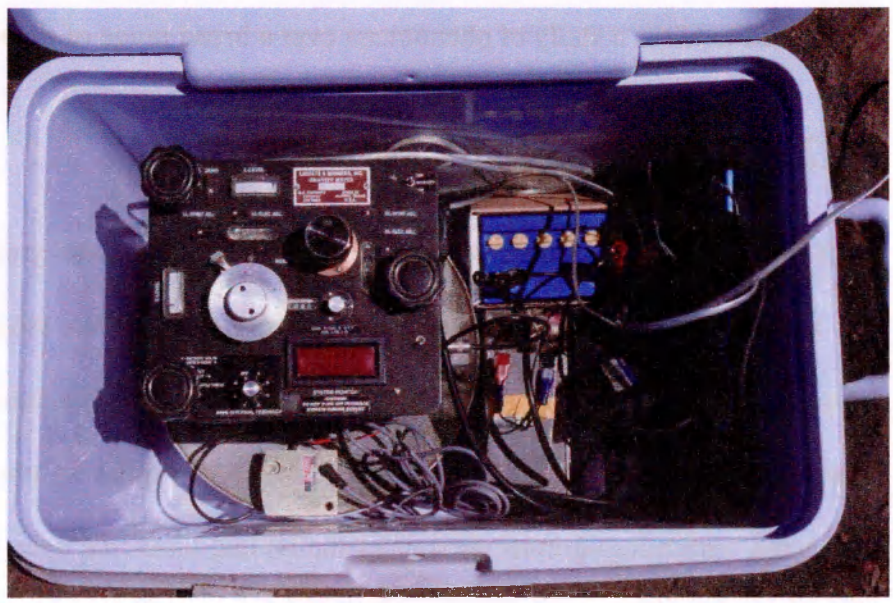

Continuous gravity and seismic recording

4.1. Introduction

Micro-gravity monitoring of volcanoes is usually performed with the aim of determining temporal variations of the gravity field. To achieve this, measurements at networks of stations are typically at intervals of week, months or years (Brown et al., 1987; Rymer et al., 2000). There are two main limitations of this approach: first of all, this method is heavy on resources such as time, person-power and money as researchers have to be physically present in the field and manually take measurements with the gravity meters. When researchers are in the field, the scope to carry out other studies is very limited. Secondly, results can only be interpreted for time scales of the same order as the frequency of repeat measurements. Thus phenomena occurring on short time scales (e.g., shallow conduit processes) are generally impossible to detect. These shortcomings led to the development of an automated, functional and easy-to-use methodology for continuous micro-gravity recording and data processing. The system is designed to allow a study of phenomena over a broad range of timescales.

4.2. Timescale of volcanic processes

In order to assess volcanic processes using continuous micro-gravity measurements, it is necessary to define the range of timescales over which these phenomena occur. Equally, when analysing continuous data, knowledge of the timescales involved can assist in the interpretation of the signal. A few examples of phenomena that can be assessed with micro-gravity as well as the typical timescale over which they occur are given here.

- Magma chamber dynamics (e.g. magma convection) may occur at scales of days to months, depending on the size and depth of the magma reservoir, the magma rheology and the eventual input of new magma from below. Thus,

injections of lighter magma in the chamber can theoretically be studied using conventional micro-gravity techniques.

- Earth tides are suspected to influence volcanic systems (Beaulieu et al., 1998). The opening/closing of shallow cracks by tidal forces could open/close pathways allowing magma to travel up and down. Such processes must clearly be studied at the timescale of Earth tides (i.e. minutes to hours; **Fig 4.1**).
- Conduit processes (e.g. puffing, Ripepe et al., 2002) can occur over timescales of seconds to hours. They typical involve temporal changes of the magma level in the conduit. If these phenomena are to be investigated, it implies a shorter sampling rate than the one we would consider to study Earth tides.

In all cases, it only feasible to study phenomena with a frequency which is less than half the sampling frequency (e.g., at a sample-per-second sampling rate, only phenomena occurring at periods greater than 2 seconds are well resolved). In other words, only phenomena with an event frequency below the Nyquist frequency of our continuous recording will be observable.

4.3. Technology

Continuous micro-gravity monitoring involves the use of appropriate technology, both hardware and software wise. The work reported here was carried out using Lacoste & Romberg gravity meters D41 and D61. The instruments have been fitted with Aliod digital feedback and data recording involved the development of new software.

4.3.1. Instrument characteristics

Lacoste & Romberg gravity meters have been extensively used for decades in volcanology (Brown et al., 1987; Rymer et al., 1994, 2000) but the Aliod feedback system has only been available since 2000. This modification provides an automatic beam nulling system (Lacoste & Romberg, 2000) that streams gravity readings at a

frequency of 2 Hz in ASCII code via an external RS-232 port. The data stream may be accessed using computers capable of serial port communication.

The system is based on a Capacitance Beam Indicator (CPI; **Fig 4.2**). It is a capacitance bridge with a capacitance plate on the beam and a fixed plate above the beam and another fixed plate below the beam. This system is sometime referred to as "electronic readout". The capacitance bridge senses the position of the meter's beam and reports this to a galvanometer or liquid crystal display (LCD) on the meter lid. It has several advantages:

- Operator fatigue is reduced since the microscope need only be used when checking or adjusting the CPI.
- The galvanometer can be set to have greater sensitivity than the optical system, allowing more accurate reading.
- An electric outlet is provided for the signal that drives the galvanometer. A recorder can be driven by this signal to demonstrate earth tides and long period seismic waves.
- An external RC filter and voltage indicator (galvo or digital multimeter) can be used to read the meter when ground vibration is troublesome.

Under normal operation the gravity meter mechanically balances the force of gravity on the mass of the beam by adjusting the upward force of the main spring. Another method of nulling the forces on the mass is available. The majority of the gravitational force may be balanced by the main spring. That mechanical force can then be held constant by clamping the nulling dial and the fine adjustment of the nulling accomplished with electrostatic force on a capacitance plate affixed to the meter's mass.

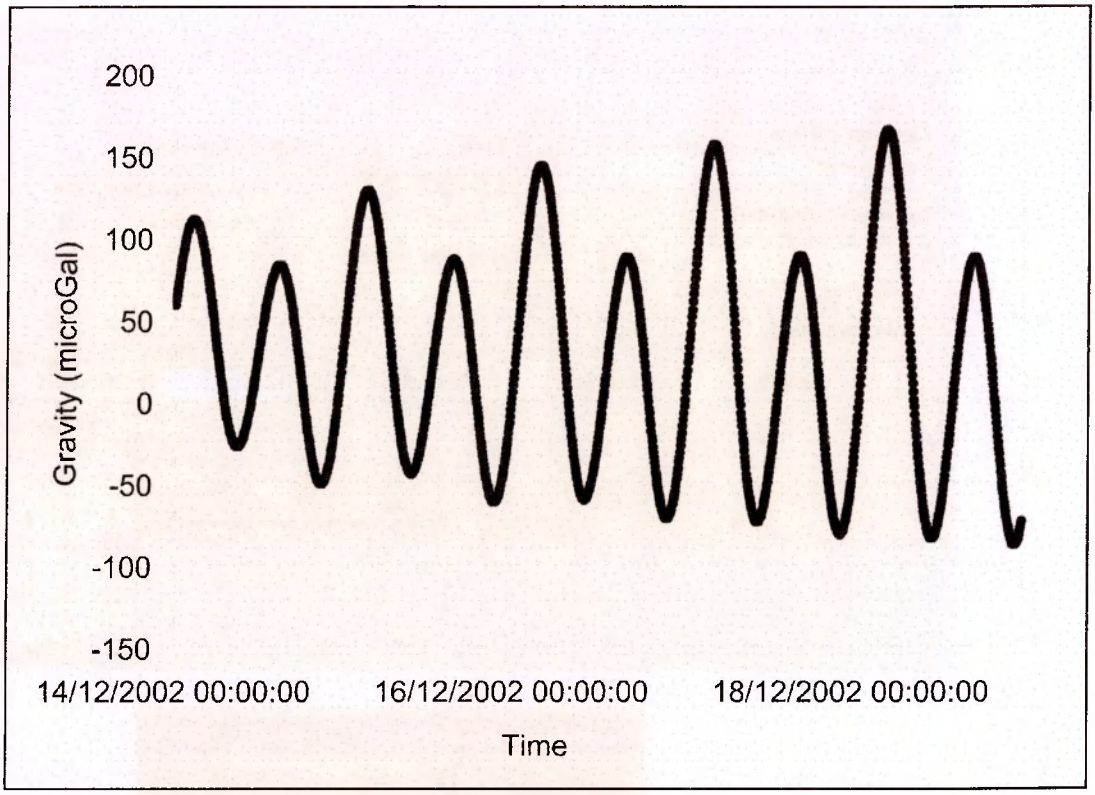

Fig 4.1. Earth Tides gravity correction calculated using TideCalc software. This is added to raw gravity data. Example here for coordinates of Masaya volcano, Nicaragua, from 14/12/2002 to 19/12/2002.

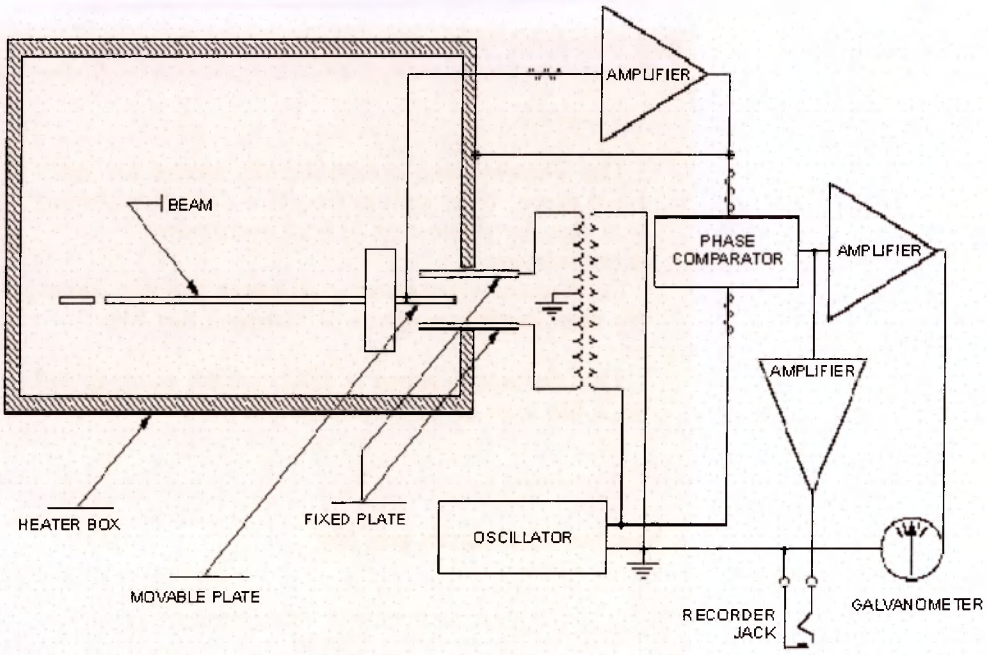

Fig 4.2. Scheme of the Capacitance Beam Indicator for Lacoste & Romberg D-meters.

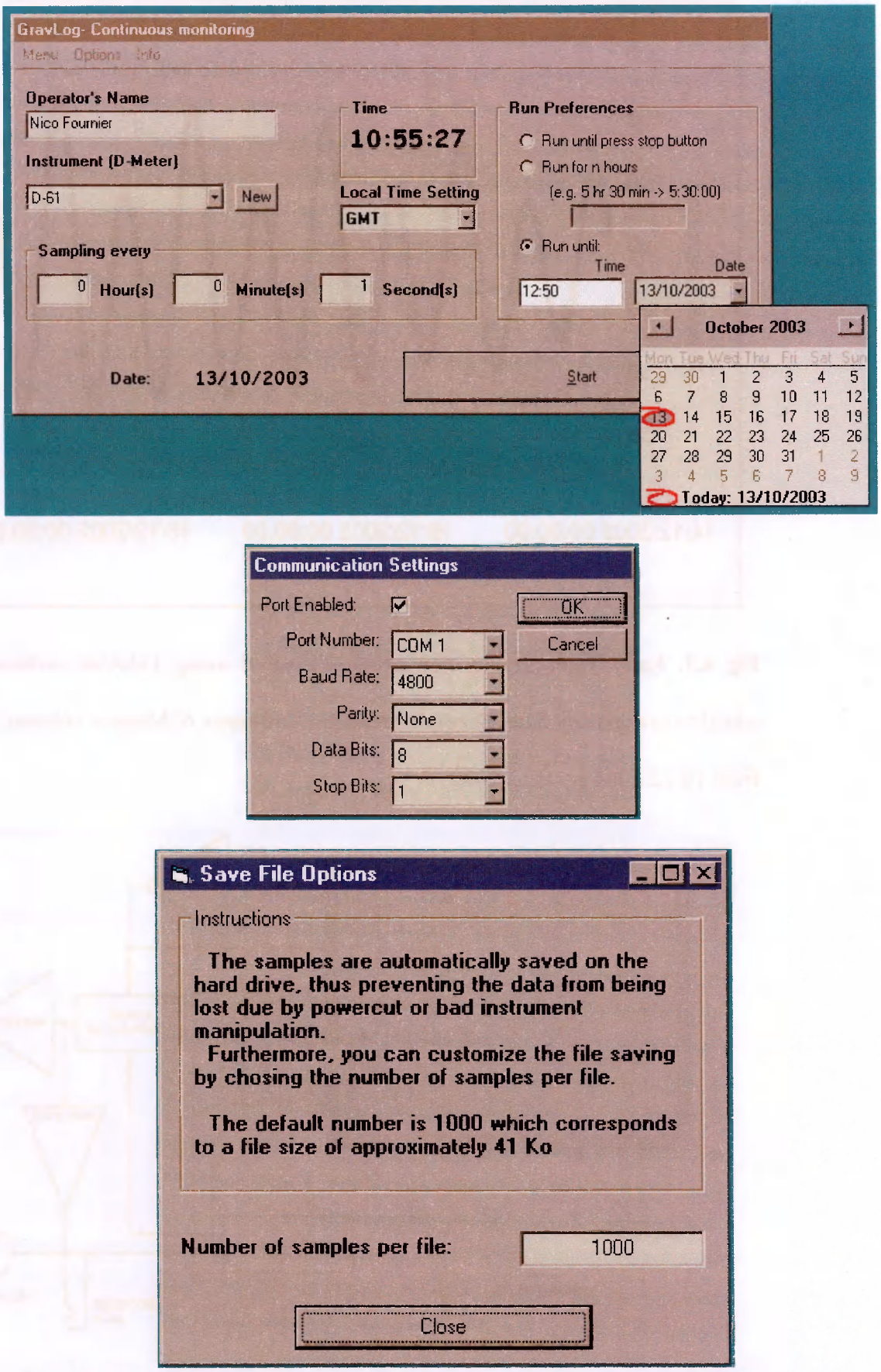

Fig 4.3. Screen shots of g_log software. *Top*: Main form where the user sets up the sampling rate, the instrument used, length of the recording (if desired). *Middle*: Communication settings form. *Bottom*: Save file options form.

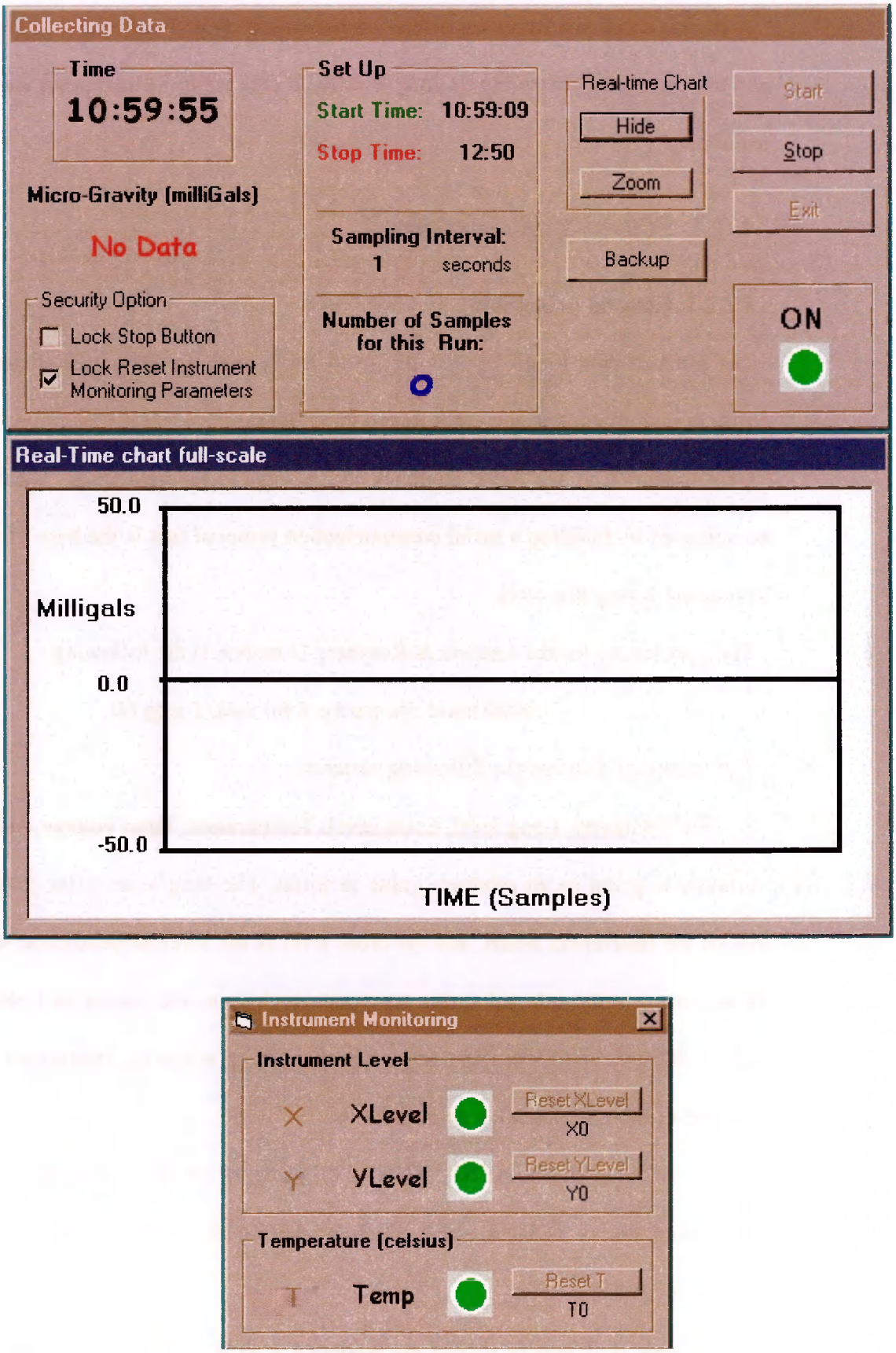

Fig 4.4. Screen shots of g_log software. *Top*: Logging form with real time graph (here, no data are recorded). *Bottom*: Instrument monitoring form; green lights indicate good instrument stability whereas red lights indicate off-levelling or internal temperature problems.

A digital electrostatic nuller offers long-term stability, flexibility in selecting filters and the capability of sending its data to a digital data logger or computer via its RS232C serial port.

4.3.2. Software development

4.3.2.1. General principles

The aims of data logging software are to firstly pick up the signal streamed out the emitting instrument and secondly record these data.

Data streams from the Aliod feedback stream via a serial connection. The first aim can be achieved by building a serial communication protocol that is the basc of all software developed during this work.

The port setting for the Lacoste & Romberg D-meters is the following

4800 baud, No parity, 8 bit data, 1 stop bit.

The stream of data has the following structure:

<SYN>Gravity, Long level, Cross level, Temperature, Input voltage, <CR><LF>

Gravity is given as an arbitrary value in mGal. The long level is the level along the axis of the instrument beam, and the cross level is the level perpendicular to the beam. Temperature is the internal meter temperature close to the sensor in Celsius and the input voltage of the instrument (e.g., battery voltage when the instrument is powered with one or more batteries) is given in volts.

The SYNC character is ACSII "SYN" 22 decimal or 16 Hex, not printable as the two END characters are <CR> + <LF> which are ASCII 13 decimal (or D Hex) + ASCII 10 decimal (or A hex).

For Lacoste & Romberg meters not equipped with liquid electronic levels, the values for long level and cross level are arbitrary and meaningless (i.e., not related to the actual instrument levels). It is therefore not possible to monitor the levelling for such instruments.

The data stream has then to be stored as well as the time (second precision) at which it has been recorded. As the output frequency from the meter is 2Hz,this should be the maximum sampling frequency achieved. However, to isolate occasional irregularities in the data stream, and hence the loss of data, the maximum sampling frequency used here is 1Hz, with a check for errors in the stream.

Serial port communication software was developed here to allow the user to automatically log data from Lacoste & Romberg gravity-meters with Alliod 100 or Alliod 100x feedback installed. As the software could be used by a large number of users, it has been designed to be as user-friendly and reliable as possible. Two families of software have been designed for logging respectively with PCs equipped with usual Windows® platform and Palm® handheld computers (PDA).

MICROSOFT® VISUAL BASIC® appeared to be the ideal programming environment for the required task as it allows for creation of Windows®-like and easy-to-use applications. Indeed, VISUAL BASIC® enables engaging GUI (Graphical User Interface) coding which is can be controlled by the user without the need of any knowledge of coding.

The output format (i.e., Comma Separated Values (CSV)) has been chosen for both families of applications in order for the data to be easily imported into data processing applications such as MICROSOFT® EXCEL® or MATLAB®. It includes the data stream plus the date and time.

4.3.2.2. PC platforms

Two main applications have been developed: g_logbasic and g_log.

- g_logbasic is a simple one-window application for use with low RAM and processing capabilities PCs. It is a "black box" logging the data stream at 1 Hz sampling frequency.

- g_log is a more complete application for use with newer computers. It has additional features compared with the g_logbasic program. Indeed, it offers a wide range of user-defined sampling rates (i.e., from 1 sample per second (sps) to user-defined sampling rate) as well as visual instrument parameters monitoring (i.e., internal temperature, long and cross levels) and it allows real-time visualization of the data. Additional features such as port communication setting and preferences for data saving are also available. The software presents several GUI depending on what options are selected. The main form (i.e., GUI) is loaded when starting the application. It is the main interface where the user chooses the settings. Once the logging has started, another form appears and shows the last measurement as well as the amount of data collected. One additional form opens and shows visual warning when instrument parameters such as internal temperature or the battery voltage change. Finally an optional form is available for real-time graphics of the data series. Screen shots of the major forms are illustrated in **Fig 4.3 and 4.4**.

4.3.2.3. Palm® handheld computers: g_log4PDA

g_log4PDA is written in MICROSOFT® VISUAL BASIC® using the commercial add-in software package MobileVBLite™ offered by APPFORGE™ which enables Graphical User Interface coding in VISUAL BASIC® for Palm OS® computer platforms. The software is designed to be operated on a Palm OS® (Version 3.0 or higher) run Personal Digital Assistant (PDA).

We have chosen coding for PDA and Palm OS® for two main reasons:

- Lacoste & Romberg's Aliod 100 systems are provided with a Palm OS® run PDA, thus any Lacoste & Romberg user may directly employ our software for data retrieval,

- continuous data retrieval onto a PDA in the field uses less electrical power consuming than onto a desktop or laptop reducing the need and costs for extensive electrical power supply,

Moreover, PDAs are less costly than laptop or desktop computers installed at continuously operating gravity stations.

g_log4PDA (Version 1.0) consists of four different forms: a start-up form ('g_log4PDA'), a form to access and read from the Palm OS® 'memo' database ('main'), a form that creates a new entry into the database ('memo'), and a form that provides information about the application itself ('about').

As the memory capabilities of Palm OS® run handheld computer are limited, the maximum sampling rate is 1 sample per minute (the minimum sampling rate being 1 sample per 12 hours).

Recorded data can subsequently be downloaded to PCs using the conventional PDA connection protocol and software provided with the PDA.

4.3.3. What software for what use?

The physical processes of interest will determine the computer and software to be used. If a sampling rate greater than 1 sample per minute is desired, one must use one of the PC based software whereas the PDA software is perfectly suitable for sampling rate below 1 sample per minute.

Power consumption in the field is also an important factor in deciding the recording medium. Although a Lacoste & Romberg D-meter can run one day on a 12V 7.2 Ah gel-cell battery, the PC used for data logging is much more power consuming. Therefore, unless several gel-cell batteries are connected in parallel or solar panels or other power supplies are available, the handheld computer – much less power demanding than a PC – is the preferred logging medium. Key parameters to make the choice between logging media and software are summarised in **Fig 4.5**.

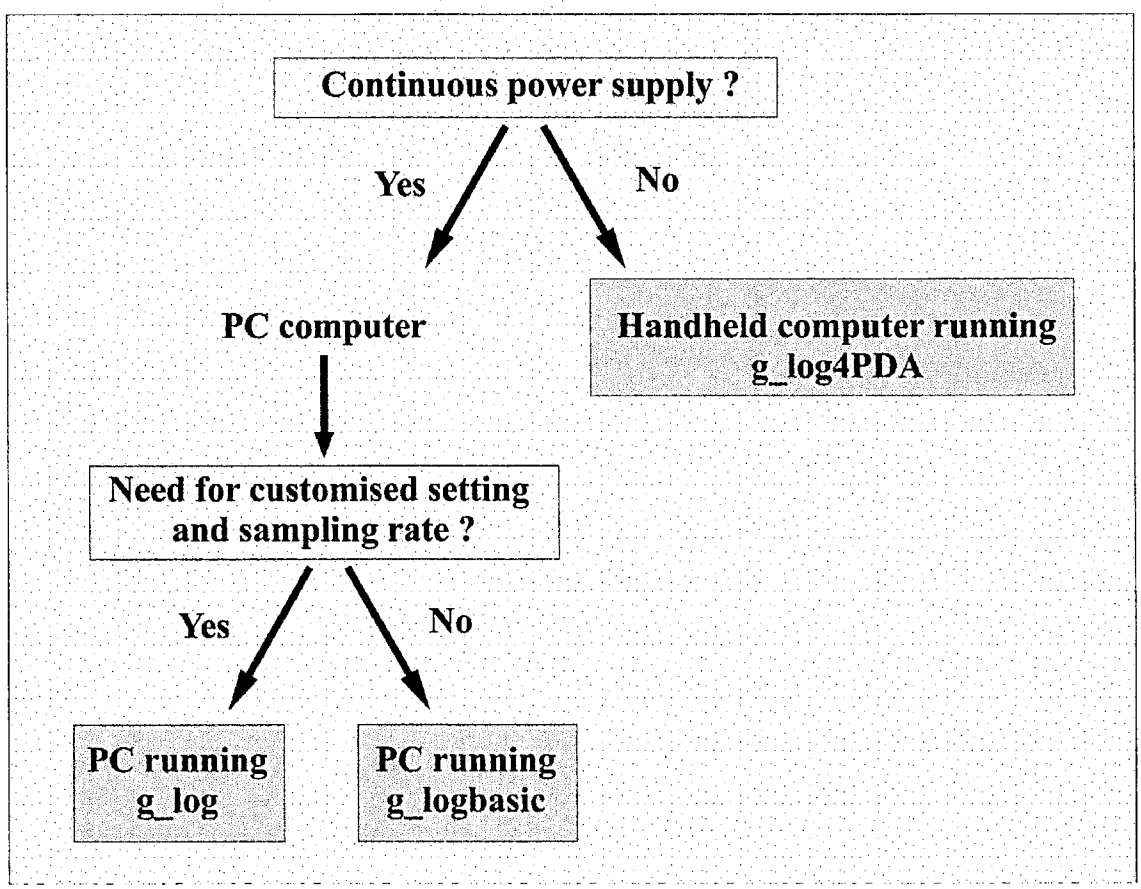

Fig 4.5. Flow diagram for the choice of the appropriate logging software in the g_log family.

4.3.4. Time stamp

Intervals between the measurements during the continuous recording are obviously based on a clock. In the case of this work, it is based on the computer clocks, which raises the following question: is the time stamp accurate? Indeed, computer clocks are generally not accurate and, for instance, a drift of a few seconds every few hours may be expected for computers with 500 MHz processors. This is worse for old computers with lower speed processors. It therefore raises up two major issues. Firstly, a drifting computer clock induces a non-linearity of the time stamp, which can become a real handicap when assessing phenomena with an event period of a few seconds. Secondly, if micro-gravity continuous data are to be coupled with continuous recording for other techniques (e.g., seismic, thermal data), the overall data set must have a correct and common time stamp.

A low-tech solution to this problem is a regular manual computer clock adjustment. A better option is to have the computer clock continuously reset by the GPS clock. Thus, one can connect the computer to both the gravity meter and a GPS and run a routine that automatically sets up the computer clock by the GPS clock, for instance every minute. This will insure a proper time stamp and rigorous comparison of gravity data with other data sets. Another option is to get the "radio clock" signal from a local atomic clock but this has two major disadvantages: first of all the radio signal has to be post-processed, which is not straightforward. Secondly, the radio signal is transmitted with a limited radius (e.g., 1500 km radius for the Mainflingen atomic clock in Germany, at a frequency of 77.5 kHz). It means that not all volcanoes are within transmission distance from the few atomic clocks available in the world. Using GPS clock (e.g., from a handheld GPS) is thus much more straightforward and suitable almost everywhere around the globe.

4.4. Data processing

Once the time series has been recorded, numerous options are available for the data processing. These are listed below.

4.4.1. Adjustment of the time stamp: filling the gaps

The g_log software family is based on timer events relying on the computer clock. Inaccuracies of the computer clock and data stream induce some irregular time stamps (e.g., for a sampling rate of 1 sps, some gaps of 2 seconds may appear). If we want to perform spectral analysis, we need a regular time stamp so we must insert missing data.

A simple routine written in MATLAB® can easily perform this task (code given in Appendix D). Missing data are interpolated by comparison with the surrounding data. Thus, we check the time stamp between 2 points and if it exceeds the selected time stamp (i.e., 2 or 3 seconds instead of the expected 1 second) the routine averages the gravity data between the previous data point and the following one.

4.4.2. Tide correction

An automated correction for the effects of Earth Tides is necessary when dealing with thousands of data points. We use the TideCalc software (Brouke et al., 1972) to generate ASCII files of gravity correction factors for given dates that are to be added to the actual data. Afterwards, MATLAB® routines (cf. Appendix D) can be used to import both gravity data and Earth tides correction and make the correction automatically. Please note here that data set time must be converted to GMT to fit with Earth Tide correction calculation with TideCalc.

4.4.3. Frequency analysis

Continuous gravity data must be analysed as time series. Interpretation of the data remains ambiguous if the analysis is restricted to the time domain. Indeed, a given

gravity signal might be the result of the convolution of several periodic or non-periodic events. While some of these events are known and can be calculated (e.g., Earth Tides), many others remain hidden in the overall signal. It is therefore appropriate to carry out a frequency analysis to try to determine the diverse phenomena affecting the gravity.

Fast Fourier Transform (FFT) and conventional power spectrum give density plots of the signal over a range of frequencies. For an arbitrary function $f(t)$, a set of harmonic terms exists and can be represented as follows (Thorne & Wallace, 1995)

$$f(t) = \frac{1}{2\pi} \int_{-\infty}^{\infty} F(\omega) e^{i\omega t} d\omega \tag{4.1}$$

where

$$F(\omega) = \int_{-\infty}^{\infty} f(t) e^{-i\omega t} dt \tag{4.2}$$

with ω the angular frequency, t the time and $i = \sqrt{-1}$.

Equation (4.1) illustrates that the convolution of several harmonic functions can simply be represented as a sum of monochromatic functions in the frequency domain. An important point here is that while this is a powerful tool for treating convolution of periodic functions, it remains inappropriate when dealing with non-periodic signals.

For this work, data processing using power spectrum has been tried for various sets of continuous gravity data recorded in the lab and in the field at Masaya (Nicaragua), Poás (Costa Rica) and Stromboli (Italy) volcanoes. Power spectrum is a density plot of the time series data in the frequency domain. It has no unit on the vertical axis and the range of frequencies is represented on the horizontal axis. The signal is truncated at its right end for it is meaningless to represent data above the Nyquist frequency.

The mathematical treatment for power spectrum analysis was achieved using coding with MATLAB®, using the integrated FFT function (cf. Appendix D).

4.5. Preliminary results

Power spectrum of time series data was performed for both lab and field data for which we chose to record gravity at the maximum sampling rate allowed by the g_log software (1 Hz), in order, for this first step, to compare data with the same intervals. Consequently, the Nyquist frequency is 0.5 Hz, which means that we will only be able to assess phenomena with a periodicity of 2 seconds and more. Data shown here have all been recorded with the same instrument (Lacoste & Romberg D-61) to avoid instrumental effect. They have not been corrected for Earth tides, as their visualisation can be useful when intending to spot any possible relationship between volcanic processes and Earth deformation.

4.5.1. Lab experiment

Gravity has been recorded continuously at the Open University at different stages of the project to test the logging softwares. Ultimately, the goal has been to determine the most stable place available, and leave the instrument running for several hours. The D-61 gravity meter was thus set up on a concrete platform, well isolated from local vibrations (i.e. not influenced by people walking around, machines running nearby), and left running for several hours. During the run, the atmospheric temperature and pressure were relatively stable and the room remained locked at all time to avoid ground vibrations and and suddent pressure changes. Here we show preliminary results from this ultimate experiment.

This first example shows continuous gravity data recorded during slightly more than 19 hours and not corrected for the Earth Tides (**Fig 4.6**). The time series thus shows the typical periodic oscillations due to this phenomenon (**Fig 4.6 top**). These data were supposed to be recorded in a fairly stable site, which means that gravity changes through time should only be due to Earth Tides and possible large-scale seismic events.

Stability of the signal is relatively good, as the instrument noise does not exceed 10 μGal. One interesting point here is that it seems that the instrument noise is the greater when the gravity gradient $\frac{\partial g}{\partial t}$ through time is the lowest.

When looking at the power spectrum of the same sequence of data, in a log(amplitude) vs. log(frequency) we can observe that amplitude of gravity variations clearly drop down for frequencies between 0.001 and 0.5 Hz (**Fig 4.6 middle**). If we consider that the observed signal can be regarded as a convolution of periodic gravity changes, it means that gravity changes occurring at periods between 1000 sec (~16 min 40 sec) and 2 sec are minimal and actually not well defined.

A closer look at the power spectrum, but this time with non-logarithmic axis, shows an interesting feature of the signal (**Fig 4.6 bottom**). Indeed we can observe one distinct peak in the power spectrum at a frequency of 0.04 Hz. In other words, a distinct periodic signal (period of 25 sec) contributes to the overall gravity signal during this lab recording. As the Earth Tides induced gravity changes have a period much greater than a few seconds, it means that this signal relates to another phenomenon. Unfortunately, the lack of seismic data prevents isolation of the source of this signal, but we can still state that despite the small gravity variations during the logging (other than Earth Tides), the signal can hide some interesting features. Another interesting point is the occurrence of a cyclic increase of the amplitude with peaks at respectively 0.220, 0.280, 0.337 and 0.395 Hz. Again we cannot determine the origin of this signal but it shows that continuous gravity can show potentially interesting information despite small gravity changes.

There are two major possibilities for the origin of these 5 peaks. The first one is that they correspond directly to an external phenomenon like ground vibration. The second possibility is that we are here assessing the instrument noise and its treatment (e.g., damping). As there is no linear relationship between the peaks frequencies, we are

obviously not here in presence of harmonics of a vibration at a typical frequency. The question that follows is: Is the instrument noise only mechanical (i.e., related to the mass oscillation) or does at least part of it come from the analogue to digital (A/D) conversion and the damping system? The lack of available information about the instrument damping system and A/D conversion does not allow us to make the discrimination between these two possibilities.

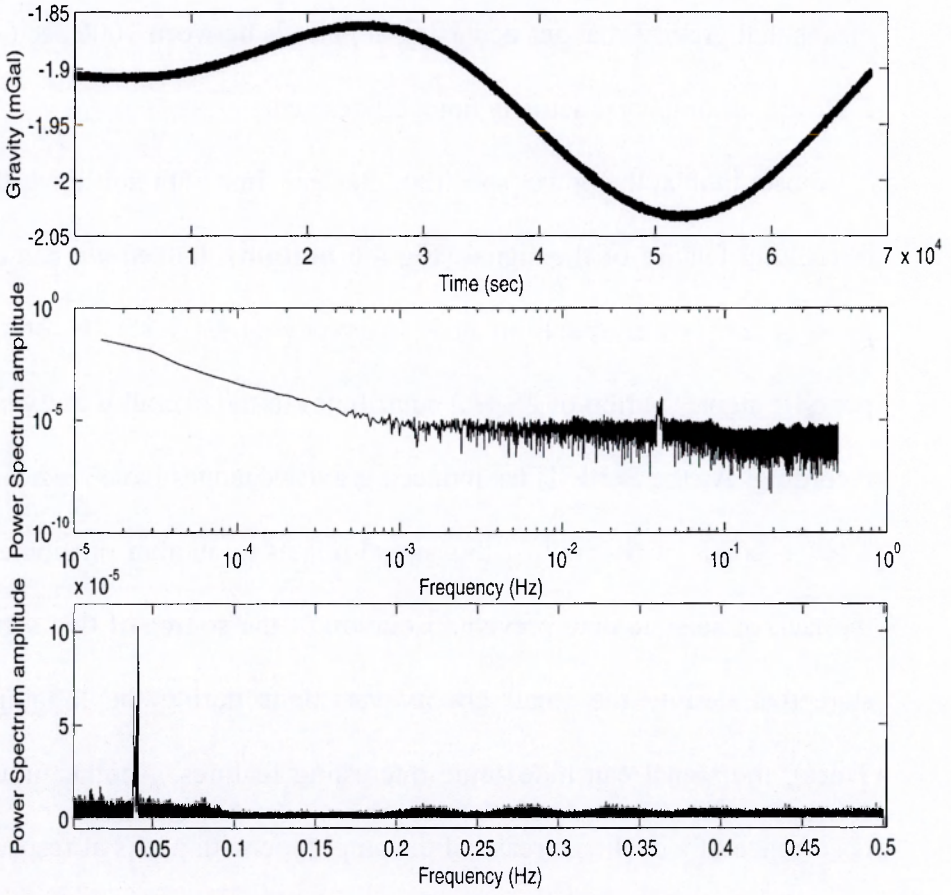

Fig 4.6. Time series analysis of continuous gravity recorded at **The Open University on the 01/06/2003**. *Top*: Gravity changes through time, not corrected for Earth tides. *Middle*: Power Spectrum of the same time series in logarithmic scale. *Bottom*: Power spectrum of the same time series in linear scale; Frequencies near zero are ignored as subject to alias. Time zero represents the beginning of the recording.

4.5.2. Masaya volcano (Nicaragua)

The D-61 gravity meter was installed in a cave in Nindiri lava lake (**Fig 4.7**) in order to be as close as possible to the magmatic processes occurring at Masaya. The lack of available power source only allowed recording for a few hours in a row (6 h 25 min for this example), coupling the 12 V batteries to power both the D-meter and the computer for logging.

The time series (**Fig 4.8 top**) provides valuable information. Indeed, apart from the cyclic gravity changes due to the Earth Tides, gravity changes with an amplitude of about 200 μGal occur frequently, the background noise being of about 70 μGal (against 10-20 μGal usually, further away from the active vent). As the conditions of recording are similar to those of the usual gravity survey at this volcano (actually even more protected from the wind) it raises a critical question of the validity of the gravity data collected at Nindiri lava lake for the conventional micro-gravity monitoring. Indeed, while manual gravity measurements typically last 2-5 minutes (i.e., 120-300 sec), continuous recording shows here gravity variations of up to 200 μGal in time laps of no more than 30 sec, some of them peaking during up to one minute. With such conditions it is obviously extremely difficult to get stable data during a conventional micro-gravity survey and explains the very unstable reading observed during the attempt of Bouguer survey at Nindiri frozeon lava lake in 2002.

A critical conclusion here is that gravity changes at Masaya volcano cannot be assessed too close to magmatic processes (i.e., at the bottom of Nindiri lava lake). Obviously (and ideally), any attempt at carrying out a micro-gravity survey close to the centre of activity at any volcano should be preceded by a continuous gravity study in order to assess the stability of every station location. Conventional measurements and previous attempts to continuously record gravity at the summit cark park stations do not show short timescale gravity changes so data collected in the past at the summit are not

to be called into question. Station stability is site dependent and the bottom of Nindiri lava lake, where ground vibration due to magmatic puffing makes the instrument unstable, is unsuitable for gravity measurements. We can note here that reading stability may also be time dependent. Indeed, an increase of seismic activity – due, for instance, to a more vigiorous volcanic activity- may induce reading instability at stations which were previously suitable for gravity measurements. Station stability must therefore be assessed for every field campaign.

Power spectrum analysis of the same data set (**Fig 4.8 middle**) does not tell us very much in terms of signal periodicity. A more detailed investigation of the spectrum (**Fig 4.8 bottom**) shows however similar low amplitude cyclic patterns to those observed in the lab experiment. The main difference between figures 3 and 5 is that the data in Fig 5 are not surprisingly noisier.

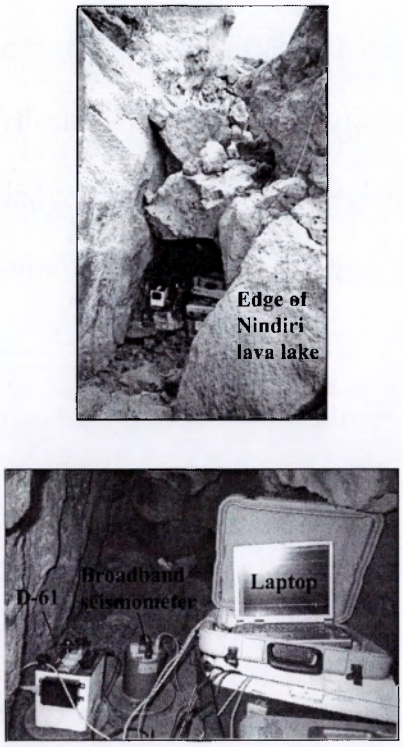

Fig 4.7. Instrumental set-up on the floor Nindiri lava lake, at **Masaya volcano, Nicaragua**. *Top*: General view of the site, taken from the lava lake. *Bottom*: Closer view of the installation. From left to right: D-41 gravity meter, Broadband 3-component seismometer (6-T seismometer from Guralp®), Laptop for data logging.

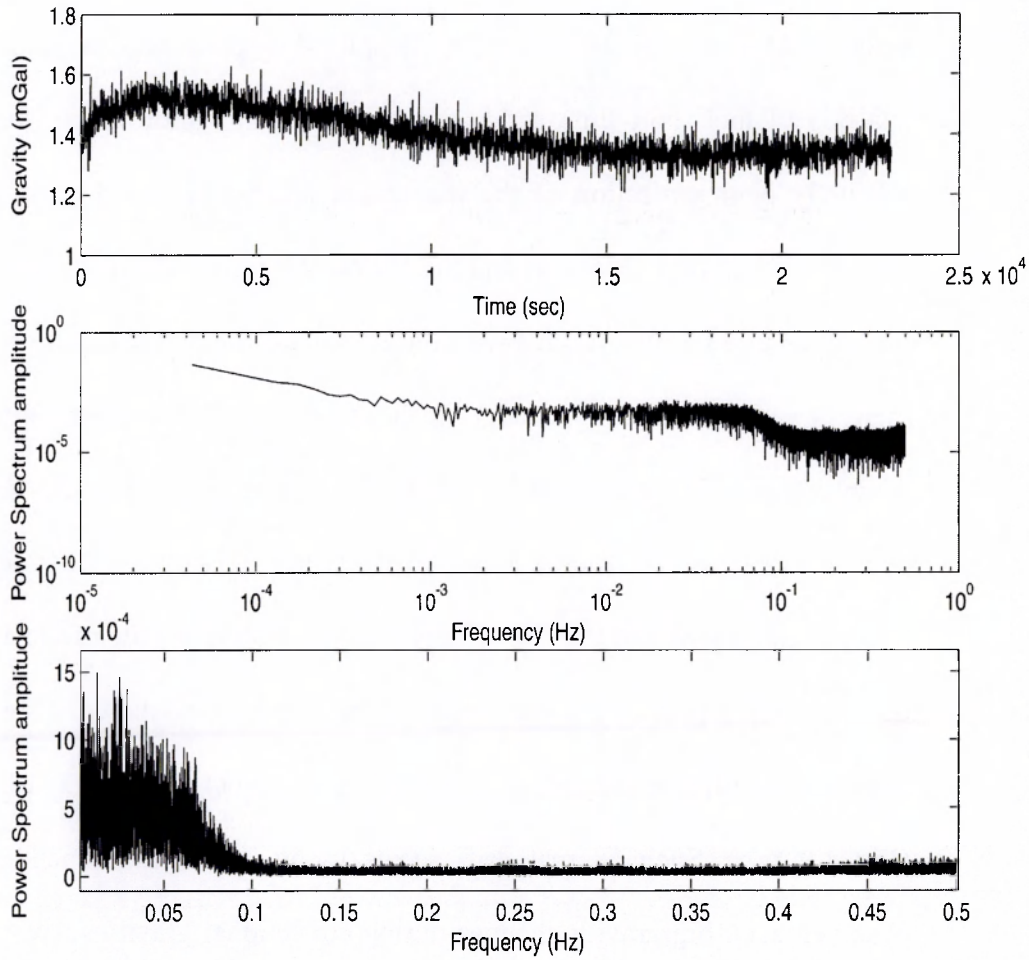

Fig 4.8. Time series analysis of continuous gravity recorded at **Masaya volcano, Nicaragua, on the 14/12/2002**. *Top*: Gravity changes through time. *Middle*: Power Spectrum of the same time series in logarithmic scale. *Bottom*: Power spectrum of the same time series in linear scale; Frequencies near zero are ignored as subject to alias. Time zero represents the beginning of the recording.

4.5.3. Poás volcano (Costa Rica)

The D-61 gravity-meter was left running for almost 3 hours at the bottom of Poás crater, in a rudimentary stone frame to protect it from the wind. The instrument was left running for one hour before starting the logging in an attempt to stabilize it as usual when making continuous recording. Despite the small amount of data available, the analysis of this short time series gives some useful information. Firstly, despite the relatively poor protection of the instrument against the wind (e.g., compared to the experiment setting at Masaya) and the surrounding hydrothermal activity (i.e., high flux fumaroles at less than 100 m) we noticed a small instrument noise (~10 μGal). Thus, there is very little gravity change in the high-frequency domain (**Fig 4.9 bottom**). It follows that Poás crater floor is suitable for a relatively stable site for detailed micro-gravity survey unlike Nindiri lava lake at Masaya, hence the successful high-resolution Bouguer survey we did there (cf Chapter 3). Secondly, in spite of the attempt of leaving the instrument to stabilize for an hour, the time series shows a significant negative instrumental drift of the data (- 820 μGal) that cannot be explained by the Earth tides (**Fig 4.9 top**). Such a great drift seems to be instrument dependent for we never observed such big gravity changes during convetional gravity survey at the bottom of Poás crater. Therefore, gravity data from conventional gravity survey (using a G-meter), are not to be called into question. Indeed, G-meters are much less sensitive to instrumental drift and what counts in terms of station reliability is the noise amplitude (typically due to ground vibration or wind). Regarding the D-meter's drift at Poás, the lack of continuous data unfortunately does not allow us to draw conclusions. Concerning the site stability, it seems that shallow magmatic activity (e.g., Masaya) has a bigger influence on the instrument stability than shallow hydrothermal processes (e.g., Poás). Care must be taken though as transmission of seismic waves from the source (e.g., magmatic or hydrothermal processes) to the surface is highly dependent on the

nature of the substratum. For instance ash deposit will tend to dampen the high frequencies while cold lava body will transmit them well.

Power spectrum analysis does not give much information apart from the almost straight spectrum when plotting amplitude versus frequency on logarithmic scale (**Fig 4.9 middle**). Indeed most of the spectra were so far "knee shaped" whereas this one is rather straight with a negative overall slope. We can also note the relatively periodic peaks of amplitude for frequencies between 0.11 and 0.19 Hz (**Fig 4.9 bottom and Fig 4.10**).

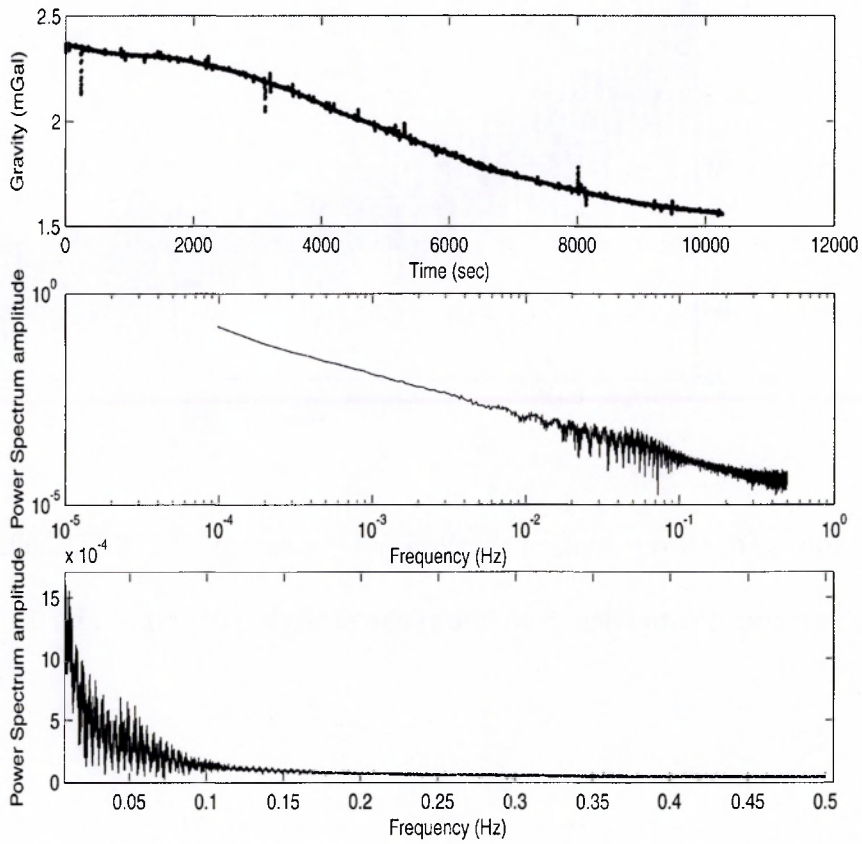

Fig 4.9. Time series analysis of continuous gravity recorded at **Poás volcano, Costa Rica, on the 20/12/2002**. *Top*: Gravity changes through time. *Middle*: Power Spectrum of the same time series in logarithmic scale. *Bottom*: Power spectrum of the same time series in linear scale; Frequencies near zero are ignored as subject to alias. Time zero represents the beginning of the recording.

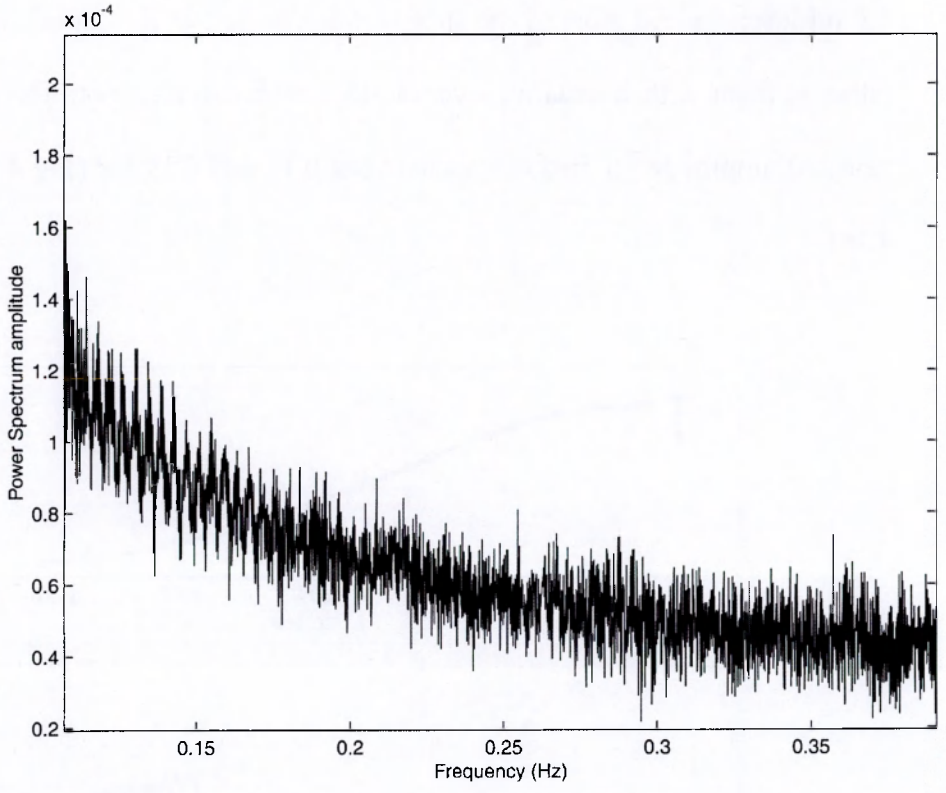

Fig 4.10. Closer look at the Power Spectrum of the **20/12/2002 data set from Poás volcano, Costa Rica.** Note the cyclic peaks between 0.11 and 0.19 Hz.

4.5.4. Stromboli volcano (Italy)

Continuous gravity data were recorded at Stromboli volcano in May 2002 during a multidisciplinary experiment involving The Open University, the Universities of Florence (Italy) and Hawaii (USA) and the Alaska Volcano Observatory (USA). The D-61 gravity meter was installed in a concrete bunker at the top of the volcano while the D-41 was logging at the observatory. The data presented here were all collected on 20/05/2002 on Stromboli.

The most characteristic feature of this data set is the succession of sharp peaks of gravity (sharp oscillation with generally a positive onset) all along the time series (**Fig 4.11 top**). They have an average amplitude of 100 μGal and usually last for ~30-40 sec (**Fig 4.12**). In order to determine the source of these peaks, one must first understand the significance of the recorded signal. Indeed, such reversible gravity changes with an amplitude of 100 μGal occurring in only 30 to 40 sec are difficult to explain with mass changes underground, especially because the instrument was obviously not located right above the vent but off-centred on a relatively stable site (i.e., no great change of mass expected under the station). Another possibility for the source of these gravity peaks would be ground deformation. However, with an average free-air gradient of 0.3086 mGal m^{-1}, it would mean ground vertical displacement, up and down, of ~ 32 cm in less than a minute, in order to account for the 100 μGal average gravity peaks amplitude. The lack of traces from such ground deformation on the nearby installations (e.g., cracks, displacement of the gravity meter) obviously dismisses this hypothesis. Therefore the gravity changes during these peaks must not be interpreted in terms of proper gravity signal, but rather in terms of movement of the internal instrument mass, which was "translated" meaninglessly in mGal. A gravity meter is similar to a broadband seismometer as it is based on an inertial pendulum system. When its mass is steady, the gravity meter can record small gravity changes. However, when strong and

sudden movements of the instrument mass overwhelm the damping system, it no longer acts as a gravity meter but as a proper seismometer and records ground motion or velocity. Coupling of gravity data with seismic data shows that the gravity peaks are actually identical to the signal recorded by the broadband seismic vertical component. Seismic data were unfortunately not available for use at the time this thesis was printed but they may be available by contacting Maurizio Ripepe at the Univ. of Florence, Italy.

The power spectrum analysis (**Fig 4.11 middle and bottom**) shows that the gravity signal is dominated by frequencies essentially lower than 0.12 Hz (i.e., periodic event with period greater than 8 sec). Oscillations of the spectrum between 0.12 and 0.5 Hz are though still noticeable. Again, the lack of direct relationship between these peaks frequencies shows that these are not harmonics.

The greater amount of data available, the better from a statistical point of view. However, the analysis of time series much longer than the expected period of a studied phenomenon can actually increase the noise in the lower frequency range of the power spectrum, thus hiding smaller peaks of interest. As the occurrence of the peaks so far observed in the gravity signal is in the order of a few minutes, we chose to study a shorter time slot of less than 4 hours, at the same sampling rate of 1 sps (**Fig 4.13 top**). The corresponding power spectrum (**Fig 4.13 middle and bottom**) thus shows features that were hidden in the power spectrum of the whole data set (**Fig 4.11 bottom**). Indeed, if we observe the same general pattern in the spectrum (i.e., frequencies lower than 0.1 Hz dominate), it also shows that the maximum amplitude in the lower frequency part of the spectrum corresponds to frequencies around 0.03 Hz. In other words, for the 4 hours considered, the gravity signal is dominated by periodic events with a period of about 20 sec. This is even clearer if we further reduce the studied time slot (e.g., 17 min 30 sec, **Fig 4.14**). The 0.03 Hz frequency fits rather well with the frequency of the observed peaks.

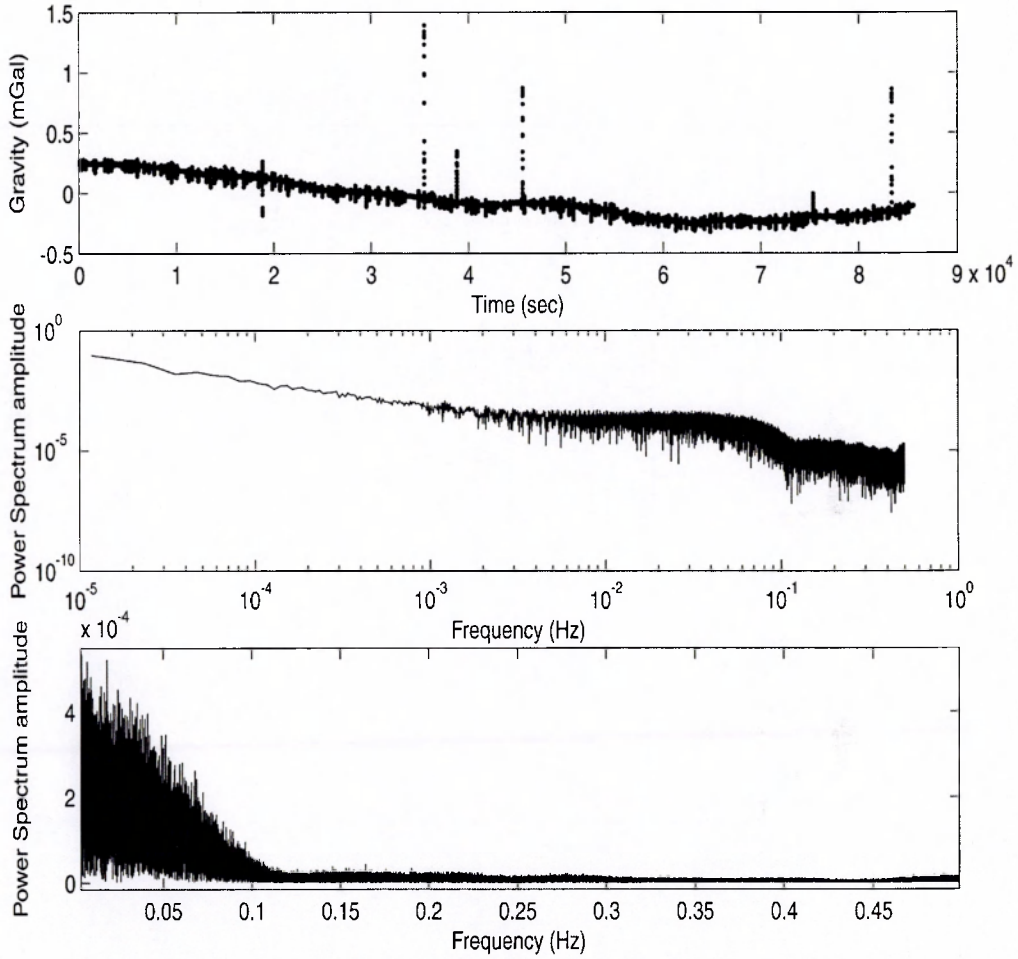

Fig 4.11. Time series analysis of continuous gravity recorded at the **top of Stromboli volcano, Italy, on the 20/05/2002**. *Top*: Gravity changes through time. *Middle*: Power Spectrum of the same time series in logarithmic scale. *Bottom*: Power spectrum of the same time series in linear scale; Frequencies near zero are ignored as subject to alias. Time zero represents the beginning of the recording.

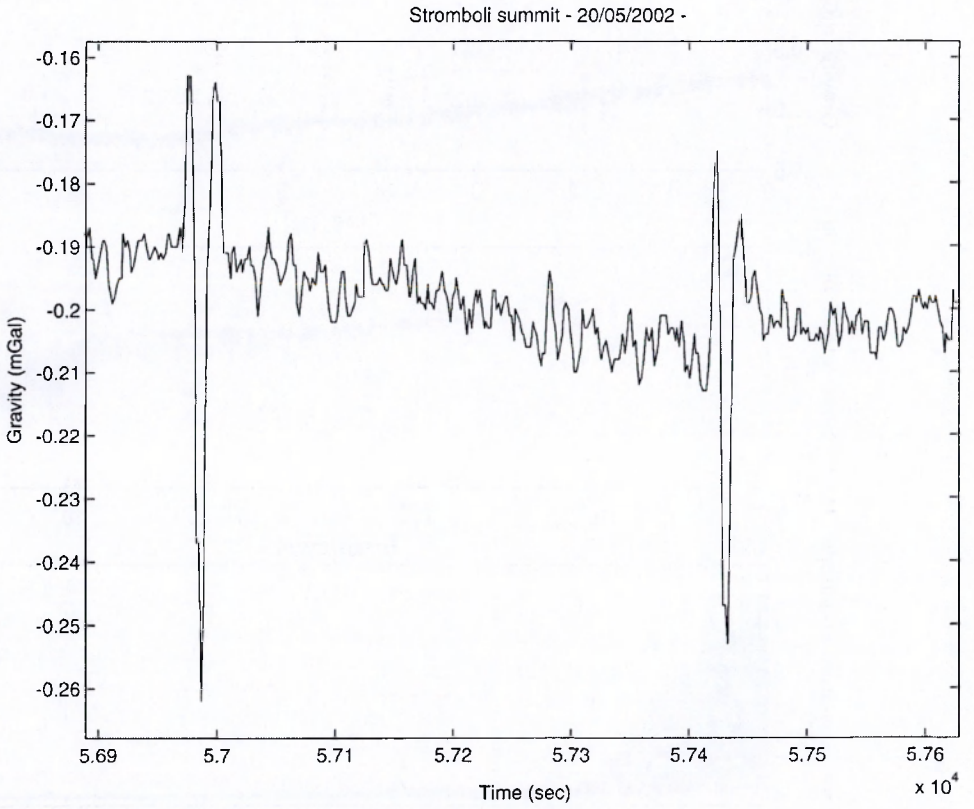

Fig 4.12. Close look at two representative gravity peaks recorded at the **top of Stromboli volcano, Italy, on the 20/05/2002**.

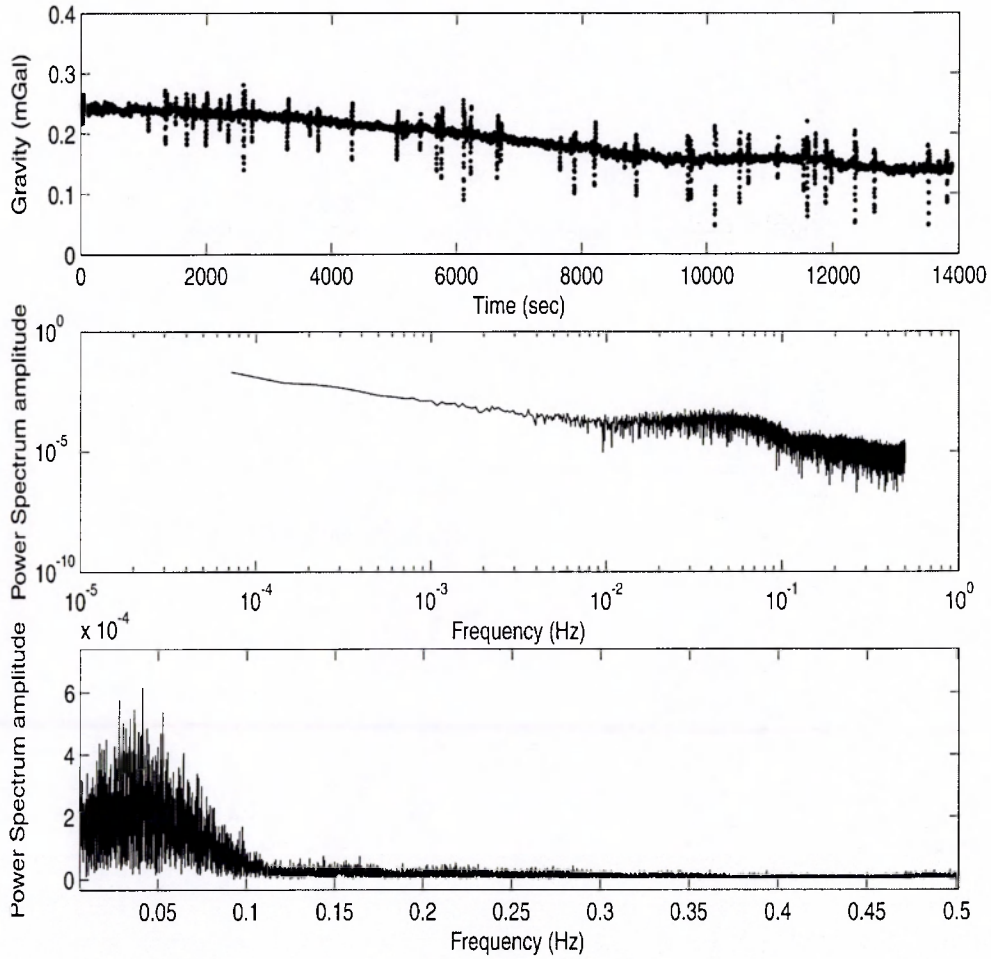

Fig 4.13. Time series analysis of part (~4 hours) of the continuous gravity recorded at the **top of Stromboli volcano, Italy, on the 20/05/2002**. *Top*: Gravity changes through time. *Middle*: Power Spectrum of the same time series in logarithmic scale. *Bottom*: Power spectrum of the same time series in linear scale; Frequencies near zero are ignored as subject to alias. This sample is an example of parts of the signal randomly selected for closer inspection.

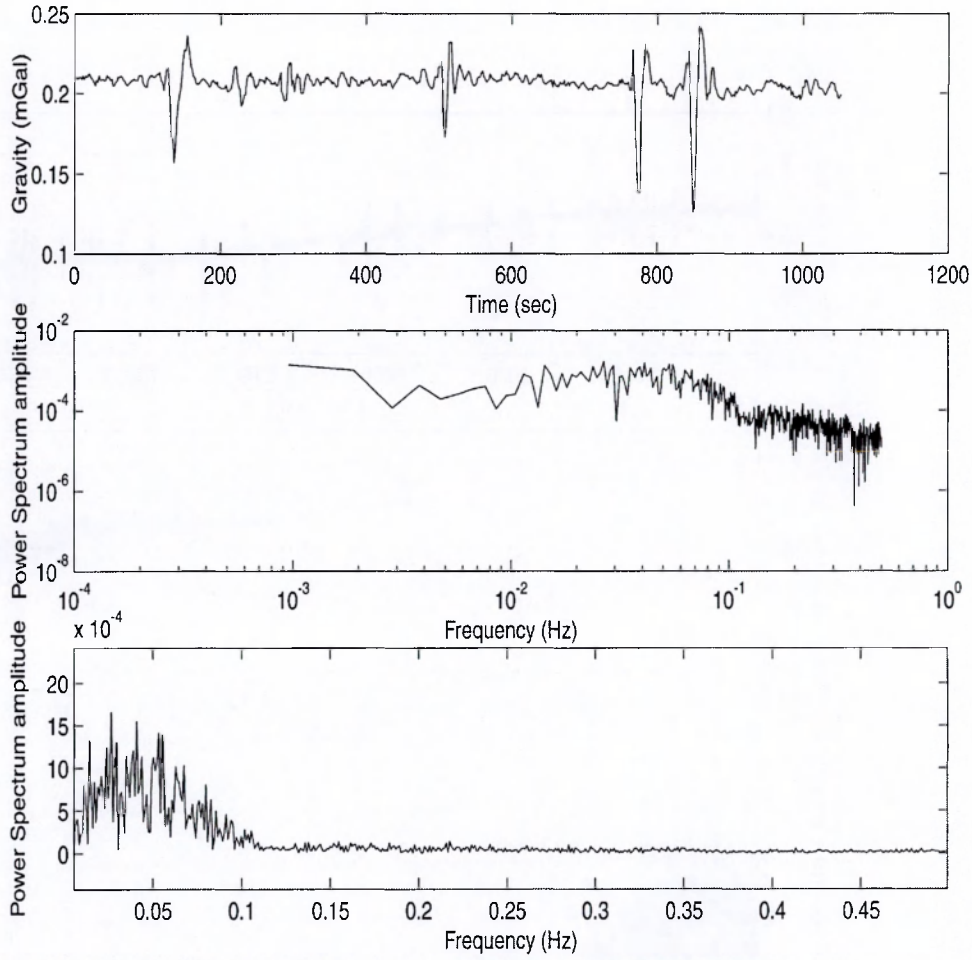

Fig 4.14. Time series analysis of part (~17 min 30 sec) of the continuous gravity recorded at the **top of Stromboli volcano, Italy, on the 20/05/2002**. *Top*: Gravity changes through time. *Middle*: Power Spectrum of the same time series in logarithmic scale. *Bottom*: Power spectrum of the same time series in linear scale; Frequencies near zero are ignored as subject to alias. This sample is an example of parts of the signal randomly selected for closer inspection.

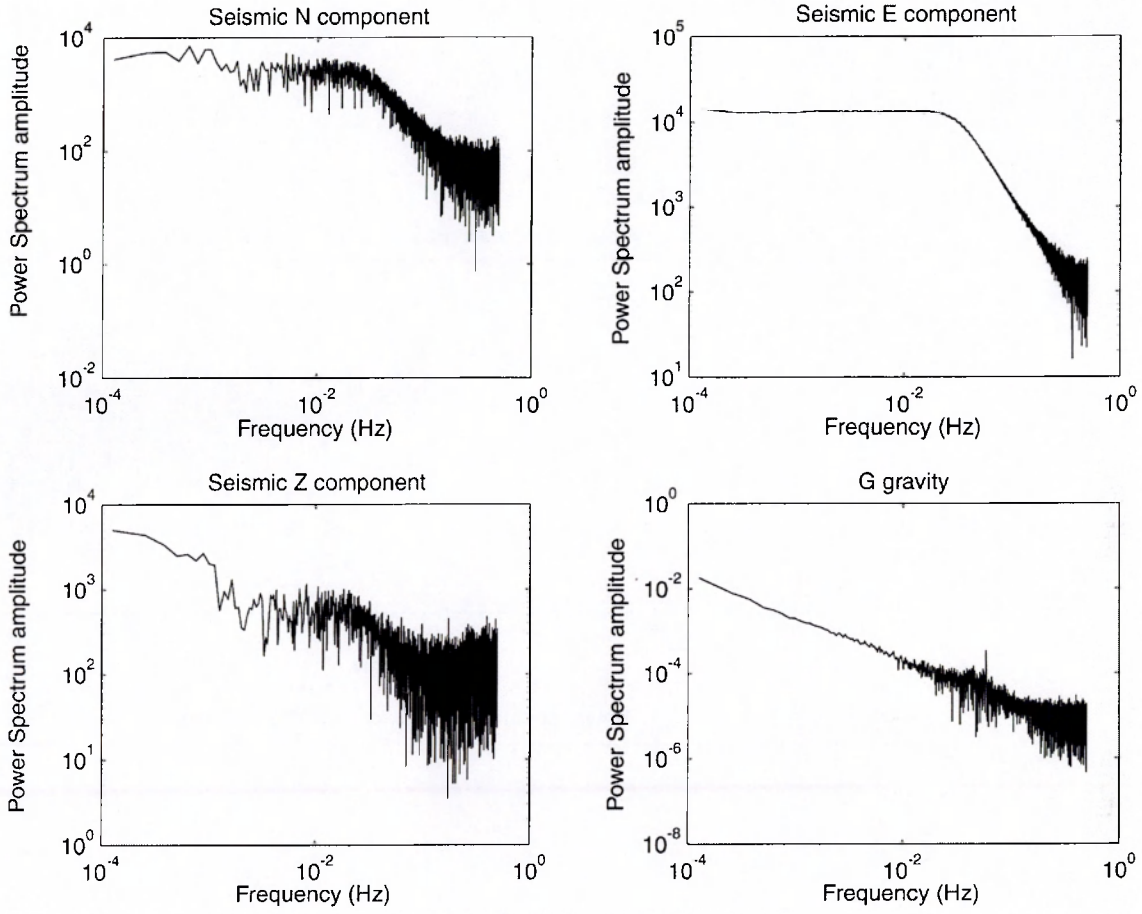

Fig 4.15. Power spectrum of both seismic and gravity time series for the whole experiment at The Open University. *Top left*: Horizontal North-South seismic component. *Top right*: Horizontal East-West seismic component. *Bottom left*: Vertical seismic component. *Bottom right*: gravity.

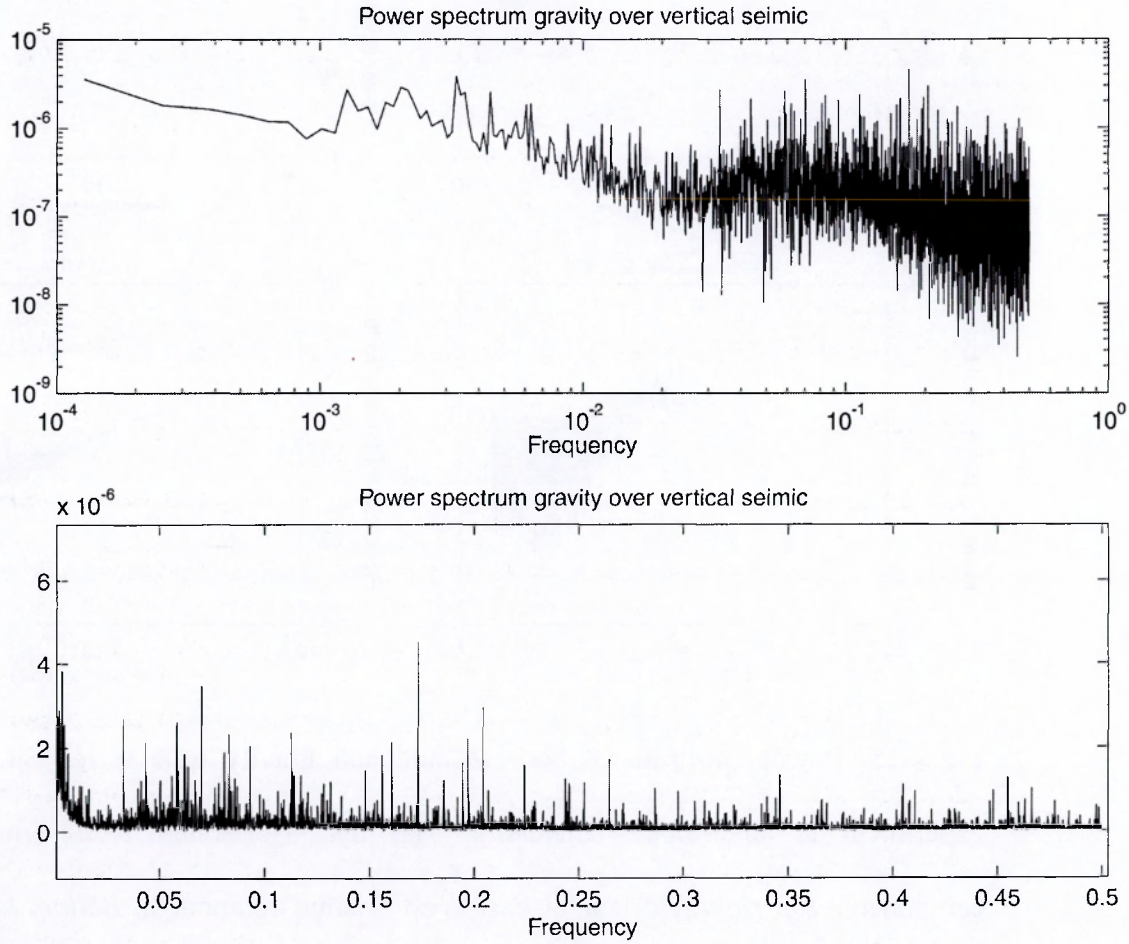

Fig 4.16. Response function of D-41 gravity meter over the 6-T seismometer vertical component. *Top*: Logarithmic scale. *Bottom*: linear scale.

4.6. Discussion

Some important conclusions can be drawn from these preliminary results. The first one concerns the ability of the D-meter gravity meters to continuously record gravity changes while being subject to ground motion or acceleration. This is very well illustrated by the preliminary results from Stromboli where the recorded waveforms during summit activity are the same for both gravity and seismic (vertical component) recording. It therefore raises a fundamental question: when the gravity meter records ground motion or velocity, is it still able to record gravity changes? In other words, is there any gravity signal hidden within the overall waveform when the instrument is subject to strong ground motion/velocity? It is difficult to answer this question from these preliminary results but we can make here a few suggestions that would help solve this problem.

The first step is to determine the "seismic" response of the meter. The easiest way to do so is to couple gravity recording with that of a broadband seismometer. For that, we used the D-61 gravity meter from Lacoste & Romberg and a 6-T broadband 3 component-seismometer from Guralp® and simultaneously recorded data for a few hours. Both instruments were set up on the ground in a lab at The Open University. The gravity meter allows up and down movements of its internal mass, exactly as the vertical component of the broadband seismometer does. Therefore, if both instruments are subject to exactly the same ground motion/velocity, they will act in a similar way. Consequently, in laboratory-based experiment, where the gravity meter is not influenced by any gravity variation apart from the Earth tides (which can be calculated), both instruments are subject to the same stress (**Fig 4.15**). It is next possible to determine a response function of the gravity meter versus the seismometer, which is the ratio of the gravity power spectrum over the vertical seismic power spectrum (**Fig 4.16**; Appendix

D). Once this known, it is possible, when using the same instruments together in the field, to extract the seismic signal from the gravity signal waveform. The residual can then be assessed as a non-seismic signal, which is possibly a gravity signal. The lack of such a residual would prove that no gravity signal has been recorded while the instrument was subject to strong ground motion or velocity. Of course, it is important to be aware that real variations of gravity may occur during a field-based experiment.

As this method is instrument dependent, the same instruments must be used in the field. Unfortunately, this is not always practical. However, there is a way round this problem by determining the response function of the gravity meter versus seismicity in general but it involves a thorough knowledge of the seismometer response and therefore collaboration with the seismometer manufacturer.

A second important point raised by this preliminary work is the occurrence of reversible tares due to the resonnance of the beam/spring when the gravity meter is subject to ground vibrations at specific frequencies. Such tares have been previously identified (pers. comm. Mark Davis) and are of particular importance. Indeed, it seems that when the Lacoste & Romberg gravity meters are subject to such reversible tares induced by particular frequencies, stable but erroneous gravity readings may result. Consequently, it is critical to know if the instruments are subject to such tares, especially when using them for the monitoring on active volcanoes on which ground vibrations are frequent. Obviously, due to the nature of the gravity meters, these tares could also happen with other types of astatic spring gravity meter (e.g., Scintrex®).

In conclusion, the analysis of continuous gravity data highlights instabilities of the instrumental set up and the influence on the readings of external factors such as ground vibrations. These instrument instabilities also appear to be more important close to active volcanic processes than to hydrothermal vents (i.e., fumaroles).

Chapter 5

Conclusions from the Poás study

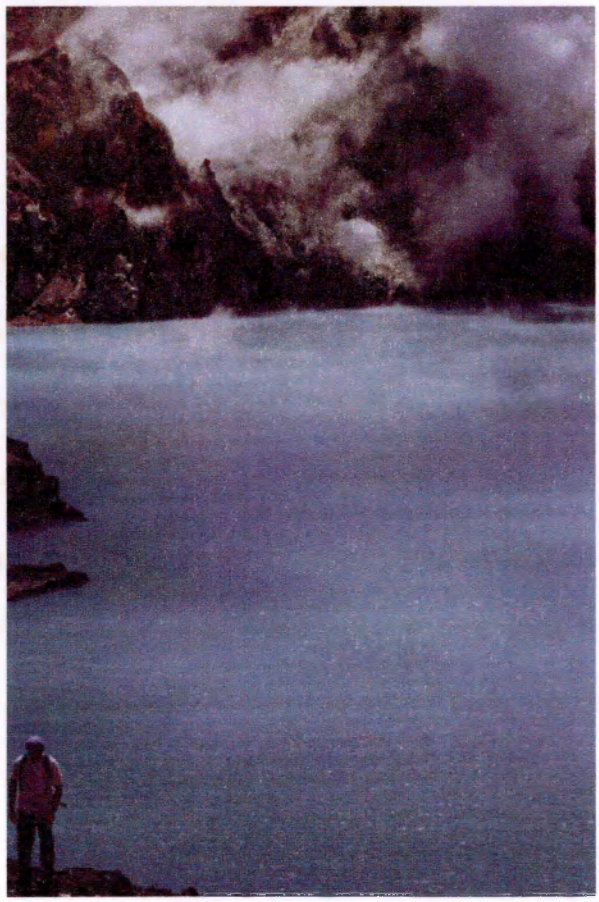

End of a day spent in the field at Poás volcano, Costa Rica

The conclusions can be subdivided into two distinct parts: The gravity monitoring methodology in volcanology and volcanic processes at Poás.

5.1. Micro-gravity monitoring and gravity surveys in Volcanology

Gravity methods are used in two ways in volcanology. Micro-gravity monitoring assesses subsurface mass changes through time and is carried out either continuously or, more traditionally, by repeating measurements manually at the stations of a given network. On the other hand, static surveys (i.e., Bouguer surveys) give snapshot information of subsurface structural features (Thorpe et al., 1981, Locke et al., 1993). This work has explored each technique and brings new insights from integrating them altogether.

5.1.1. Continuous gravity recording

Micro-gravity monitoring through time is normally performed manually but new technological advances (i.e., D-meters from Lacoste & Romberg with feedback) now allow continuous micro-gravity data to be streamed from the instrument. Development of logging software during this project allows automated micro-gravity recording via conventional serial port communication. Continuous gravity measurements on several volcanoes show that, in some cases (e.g., Masaya, Stromboli), when the measurements are made too close to the centre of volcanic activity, recorded data might no longer correspond to real gravity changes but reflect ground vibrations. Thus, Nindiri lava lake at Masaya must be avoided for such monitoring, being too close to the magmatic system and subject to significant ground variations. On the other hand, the crater floor at Poás volcano seems suitable for micro-gravity and gravity surveys, as no important short-term signal variations have been recorded.

5.1.2. High-resolution Bouguer survey

Bouguer surveys on volcanoes are typically made at the scale of the whole volcanic edifice to investigate the overall structure. The main factors that influence survey resolution are the spatial density of measurement sites and the accuracy of the terrain correction. Conventional Bouguer surveys investigate gravity differences of the order of one mGal and above. Consequently, terrain correction using topographic maps at 1:50,000 or 1:25,000 (and, more recently, Digital Elevation Models based on these maps) are usually precise enough to ensure appropriate terrain correction accuracy. However, such large-scale gravity surveys cannot assess small subsurface density contrasts. This work presents the methodology and results of a new high-resolution gravity survey carried out at the top of Poás volcano. This has proved to be a powerful tool to investigate subsurface features on active volcanoes (e.g., near-surface magmatic intrusions).

The corner stone of a high-resolution Bouguer survey is accurate terrain correction. This can be achieved by combining digitised x,y,z topographic coordinates (from 1:50,000 maps) and Real-Time Kinematic GPS to produce a high-resolution Digital Elevation Model (DEM).

Modelling of high-resolution Bouguer anomalies at Poás crater floor has shown that shallow magmatic intrusions cannot be determined from conventional Bouguer survey. As these shallow features are likely to be responsible for temporal variations of micro-gravity, a high-resolution Bouguer survey should ideally always precede the installation of a micro-gravity monitoring network in order to better understand the source of the micro-gravity changes through time.

5.1.3. General methodology for micro-gravity monitoring

In order to install a robust micro-gravity monitoring programme on volcanoes, the following methodology be adopted:

1. Undertake continuous micro-gravity recording at each of the proposed micro-gravity stations in order to determine reading stability. Recording during one to three hours is sufficient to discriminate viable monitoring sites. Although gravity meters used for continuous recording (D-meters) are generally more sensitive to instrumental drift than G-meters, they react in a similar fashion to ground vibrations. Therefore, they can be used successfully to assess site stability for both types of meters.

2. High-resolution Bouguer survey at the site of interest in order to develop insights about subsurface structural features that may be responsible for micro-gravity changes through time (e.g., magma body)

3. Automated (i.e., continuous) or manual (i.e., manually repeated through time) micro-gravity monitoring, depending on instrument availability and logistical constraints. When monitoring volcanoes with aquifers in the monitored zone, extension and temporal variability of the water table and aquifer extension must also be monitored in order to be able to correct gravity data for the "aquifer effect" (cf.section 5.2 below).

As gravity meters are sensitive to ground vibrations, measurement sites with low vibrations are preferred. Stations are usually located on hard rock (e.g., lava flows) for two main reasons. Firstly, it ensures that the station emplacement does not move and, secondly, it makes the site recognition easier. The problem with using hard ground surface is that it efficiently transmits the seismic waves. Light scoria would, on the other hand, dampen the ground vibration and possibly limit instrument noise. The problem with non-consolidated ground is that it is more difficult to ensure the stability of the station's exact location (e.g., a pin cannot be fixed). A compromise would be to leave a hard plate (e.g. metal or wooden dish- size plate) on the ground at each station.

Before every measurement, the plate can be removed, the centre of the emplacement where the plate is geo-located by using differential GPS and finally the gravity is measured with the bottom of the regular gravity plate touching the ground and the plate legs set in the ground. Once the gravity is measured, the station plate can be reinstalled at its original place. Obviously, leaving metal plates on site raises other problems as they may be stolen. In order to avoid any disappearance, the plates would have to be hidden with scoria. In terms of station stability, the scoria would ideally be lying over a more solid material (e.g., lava flow) in order to ensure a relative stability over periods of heavy rain.

5.2. Volcanic processes and monitoring at Poás volcano

Monitoring at Poás volcano by the VDG group at the Open University relies mainly on micro-gravity, coupled with other techniques (seismology, magnetics, fluid/gas chemistry, energy budget). Micro-gravity changes through time are used to retrieve the mass of possible intrusions beneath the crater floor. However, if gravity changes arising from the hydrothermal water table changes were not taken into account in the gravity modelling, it would invariably lead to an underestimate of the amount of magma intruded. Indeed, gravity increase due to the intrusion of a dense magma body can at least partially be compensated by the gravity decrease due to the associated drop of the hydrothermal water table (herein referred as "aquifer effect"). The major insight from this project is the modelling and quantification of this phenomenon. My reinterpretation of the 1986-1989 crisis data shows that the mass of magma intruded at the time was 30 times greater than the previously published results (Rymer et al., 2000). If a volcano has an aquifer in the area of micro-gravity monitoring, mass transfers due to variations of the water table must be taken into account in terms of gravity changes. As most of the micro-gravity monitoring stations at Poás are located at the top of the edifice, the

aquifer in question is the hydrothermal system, the lake being the top of the hydrothermal system. However, if monitoring was to be pursued on other parts of the volcanoes, local aquifers should be assessed.

Once the effects of the hydrothermal system have been removed, temporal micro-gravity monitoring and the high-resolution Bouguer survey can provide information on the size of magma intrusions beneath the crater floor at Poás. This has been suggested by previous studies (Rymer et al., 2000) but not quantified (apart from an attempt at modelling for the 1986-1989 intrusion). Our modelling suggests that 149 x 10^9 kg of magma has been intruded above the top of the upper magma reservoir (~500 m below the crater floor), and it almost reached the surface (the top is inferred to lie a few meters below the crater floor). This mass of magma represents at least two phases of intrusion and less than 20% of this mass was emplaced during the 1986-1989 crisis.

As shown by the continuous gravity experiment, Poás crater floor is a suitable place to monitor micro-gravity. As the subsurface intrusion of magma is a significant and possibly recurrent phenomenon at Poás, ongoing micro-gravity monitoring at the crater floor is highly encouraged, taking into account the aquifer effect on gravity at the stations.

One step forward would be to automate the "aquifer effect" correction for micro-gravity monitoring at Poás, by monitoring precisely the crater lake level using differential GPS.

Volatile solubility in magma is almost nil at depths less than that 500 m (i.e., top of the upper magma reservoir at Poás). It implies that volatiles will invariably exsolve from the magma and form bubbles. It follows that a volume increase will result from a magma movement upwards if the volume change cannot be accommodated laterally or at depth. In the case of subsurface intrusions (e.g., Poás), it results in an upward movement of the magma. As the magma rises, confining pressure decreases and the

bubbles will tend to expand and provoke a self-sustained and irreversible acceleration of the magma upward, finally leading to a magmatic eruption. The lack of magmatic eruptions associated with the episodes of intrusion at Poás implies that the magma was already largely degassed prior to emplacement. It follows that most of the magma degasses in or below the upper magma reservoir at Poás. Retrieving the amount of magma intruded by using the gas flux (via sulphur budget study) at the top would therefore be irrelevant, as most of the magma degassing may be recycled in the magma reservoir. Hence, gas flux cannot replace micro-gravity for monitoring the possible magmatic intrusions in subsurface. However, monitoring the amount of gas exiting the magma via the sulphur budget developed during this project would allow for an estimate of the overall amount of magma degassing through time. An increase of the degassing would then reflect changes occurring in the magma reservoir or below, such as arrival of new hot and gas-rich magma. Such a significant mixing with new magma would probably induce more vigorous magma movement within the magma reservoir and increase the pressure in the reservoir, which would in turn favour the emplacement of shallow intrusions. Monitoring of the mass ratio "magma intruded" (from micro-gravity) over "magma degassing" (from sulphur budget) is therefore important to understand how the magmatic system evolves through time at Poás.

We can note here that the amount of magma erupted at Poás in the last 50 years is negligible compared with the amount of magma that must have degassed (Poás has been persistently degassing for at least 50 years). Since the last crisis (1986-1989), no significant gravity increase has been recorded, which means that no or very little magma was intruded at high level in the volcano. Degassed magma must then have been recycled at depth. Such a recycling implies permanent, or at least frequent, convective movements within the upper magma reservoir.

Chapter 6

Implications for persistently active volcanoes

Gas monitoring at Poás volcano, Costa Rica

Persistent degassing with little or no magma erupted implies the combination of three parameters. Firstly there is a need for a regular source of volatile-rich magma. The origin of this source can be assessed by large scale seismic surveying and geochemistry and is beyond the scope of this project. One can only reasonably assume that such a source exists when persistent degassing is observable and a range of gas species are being emitted. Indeed, large carbonate provinces below volcanoes can be a viable source of CO_2 when heated up by magma (Cortini et al., 1985, Allard et al., 1997). All the same, regional scale gas emission is not always related to volcanic activity and CO_2 can originate from the mantle (Sano and Williams, 1996). However, gas coming from the substratum being assimilated, or from deep sources (e.g. mantle) will be mostly CO_2 and insoluble species. A significant amount of combined SO_2, HCl, HF and other acids indicates that the gas most likely comes from a shallower magma body.

Secondly, once exsolved, the gas must be able to escape the magma and reach the surface. This depends on magma viscosity which, in turn, is highly sensitive to among other things, magma composition, temperature and volatile content. Such phenomenon can be studied with experimental petrology and is also beyond the scope of this project. One must note, though, that quantification of viscosity over a whole range of magma compositions, temperatures and volatile contents is extremely valuable for validating -or otherwise - models derived from geophysics and geochemistry, especially when it comes to assessing kinetics of magma emplacement.

Finally, persistent degassing is only possible if the degassed magma is able to quit the gas exsolution zone (e.g. recycling in depth, intrusion into the country rocks) and to be replaced by new gas-rich magma. This project brings some insights about the fate of the degassed magma at Poás volcano with a combination of both magma convection and shallow intrusions (see Chapter 5 – Conclusions). It also has further implications for our general knowledge of these processes and these are discussed here.

6.1. Upper magma reservoirs as a controlling factor of persistent passive degassing

Extremely shallow magmatic intrusions, not associated with any eruption, must be almost entirely degassed when emplaced (e.g., Poás). It implies that the degassing occurs lower down, in an upper magma reservoir or below. The depth of degassing (i.e., exsolution depth) depends on the magma chemical composition, temperature and volatile diffusivity (Sparks et al., 1994) as well as magma viscosity which is temperature and magma composition dependent. Burnham models (Burnham, 1994) allow calculation of water solubility for various magma compositions. As water is the main component of volcanic gases (Symonds et al., 1994, Giggenbach, 1996), it is a reasonable assumption to consider that exsolution of water is the main factor controlling significant bubble formation (Sparks et al., 1994). It is however difficult to determine precisely the water exsolution depth because of the interdependent parameters that drive this phenomenon. The important point here is that, when the degassing occurs, bubble nucleation and expansion will provoke a global increase of volume in the magma, especially in the case of a relatively viscous magma. Bubbles will tend to grow as long as allowed by magma viscosity and, when bubbles grow, the associated volume change has to be accommodated.

If the magma is located in an open conduit when nucleation occurs, it will tend to rise and, as the water solubility in a water saturated melt decreases, to a first approximation as the square root of pressure (Sparks et al., 1994), the higher the magma in the volcanic edifice, the more bubbles will nucleate. In addition to that, as confining pressure decreases when the magma rises, bubbles will generally tend to expand. This finally leads to an irreversible acceleration of the magma upward and finally to an eruption.

On the other hand, if nucleation occurs when the magma is in a closed space (i.e., no open conduit), pressure will increase gradually within the magma. The pressure increase will first tend to suppress bubble nucleation and growth but, ultimately, will eventually overwhelm the capacity of the surrounding rocks to maintain this pressure and lead to a catastrophic eruption. However, if the magma starts to degas in a magma reservoir which is wide enough to allow convection at the given magma viscosity, volume increase due to bubble nucleation and growth can be dissipated through magma movement (i.e., convection). Stevenson and Blake (1998) modelled the convective overturn of dense degassed magma with buoyant volatile-rich magma in conduits of diverse sizes. The main parameters driving convection were magmas (i.e. degassed and volatile-rich) density and viscosity contrasts as well as crystal, water and CO_2 content and conduit geometry. Whereas magma density contrast and conduit size can be estimated, we do not have data for H_2O and CO_2 flux or crystal content for recent Poás lavas. Furthermore, viscosity is poorly constrained experimentally for andesite and varies greatly (i.e. several orders of magnitude) according to dissolved volatile content and temperature. It means that such convection models cannot be applied to Poás volcano at the moment due to the lack of such data. The capacity of magma to convect varies greatly with composition, volatile content and conduit geometry. Examples from Stevenson and Blake (1998) showed that convection was possible for conduit widths ranging from a few metres at Stromboli (with basaltic magma) to 10s of metres for Mount St Helens (dacite). Therefore, although we cannot model convection for thePoás upper reservoir, it seems reasonable to assume that convection can occur as the upper magma reservoir width greatly exceeds 100 m. This is consistent with continuous feeding of the chamber by deeper volatile-rich magma and the subsequent continuous degassing. Convective overturn of denser degassed magma is then a viable way of

freeing space in the chamber for rising volatile-rich magma and to accommodate the volume change due to bubble nucleation and growth.

If a subduction zone volcano contains an upper magma reservoir which is high enough to ensure a low volatile solubility (i.e., favours magma degassing) and wide enough to allow magma convection, the result will be steady state convection associated with persistent degassing but very low effusion rate (or even no magma erupted at all). Magma intrusions will be mainly degassed as gas exsolution occurs deeper than their level of emplacement (i.e., in the upper magma reservoir) and will tend not to be associated with any significant magmatic eruption. If the same volcanoes have different conditions, they may lead to a dramatic pressure increase at the level of exsolution that will finally result in a powerful eruption when this pressure overwhelms the capacity of the surrounding material to contain it. The lack of significant magmatic eruptions at Poás for the past century (Rymer, 1985 and references therein), despite a significant amount of high level intrusions (this work), suggests that the 500 m deep magma reservoir is wide enough to allow convection. Records of volcanic activity and structural geophysics (to determine the presence or otherwise of a shallow magma reservoir and subsurface intrusions) may help support this theory and can be tested on all volcanoes containing viscous magma (e.g., most volcanoes in a subduction setting).

6.2. Magma emplacement in volcanic edifices: role of the hydrothermal system

This work provides strong evidence that, at subduction zone andesitic volcanoes like Poás, significant amounts of magma can be emplaced in the subsurface (a few metres below the surface) without being accompanied by magmatic eruption. If this magma were still gas rich when it emplaced, it would have led inevitably to an eruption. Therefore, the magma must have been emplaced partially, if not almost entirely,

degassed. Generally, magma emplacement is driven by gas exsolution and bubble growth within the magma but it cannot be the case here as the magma was already degassed when emplaced. In order to further understand this phenomenon, one first needs to determine the mode of emplacement of the magma.

We suspect that dykes, necks and sills are the most common ways of emplacing magma in a volcanic edifice (Marsh, 2000). Such features can be observed even in poorly-consolidated scoria in many places where part of the internal structure of volcanic edifice is visible (e.g., Etna in Italy, Mont Dore and Chaîne des Puys in France). However, it becomes increasingly difficult to identify such features when studying hydrothermally altered volcanic successions (e.g., Cantal volcano in France, Vulcano in Italy, Poás in Costa Rica) and when there are some, they tend to be much bigger (e.g., "Dent de la Rancune" and "Crete de Coq", Mont Dore volcano in France). Indeed, as volcanic successions are hydrothermally altered, parts of the rocks are dissolved and replaced by mineralization. Native elements such as sulphur (e.g., Poás) and/or clays minerals thus precipitate in the created voids (Rowe et al., 1992, this work). In terms of rocks mechanics, hydrothermally altered volcanic successions will have a ductile behaviour whereas fresher rocks will be brittle (van Wy de Vries et al., 2000). It follows that fractures are more difficult to propagate in such a medium as it will tend to deform under stress instead of breaking as a brittle solid. Another important point is that minerals that form during hydrothermal alteration are stable at the temperature and pressure at which it occurs. Temperatures of formation of such clay rich alteration tend to be much lower than magmatic temperatures (~800-1200°C depending on the magma composition). This means that if this material comes into contact with hot magma it will melt, unlike fresh scoria which will resist such temperatures. This assimilation of the surrounding formations by the magma will slowly progress. As this phenomenon is not driven by fracture propagation, there is no

particular reason why the resulting shape of the moving magma body should be dyke-like. The stocky shape of the subsurface intrusions at Poás, inferred from our gravity surveys, fits well with this mode of magma progression. Moreover, during the 1986-1989 crisis, despite the emplacement of a significant amount of magma close to the surface, no significant ground deformation was recorded (less than 10 cm maximum at the Dome). When magma propagates in a fracture, the induced 3D stress provokes ground deformation (Jonsson et al., 1999, Sigmundsson et al., 1999). One simple way of modelling ground deformation is to assume a purely elastic response of the substratum to the stress due to the magma intrusion. The lack of ground deformation during the last intrusive episode at Poás means that the volume of magma intruded had to be accommodated by assimilation of the surrounding material. During the same crisis, it took about 4 years to emplace approximately 28 x 10^9 kg of magma from 500 m below the crater floor to a few metres below the surface. This low intrusion rate is consistent with the hypothesis of the intrusion volume being accommodated by assimilation of the surrounding substratum, in a pluton-like way. We can note here that the presence of water in the hydrothermal system may also help the assimilation of the country "rocks" by the magma. Another interesting point is that if the volume of the intruded magma is slowly accommodated this way, the "Mogi model" of an elastic response of the country rocks does not apply.

The evidence for subsurface intrusions at Poás (and hence, potentially on other volcanoes of the same type) has some important consequences in terms of long-term evolution of subduction-related volcanoes.

6.3. Subsurface magma intrusions

Firstly, we showed in this work that successive episodes of partially degassed magma intrusions can occur near the surface. The question that follows is: what happens when

all the space above the upper magma reservoir at a volcano is occupied by a solid cooled magma intrusion? Indeed, intruding magma upward from the magma reservoir will become increasingly difficult, as large amounts of massive frozen magma cannot be assimilated by the same, but still liquid, magma. All the same, hydrothermal alteration cannot occur as easily on massive solid magma bodies as on vesiculated deposits because of the low porosity and permeability of these massive degassed magma bodies. The direct consequence is that if the general magma supply rate increases, the magma will tend not to travel upward but, more likely, will move laterally, which is easier because the surrounding material is subject to hydrothermal alteration and may deform or be more easily assimilated than the frozen intrusion above the reservoir roof. In terms of volcanic hazards, it means that sector collapses may occur as the magma slowly migrates laterally or as the pressure in the magma reservoir increases if no lateral magma intrusions are possible. It is therefore extremely important to assess the presence, or otherwise, of magma intrusions in the upper part of a volcanic edifice and to monitor the space available for new intrusions.

6.4. Role of hydrothermal systems in the long-term evolution of volcanoes

We described the role of upper magma reservoirs in maintaining persistent degassing without emission of magma. However, this leads to the following question: what dictates the the formation of an upper magma reservoir high in the edifice?

We discussed earlier the important role of hydrothermal alteration in facilitating the assimilation and rise of partially degassed subsurface magma through weakening of the upper part of the edifice and thus allowing an easier assimilation by the slowly rising hot magma.

It follows that, when no well developed hydrothermal is present, it may be difficult for the same magma to progress by desegregation and assimilation of the surrounding rocks and magma may mainly be emplaced as dykes. Magma migration within fractures is much faster than by assimilation and the probability of migrating magma reaching the surface (and triggering an eruption) thus greatly increases. Moreover, the developing magma reservoir may be limited, as significant room for the magma to accumulate can only be achieved by separation of blocks by fractures and collapse of these blocks in order to create voids. On the other hand, when a well-developed hydrothermal system is present, the main process of magma reservoir widening may be by assimilation of the hydrothermally altered surrounding material.

If we put this into the perspective of volcano formation and evolution through time, hydrothermal systems take time to develop sufficiently to allow significant alteration within any volcanic edifice. It follows that, during the early stages of activity at a volcano, a significant magma reservoir may be difficult to form high in the edifice. Consequently, persistent degassing may be accompanied by more magmatic eruptions. Later, when the hydrothermal alteration develops, magma migration by assimilation of the surrounding altered material may greatly help the formation of magma reservoirs high in the edifice. When such magma reservoirs are sufficiently wide, they may allow convection at the level of (or above) the vesiculation and hence lead to significant persistent degassing but less magmatic eruption. These are also conditions that may drive partially degassed magma intrusions above this upper magma reservoir, especially during episodes of increased magma supply rate into the upper magma reservoir. When the space between the upper magma reservoir and the top of the edifice is mainly filled by cooled intruded magma, the overall density of the summit zone will increase. In the mean time, as magma can no longer migrate upwards, the widening of the upper magma reservoir will accelerate by assimilating the hydrothermally-altered surrounding

material. The combined effect of the higher mass above this upper magma reservoir and its widening will result in weakening of its roof until it collapses. The high cohesion of degassed and frozen magma above the upper magma reservoir supports the idea of a piston-like block collapsing during caldera formation. There is indeed no particular reason why the roof of the magma reservoir should not disintegrate during the caldera formation, especially associated with large amplitude eruptions, if the material above the magma reservoir were mainly filled by pyroclastic deposits which are common on the upper part of stratovolcanoes. Lateral development of any magma reservoir by assimilation of altered material high in the edifice may in the mean time weaken flank stability which can, in turn, increase the probability of sector collapse. Both caldera formation and sector collapse correspond to phases of destruction of the volcanic edifice, including the destruction of most of the summit hydrothermal system. At that stage, the volcano is back at the beginning of the cycle when no developed hydrothermal system is present and, hence, no upper magma reservoir.

In summary, we suggest here that hydrothermal systems may have a greater role than previously suggested in magma chamber formation and expansion within volcanic edifices. We also propose that magma reservoirs and subsurface intrusions high in the edifice have a much more significant role in controlling both the type of activity and the evolution of stratovolcanoes than was previously recognised.

References

Allard P, Jean-Baptiste P, D'Alessandro W, Parello F, Parisi B and Flehoc C, 1997. Mantle-derived helium and carbon in groundwaters and gases of Mount Etna, Italy. Earth and Planetary Science Letters, 148: 501-516.

Andres R, Barquero J and Rose W, 1992. New measurements of SO2 flux at Poas Volcano, Costa Rica. Journal of Volcanology and Geothermal Research, 49: 175-177.

Barquero J and Malavasi E, 1985. Seminario vulcanologico conjunto USA-CR. Excursion al Volcan Poas. Boletin de Volcanologia (Universidad Nacional de Costa Rica, Heredia)(14): 117-131.

Beaulieu A, Williams-Jones G, St-Armand K, Stix J and Rymer H, 1998. Temporal gravity variations of variable timescale at Masaya volcano, Nicaragua, AGU Fall Meeting. EOS, San Francisco, USA, pp. F960.

Bennett F D and Raccichini S R, 1978. Subaqueous sulphur lake in Volcan Poas. Nature, 271: 342-344.

Brantley S, Borgia A, Rowe Jr G, Fernandez J and Reynolds J, 1987. Poas volcano crater lake acts as a condenser for acid metal-rich brine. Nature, 330: 470-472.

Brouke R A, Zurn W E and Slichter L B, 1972. Lunar tidal acceleration on a rigid Earth. Geophyical Monography Series, 16: 319-324.

Brown G, Rymer H and Thorpe R, 1987. The evolution of andesite volcano structures: new evidence from gravity studies in Costa Rica. Earth and Planetary Sciences Letter, 82: 323-334.

Burnham C W, 1994. Development of the Burnham model for prediction of H_2O solubility in magmas. In: Carroll M and J. Holloway (Editors), Volatiles in Magmas. Reviews in Mineralogy. Mineral Society of America, Washington D.C., pp. 123-129.

Carroll M and Webster J, 1994. Solubilities of sulfur, noble gases, nitrogen, chlorine, and fluorine in magmas. In: Carroll M and J. Holloway (Editors), Volatiles in Magmas. Reviews in Mineralogy. Mineral Society of America, Washington D.C., pp. 231-279.

Casadevall T, Rose W, Fuller W, Hunt W, Hart M, Moyers J, Woods D, Chuan R and Friend J, 1984. Sulfur dioxide and particles in volcanic plumes from Poás, Arenal and Colima Volcanoes, Costa Rica and Mexico: February 1982, Journal of Geophysical Research, 89: 9633-9641

Cortini M, Lima A and De Vivo B, 1985. Trapping temperatures of melt inclusions from ejected vesuvian mafic xenoliths. Journal of Volcanology and Geothermal Research, 26: 167-172.

Delmelle P, Baxter P, Beaulieu A, Burton M, Francis P, Garcia-Alvarez J, Horrocks L, Navarro M, Oppenheimer, Rothery D, Rymer H, St. Amand K, Stix J, Strauch W and Williams-Jones G, 1999. Origin, Effects of Masaya Volcano's Continued Unrest Probed in Nicaragua. EOS transaction, Am. Geophys. Union, 80(48): 575, 579, 581.

Doukas M P, 2002. A New method for GPS-based wind speed determinations during airborne volcanic plume measurements. 02-395, U.S. Geological Survey.

Foster S, Ellis A, Losilla-Penon M and Rodriguez-Entrada H, 1985. Role of volcanic tuffs in the ground-water regime of the Valle Central, Costa Rica. Ground Water, 23: 195-801.

Giggenbach W F, 1996. Chemical composition of volcanic gases. In: Scarpa R W and Tilling R I (Editors), Monitoring and Mitigation of Volcano Hazards. Springer-Verlag, Berlin, pp. 221-256.

Hammer S, 1939. Terrain correction for gravimeter stations. Geophysics, 4: 184-194.

Harris A, Sherman S and Wright R, 2000. Discovery of self-combusting sulfur flows. Geology, 28(5): 415-418.

Houghton B F and Wilson C J N, 1989. A vesicularity index for pyroclastic deposits. Bulletin of Volcanology, 51: 451-62.

Johnson M C, Anderson A T, Rutherford M J, 1994. Pre-Eruptive Volatile Contents of Magmas. In: Carroll M and H. J (Editors), Volatiles in Magma. Reviews in Mineralogy. Mineral Society of America, Washington D.C., pp. 281-330.

Jonsson S, Zebker H, Cervelli P, Segall P, Garbeil H, Mouginis-Mark P, Rowland S, 1999. A shallow-dipping dike fed the 1995 flank eruption at Fernandina volcano, Galapagos, observed by satellite radar interferometry. Geophysical Research Letter(26): 1077-1080.

Kusakabe M, Komoda Y, Takano B and Abiko T, 2000. Sulfur isotopic effects in the disproportionation reaction of sulfur dioxide in hydrothermal fluids: implication for the $d^{34}S$ variations of dissolved bisulfate and elemental sulfur from active crater lakes. Journal of Volcanology and Geothermal Research, 97: 287-307.

Lacoste&Romberg, 2000. Model G and D Meter Manual. Lacoste and Romberg.

Locke C, Cassidy J and MacDonald A, 1993. Three-dimensional structure of relict stratovolcanoes in Taranaki, New Zealand: evidence from gravity data. Journal of Volcanology and Geothermal Research, 59: 121-130.

Marsh B, 2000. Magma chambers. In: Siggurdson H, Houghton B, McNutt S, Rymer H and Stix J (Editors), Encyclopedia of Volcanoes. Academic Press, pp. 191-206.

Martinez M, Fernandez E, Valdes J, Barboza V, Van der Laat R, Duarte E, Malavassi E, Sandoval L, Barquero J, Marino T, 2000. Chemical evolution and volcanic activity of the active crater lake of Poas volcano, Costa Rica, 1993-1997. Journal of Volcanology

and Geothermal Research, 97: 127-141.

Montegrossi G, Tassi F, Vaselli O, Buccianti A and Garofalo K, 2001. Sulfur Species in Volcanic Gases. Analytical Chemistry 73(15): 3709 -3715.

Nowell D, 1999. Gravity terrain corrections - an overview. Journal of Applied Geophysics, 42: 117-134.

Oppenheimer C, 1992. Sulphur eruptions at Volcan Poas, Costa Rica. Journal of Volcanology and Geothermal Research, 49: 1-21.

Pedley R C, Busby J P and Dabek Z K, 1997. GravMag user manual: Interactive 2.5D gravity & magnetic modeling. WK/93/26/R, British Geological Survey.

Ripepe M, Harris A J L and Carniel R, 2002. Thermal, seismic and infrasonic insights into conduit processes at Stromboli volcano. Journal of Volcanology and Geothermal Research(118): 289-297.

Rowe Jr G, Ohsawa S, Takano B, Brantley S, Fernandez J, Barquero J, 1992. Using Crater Lake chemistry to predict volcanic activity at Poas volcano, Costa Rica. Bulletin of Volcanology, 54: 494-503.

Rowe Jr G, Brantley S, Fernandez M, Borgia A and Barquero J, 1992. Fluid-volcano interaction in an active stratovolcano: the crater lake system of Poas volcano, Costa Rica. Journal of Volcanology and Geothermal Research, 49: 23-51.

Rowe Jr G, 1994. Oxygen, hydrogen and sulfur isotope systematics of the crater lake system at Poás volcano, Costa Rica. Geochemical Journal, 28: 263-287.

Rowe Jr G, Brantley S, Fernandez J and Borgia A, 1995. The chemical and hydrologic structure of Poas Volcano, Costa Rica. Journal of Volcanology and Geothermal Research, 64: 233-267.

Rymer H and Brown G, 1984. Periodic gravity changes at Poas volcano, Costa Rica. Nature, 311(5983): 243-245.

Rymer H, 1985. Gravity studies of sub-surface structures and evolution of active volcanoes in Costa Rica. Unpublished Thesis, The Open University, Milton Keynes, 336 pp.

Rymer H and Brown G, 1987. Causes of Microgravity changes at Poas volcano, Costa Rica: an active but non-erupting system. Bulletin of Volcanology, 49: 389-398.

Rymer H and Brown G C, 1989. Gravity changes as a precursor of to volcanic eruptions at Poas volcano, Costa Rica. Nature, 342: 902-905.

Rymer H, 1996. Microgravity monitoring. In: Sarpa R and Tilling R I (Editors), Monitoring and Mitigation of Volcano Hazards. Springer-Verlag, Berlin, pp. 169-198.

Rymer H, van Wyk de Vries B, Stix J and Williams-Jones G, 1998. Pit crater structure and processes governing persistent activity at Masaya Volcano, Nicaragua. Bulletin of Volcanology, 59: 345-355.

Rymer H, Cassidy J, Locke C.A, Barboza M.V, Barquero J, Brenes J, Van der Laat R, 2000. Geophysical studies of the recent 15-year eruptive cycle at Poas Volcano, Costa Rica. Journal of Volcanology and Geothermal Research, 97: 425-442.

Sanford W, Konikow L, Rowe Jr G and Brantley S, 1995. Groundwater transport of crater-lake brine at Poas Volcano, Costa Rica. Journal of Volcanology and Geothermal Research, 64: 269-293.

Sano Y and Willams S N, 1996. Fluxes of mantle and subducted carbon along convergent plate boundaries. Geophysical Research Letters 23(20): 2749-2752.

Sigmundsson F, Durand P and Massonet D, 1999. Opening of an eruptive fissure and seaward displacement at Piton de la Fournaise volcano measured by Radarsat satellite radar interferometry. Geophysical Research Letter (26): 533-536.

Smithonian Institution, 1989, Scientific Event Alert Network 14 (4), 7-10.

Sparks R S J, Barclay J, Jaupart C, Mader H M and Phillips J C, 1994. Physical apect of magma degassing. I. Experimental and theoretical constraints on vesiculation. In: Carroll M and J. Holloway (Editors), Volatiles in Magmas. Reviews in Mineralogy. Mineral Society of America, Washinton D.C., pp. 413-445.

Stevenson D and Blake S, 1998. Modelling the dynamics and thermodynamics of volcanic degassing. Bulletin of Volcanology (60): 307-317.

Stoiber R E, Williams S N and Huebert B J, 1986. Sulfur and halogen gases at Masaya caldera complex, Nicaragua: Total flux and variations with time. Journal of Geophysical Research, 91: 12215-12231.

Symonds R, Gerlach T and Reed M, 2001. Magmatic gas scrubbing: implications for volcano monitoring. Journal of Volcanology and Geothermal Research, 108: 303-341.

Telford W, Geldart L and Sheriff R, 1990. Applied Geophysics. Cambridge University Press, 770 pp.

Thorne L and Wallace T, 1995. Modern Global Seismology. International Geophysics Series, 58. Academic Press, 521 pp.

Thorpe R S, Locke C A, Brown G C, Francis P W and Randal M, 1981. Magma chamber below Poas volcano, Costa Rica. Journal of Geological Society of London, 138(3): 367-373.

van Wyk de Vries B, Kerle N and Pedley D, 2000. Sector collapse forming at Casita volcano, Nicaragua. Geology, 28(2): 167-170.

Williams-Jones G, 2001. Integrated geophysical studies at Masaya volcano, Nicaragua, The Open University, Milton Keynes, UK, 237 pp.

Williams-Jones G, Horton K, Garbeil H, Mouginis-Mark P, Harris A J L, Elias T and Sutton A J. Accurately measuring volcanic plume speeds with multiple UV spectrometres, Bulletin of Volcanology, submitted.

Appendix A

Bouguer Survey data at Poás volcano, Costa Rica

(February 2002)

At each station, gravity is measured at least three times and the measurements are considered to be valid when the difference between the data doesn't exceed 10 μGals. The three –or more- valid measurements are then averaged and recorded as the raw data. This ensures that the instrument was stable during the measurement and allows us to rid of erroneous recording due to wind blows or reader errors. During the measurements at each station, as values are compared without taking into account the Earth Tide, data are collected as quickly as possible to ensure a negligible error due to the Earth Tide varying with time (typically 1 to 5 μGals variation from the beginning do the end of the measurements at each station). Data reported below are thus the average of three –or more- measurements.

A.1. Field data

Bouguer survey - Poas Volcano crater floor. Instrument: L&R G-403

Date/Stations	Raw gravity (mGal)	Local Time	Tide (mGal)	Tide Corrected (mGal)	Drift (mGal)
17/02/02					
BA1	1373.630	12:08	0.055	1449.585	0.000
BA2	1374.002	12:22	0.063	1449.986	0.003
BA3	1374.180	12:32	0.069	1450.180	0.005
BA4	1374.070	12:41	0.075	1450.070	0.007
BA5	1374.001	12:48	0.079	1450.001	0.008
BA6	1373.725	12:58	0.084	1449.714	0.010
BA5	1373.970	13:07	0.089	1449.978	0.012
BA3	1374.175	13:19	0.094	1450.199	0.014
BA1	1373.604	13:29	0.098	1449.601	0.016
BB1	1374.123	13:39	0.102	1450.153	0.018
BB2	1374.276	13:49	0.105	1450.317	0.019
BB3	1374.475	13:58	0.108	1450.530	0.019
BB4	1374.424	14:12	0.110	1450.478	0.039
BB5	1374.232	14:22	0.112	1450.278	0.054
BB6	1373.871	14:33	0.113	1449.897	0.061
BB5	1374.245	14:43	0.113	1450.292	0.068
BB3	1374.534	14:56	0.113	1450.597	0.086
BB1	1374.179	15:07	0.112	1450.222	0.087
BA1	1373.683	15:38	0.105	1449.691	0.106
BB1	1374.212	15:48	0.102	1450.247	0.112
BC1	1374.572	16:03	0.097	1450.622	0.121
BC2	1374.770	16:15	0.092	1450.826	0.128
BC3	1374.811	16:26	0.087	1450.864	0.135
BC4	1374.801	16:38	0.081	1450.847	0.142
BC5	1374.621	16:46	0.077	1450.653	0.148
BC4	1374.819	16:54	0.073	1450.858	0.153
18/02/02					
45a	1330.781	9:39	-0.030	1404.259	0.000
Step mirador	1315.237	10:10	-0.023	1387.855	0.002
BC5	1374.672	10:54	-0.007	1450.623	0.005
BC4	1374.882	11:05	-0.003	1450.849	0.006
BC1	1374.675	11:17	0.003	1450.636	0.007
BB1	1374.331	11:28	0.008	1450.278	0.009
BC1	1374.662	11:36	0.012	1450.632	0.010
BD1	1374.905	11:50	0.019	1450.895	0.013
BD2	1375.139	12:00	0.025	1451.148	0.018
BD3	1375.103	12:09	0.030	1451.115	0.022
BD4	1375.041	12:20	0.036	1451.056	0.027
BD3	1375.076	12:32	0.042	1451.099	0.032
BD1	1374.901	12:42	0.047	1450.919	0.037
BC1	1374.652	12:53	0.053	1450.662	0.037
BD1	1374.890	13:05	0.060	1450.920	0.037
BE1	1375.151	13:39	0.076	1451.212	0.037

BE2	1374.825	13:52	0.081	1450.873	0.037
BD1	1374.864	14:06	0.086	1450.919	0.037
BE1	1375.172	14:16	0.081	1451.239	0.037
BF1	1374.998	14:28	0.092	1451.066	0.037
BF2	1375.122	14:42	0.096	1451.201	0.041
BF3	1374.639	14:56	0.099	1450.694	0.044
BF2	1375.130	15:13	0.101	1451.215	0.049
BE1	1375.177	15:23	0.102	1451.265	0.051
BF1	1375.004	15:33	0.102	1451.083	0.054
BG1	1375.610	15:47	0.101	1451.722	0.055
BG2	1375.609	15:56	0.106	1451.725	0.055
BG3	1374.453	16:08	0.099	1450.498	0.056
BG1	1375.645	16:31	0.095	1451.753	0.058
Step mirador	1315.205	17:23	0.078	1387.922	0.061
45a	1330.745	17:40	0.070	1404.321	0.062
19/02/02					
45a	1330.826	10:20	-0.019	1404.318	0.000
BF1	1375.065	11:59	0.003	1451.048	0.003
BG1	1375.710	12:10	0.007	1451.733	0.004
BH1	1376.077	12:21	0.011	1452.125	0.004
BH2	1375.679	12:32	0.016	1451.709	0.006
BG1	1375.730	12:43	0.020	1451.767	0.008
BH1	1376.071	12:52	0.024	1452.131	0.010
BI1	1376.413	13:15	0.034	1452.502	0.015
BI2	1375.082	13:26	0.037	1451.100	0.017
D3	1374.723	13:50	0.049	1450.733	0.022
BI2	1375.051	14:04	0.055	1451.085	0.025
BH2	1375.659	14:16	0.059	1451.731	0.028
BF3	1374.707	14:28	0.064	1450.731	0.028
45a	1330.760	15:19	0.081	1404.348	0.030

A.2. Final data

Stations	Drift corrected Bouguer raw data (mGal)	Longitude (degres, WGS84)	Latitude (degres, WGS84)	Elevation a.s.l. (m)
BA1	1449.585	84.2322	10.1963	2348.20
BA2	1449.983	84.2323	10.1960	2347.40
BA3	1450.175	84.2324	10.1957	2347.30
BA4	1450.063	84.2325	10.1953	2347.62
BA5	1449.993	84.2327	10.1951	2347.39
BA6	1449.704	84.2328	10.1948	2347.31
BB1	1450.135	84.2319	10.1959	2346.70
BB2	1450.298	84.2320	10.1956	2346.90
BB3	1450.511	84.2320	10.1953	2346.34
BB4	1450.439	84.2321	10.1949	2346.22
BB5	1450.224	84.2322	10.1946	2346.34
BB6	1449.837	84.2321	10.1943	2346.62
BC1	1450.500	84.2315	10.1957	2346.03
BC2	1450.697	84.2315	10.1955	2345.67
BC3	1450.729	84.2315	10.1952	2345.70
BC4	1450.705	84.2315	10.1948	2345.63
BC5	1450.505	84.2315	10.1945	2345.66
BD1	1450.747	84.2310	10.1956	2345.38
BD2	1450.996	84.2309	10.1953	2344.95
BD3	1450.959	84.2308	10.1951	2344.95
BD4	1450.894	84.2308	10.1948	2344.68
BE1	1451.062	84.2302	10.1955	2343.82
BE2	1450.701	84.2301	10.1952	2344.70
BF2	1451.028	84.2296	10.1955	2343.30
BF3	1450.515	84.2296	10.1951	2344.25
BG1	1451.532	84.2294	10.1965	2340.50
BG2	1451.535	84.2292	10.1963	2339.92
BG3	1450.307	84.2288	10.1962	2342.26
BH1	1451.933	84.2293	10.1971	2337.55
BH2	1451.516	84.2290	10.1970	2337.28
BI1	1452.300	84.2293	10.1977	2334.38
BI2	1450.872	84.2290	10.1976	2338.08

Appendix B

Processed topographic data from RTK GPS Survey at Poás volcano, Costa Rica (February 2002)

Coordinates of the 765 GPS points used for the topography survey.

Easting and Northing are given in WGS84 decimal degrees

Elevations are in metres above sea level (a.s.l.)

Note: More than 2600 points were originally recorded but only 765 were really relevant for the purpose of this survey (i.e. some points were distant of only a few centimetres which is meaningless at the scale of the survey).

RTK GPS data (WGS84 decimal degres)

Easting	Northing	Elevation
-84.2345	10.1953	2466.88
-84.2345	10.1954	2466.88
-84.2344	10.1949	2460.16
-84.2344	10.1950	2459.99
-84.2344	10.1950	2460.16
-84.2344	10.1955	2466.88
-84.2344	10.1956	2466.88
-84.2344	10.1957	2466.88
-84.2344	10.1958	2458.23
-84.2344	10.1960	2458.23
-84.2344	10.1961	2458.23
-84.2344	10.1962	2458.23
-84.2344	10.1963	2457.84
-84.2344	10.1963	2458.23
-84.2343	10.1944	2471.01
-84.2343	10.1944	2471.03
-84.2343	10.1944	2471.33
-84.2343	10.1944	2471.37
-84.2343	10.1945	2471.33
-84.2343	10.1946	2471.33
-84.2343	10.1947	2471.33
-84.2343	10.1948	2460.16
-84.2343	10.1964	2458.23
-84.2342	10.1943	2471.33
-84.2342	10.1965	2458.23
-84.2342	10.1966	2450.09
-84.2341	10.1941	2453.63
-84.2341	10.1942	2453.63
-84.2341	10.1966	2450.09
-84.2341	10.1967	2448.68
-84.2341	10.1967	2450.09
-84.2341	10.1967	2450.61
-84.2341	10.1968	2448.68
-84.2341	10.1968	2449.09
-84.2341	10.1968	2449.10
-84.2340	10.1941	2453.63
-84.2340	10.1941	2453.73
-84.2340	10.1968	2448.68
-84.2339	10.1940	2453.73
-84.2339	10.1969	2448.68
-84.2338	10.1938	2444.52
-84.2338	10.1939	2444.52
-84.2338	10.1970	2454.93
-84.2338	10.1971	2454.93
-84.2338	10.1972	2454.93
-84.2338	10.1976	2444.23
-84.2338	10.1977	2444.23
-84.2338	10.1980	2444.23
-84.2337	10.1938	2444.52
-84.2337	10.1938	2444.67
-84.2337	10.1971	2454.93
-84.2337	10.1972	2454.93
-84.2337	10.1972	2455.27
-84.2337	10.1973	2454.93
-84.2337	10.1974	2454.93
-84.2337	10.1975	2454.93
-84.2337	10.1976	2444.23
-84.2337	10.1977	2444.23
-84.2337	10.1978	2444.23
-84.2337	10.1979	2444.23
-84.2337	10.1979	2444.47
-84.2337	10.1980	2444.47
-84.2337	10.1981	2444.47
-84.2336	10.1937	2444.67
-84.2336	10.1971	2454.93
-84.2336	10.1981	2444.47
-84.2336	10.1982	2444.47
-84.2336	10.1983	2436.91
-84.2336	10.1984	2436.91
-84.2336	10.1985	2436.91
-84.2336	10.1986	2436.85
-84.2336	10.1986	2436.91
-84.2335	10.1936	2432.04
-84.2335	10.1937	2444.67
-84.2335	10.1970	2444.41
-84.2335	10.1987	2436.91
-84.2335	10.1988	2436.91
-84.2335	10.1989	2446.46
-84.2335	10.1990	2445.98
-84.2335	10.1990	2446.46
-84.2334	10.1935	2432.04
-84.2334	10.1962	2438.75
-84.2334	10.1963	2438.75
-84.2334	10.1964	2438.75
-84.2334	10.1965	2438.75
-84.2334	10.1968	2444.41
-84.2334	10.1969	2444.41
-84.2334	10.1990	2446.46
-84.2334	10.1991	2446.46
-84.2333	10.1934	2432.04
-84.2333	10.1936	2431.21
-84.2333	10.1936	2432.04
-84.2333	10.1966	2438.75
-84.2333	10.1967	2438.69
-84.2333	10.1967	2438.75
-84.2333	10.1967	2439.11
-84.2333	10.1967	2439.12
-84.2333	10.1967	2439.19
-84.2333	10.1967	2439.43
-84.2333	10.1969	2443.57
-84.2333	10.1969	2444.41
-84.2333	10.1991	2446.46
-84.2333	10.1992	2446.46
-84.2332	10.1934	2432.04
-84.2332	10.1993	2438.10
-84.2332	10.1994	2438.10
-84.2331	10.1995	2438.10
-84.2331	10.1996	2437.41
-84.2331	10.1996	2438.10
-84.2330	10.1933	2418.93
-84.2330	10.1948	2347.31
-84.2330	10.1949	2347.31
-84.2330	10.1951	2347.31
-84.2330	10.1954	2346.39
-84.2330	10.1955	2347.69
-84.2330	10.1996	2438.10
-84.2329	10.1947	2347.31
-84.2329	10.1952	2346.39
-84.2329	10.1953	2346.39
-84.2329	10.1956	2347.69
-84.2329	10.1996	2438.10

-84.2329	10.1997	2438.10	-84.2323	10.1965	2351.13
-84.2328	10.1934	2418.93	-84.2323	10.1965	2352.02
-84.2328	10.1945	2347.31	-84.2323	10.1965	2352.03
-84.2328	10.1946	2347.31	-84.2323	10.1975	2330.41
-84.2328	10.1949	2347.31	-84.2323	10.1984	2330.41
-84.2328	10.1949	2347.90	-84.2323	10.2002	2438.84
-84.2328	10.1956	2347.69	-84.2322	10.1935	2387.45
-84.2328	10.1998	2438.10	-84.2322	10.1936	2387.45
-84.2327	10.1907	2585.40	-84.2322	10.1937	2387.45
-84.2327	10.1907	2585.64	-84.2322	10.1937	2388.17
-84.2327	10.1908	2585.13	-84.2322	10.1943	2345.82
-84.2327	10.1908	2585.43	-84.2322	10.1943	2346.62
-84.2327	10.1933	2418.93	-84.2322	10.1946	2343.73
-84.2327	10.1934	2418.34	-84.2322	10.1946	2343.77
-84.2327	10.1934	2418.34	-84.2322	10.1946	2345.55
-84.2327	10.1934	2418.85	-84.2322	10.1946	2345.71
-84.2327	10.1934	2418.93	-84.2322	10.1946	2346.31
-84.2327	10.1944	2347.31	-84.2322	10.1946	2346.32
-84.2327	10.1951	2345.46	-84.2322	10.1946	2346.33
-84.2327	10.1951	2345.53	-84.2322	10.1946	2346.34
-84.2327	10.1951	2345.75	-84.2322	10.1962	2347.25
-84.2327	10.1951	2346.39	-84.2322	10.1963	2347.01
-84.2327	10.1951	2347.38	-84.2322	10.1963	2347.06
-84.2327	10.1951	2347.38	-84.2322	10.1963	2347.25
-84.2327	10.1951	2347.39	-84.2322	10.1963	2347.29
-84.2327	10.1951	2347.42	-84.2322	10.1963	2348.20
-84.2327	10.1957	2347.24	-84.2322	10.1963	2348.35
-84.2327	10.1999	2438.79	-84.2322	10.1963	2348.37
-84.2326	10.1908	2585.76	-84.2322	10.1963	2348.38
-84.2326	10.1934	2418.93	-84.2322	10.1963	2348.40
-84.2326	10.1943	2345.82	-84.2322	10.1963	2348.41
-84.2326	10.1958	2347.24	-84.2322	10.2003	2438.84
-84.2326	10.1959	2347.38	-84.2322	10.2004	2438.84
-84.2326	10.1961	2347.38	-84.2321	10.1937	2387.45
-84.2326	10.2000	2438.79	-84.2321	10.1942	2345.82
-84.2325	10.1934	2412.48	-84.2321	10.1949	2345.53
-84.2325	10.1935	2411.72	-84.2321	10.1949	2346.09
-84.2325	10.1935	2412.48	-84.2321	10.1949	2346.22
-84.2325	10.1942	2345.82	-84.2321	10.1949	2346.24
-84.2325	10.1953	2347.62	-84.2321	10.1953	2345.25
-84.2325	10.1953	2347.69	-84.2321	10.1961	2347.25
-84.2325	10.1962	2347.38	-84.2321	10.1967	2352.02
-84.2325	10.1963	2347.25	-84.2320	10.1938	2387.45
-84.2325	10.2001	2438.79	-84.2320	10.1942	2345.82
-84.2324	10.1935	2412.48	-84.2320	10.1953	2346.34
-84.2324	10.1942	2345.82	-84.2320	10.1956	2346.50
-84.2324	10.1957	2346.34	-84.2320	10.1956	2346.90
-84.2324	10.1957	2347.24	-84.2320	10.1960	2347.13
-84.2324	10.1957	2347.25	-84.2320	10.1965	2352.02
-84.2324	10.1957	2347.30	-84.2320	10.1966	2352.02
-84.2324	10.1964	2347.25	-84.2320	10.1970	2330.41
-84.2324	10.1977	2330.41	-84.2320	10.1976	2330.41
-84.2324	10.2002	2438.79	-84.2320	10.1982	2330.41
-84.2324	10.2002	2438.84	-84.2320	10.1986	2330.41
-84.2323	10.1935	2387.45	-84.2320	10.1988	2330.41
-84.2323	10.1935	2412.48	-84.2320	10.1994	2330.41
-84.2323	10.1942	2345.82	-84.2320	10.2004	2438.84
-84.2323	10.1960	2347.10	-84.2319	10.1938	2387.45
-84.2323	10.1960	2347.38	-84.2319	10.1942	2345.82
-84.2323	10.1960	2347.40	-84.2319	10.1959	2346.70
-84.2323	10.1960	2347.47	-84.2319	10.1959	2347.13
-84.2323	10.1963	2347.25	-84.2319	10.1964	2347.25
-84.2323	10.1965	2350.85	-84.2319	10.1969	2330.41

-84.2319	10.1990	2330.41	-84.2311	10.1944	2357.25
-84.2319	10.2004	2439.93	-84.2311	10.1945	2344.68
-84.2318	10.1938	2387.45	-84.2311	10.1946	2343.59
-84.2318	10.1939	2387.45	-84.2311	10.1959	2373.02
-84.2318	10.1942	2357.52	-84.2310	10.1944	2357.25
-84.2318	10.1958	2347.13	-84.2310	10.1945	2344.68
-84.2318	10.1964	2347.25	-84.2310	10.1955	2344.79
-84.2318	10.2005	2439.93	-84.2310	10.1956	2344.79
-84.2317	10.1939	2357.52	-84.2310	10.1956	2345.07
-84.2317	10.1939	2387.45	-84.2310	10.1956	2345.29
-84.2317	10.1943	2357.52	-84.2310	10.1956	2345.33
-84.2317	10.1958	2346.03	-84.2310	10.1956	2345.34
-84.2317	10.1963	2347.13	-84.2310	10.1956	2345.38
-84.2317	10.2005	2439.93	-84.2310	10.1956	2345.49
-84.2316	10.1940	2357.52	-84.2310	10.1956	2347.37
-84.2316	10.1943	2357.25	-84.2310	10.1959	2373.02
-84.2316	10.1962	2347.13	-84.2310	10.1963	2330.41
-84.2316	10.2005	2439.93	-84.2310	10.1964	2330.41
-84.2315	10.1941	2357.52	-84.2310	10.1969	2330.41
-84.2315	10.1944	2343.59	-84.2310	10.1975	2330.41
-84.2315	10.1945	2343.59	-84.2310	10.1978	2330.41
-84.2315	10.1945	2345.62	-84.2310	10.1982	2330.41
-84.2315	10.1945	2345.66	-84.2310	10.1984	2330.41
-84.2315	10.1945	2345.66	-84.2310	10.1988	2330.41
-84.2315	10.1948	2345.63	-84.2310	10.1990	2330.41
-84.2315	10.1948	2345.73	-84.2310	10.1992	2330.41
-84.2315	10.1952	2345.70	-84.2310	10.1994	2330.41
-84.2315	10.1952	2345.70	-84.2310	10.1996	2330.41
-84.2315	10.1955	2345.67	-84.2310	10.2006	2439.76
-84.2315	10.1955	2346.04	-84.2309	10.1953	2344.95
-84.2315	10.1957	2346.03	-84.2309	10.1953	2345.32
-84.2315	10.1957	2346.20	-84.2309	10.1955	2344.95
-84.2315	10.1961	2346.20	-84.2309	10.1959	2373.02
-84.2315	10.1964	2330.41	-84.2309	10.1994	2330.41
-84.2315	10.1969	2330.41	-84.2309	10.2006	2439.76
-84.2315	10.1976	2330.41	-84.2308	10.1944	2344.61
-84.2315	10.1980	2330.41	-84.2308	10.1945	2344.61
-84.2315	10.1984	2330.41	-84.2308	10.1945	2344.68
-84.2315	10.1986	2330.41	-84.2308	10.1946	2344.61
-84.2315	10.1990	2330.41	-84.2308	10.1947	2344.61
-84.2315	10.1992	2330.41	-84.2308	10.1948	2343.69
-84.2315	10.1996	2330.41	-84.2308	10.1948	2344.36
-84.2315	10.2005	2439.93	-84.2308	10.1948	2344.61
-84.2315	10.2006	2439.76	-84.2308	10.1948	2344.65
-84.2315	10.2006	2439.93	-84.2308	10.1948	2344.68
-84.2314	10.1942	2357.52	-84.2308	10.1948	2344.68
-84.2314	10.1943	2357.25	-84.2308	10.1951	2344.95
-84.2314	10.1943	2357.52	-84.2308	10.1951	2344.98
-84.2314	10.1945	2343.59	-84.2308	10.1955	2344.95
-84.2314	10.1957	2346.20	-84.2308	10.1959	2373.02
-84.2314	10.1961	2346.20	-84.2308	10.2006	2452.61
-84.2314	10.2006	2439.93	-84.2307	10.1944	2344.61
-84.2313	10.1956	2346.20	-84.2307	10.1949	2344.61
-84.2313	10.1960	2373.02	-84.2307	10.1955	2344.95
-84.2313	10.1994	2330.41	-84.2307	10.1959	2372.96
-84.2313	10.2006	2439.93	-84.2307	10.1960	2372.96
-84.2312	10.1944	2357.25	-84.2307	10.1960	2373.02
-84.2312	10.1945	2357.25	-84.2307	10.2006	2452.61
-84.2312	10.1946	2343.59	-84.2306	10.1950	2344.98
-84.2312	10.1956	2344.79	-84.2306	10.1959	2372.96
-84.2312	10.1959	2373.02	-84.2306	10.1960	2372.96
-84.2312	10.2006	2439.76	-84.2306	10.1961	2372.96
-84.2311	10.1943	2357.25	-84.2305	10.1951	2344.98

-84.2305	10.1954	2344.41	-84.2300	10.1964	2330.41
-84.2305	10.1960	2372.96	-84.2300	10.1964	2360.79
-84.2305	10.1961	2372.96	-84.2300	10.1972	2330.41
-84.2305	10.1962	2360.79	-84.2300	10.1979	2330.41
-84.2305	10.1964	2330.41	-84.2300	10.1984	2330.41
-84.2305	10.1970	2330.41	-84.2300	10.1988	2330.41
-84.2305	10.1976	2330.41	-84.2300	10.1990	2330.41
-84.2305	10.1979	2330.41	-84.2300	10.1990	2337.49
-84.2305	10.1984	2330.41	-84.2300	10.1994	2340.11
-84.2305	10.1986	2330.41	-84.2300	10.2006	2452.61
-84.2305	10.1988	2330.41	-84.2299	10.1955	2343.43
-84.2305	10.1992	2330.41	-84.2299	10.1962	2360.79
-84.2305	10.1994	2330.41	-84.2299	10.1962	2368.23
-84.2305	10.2006	2452.61	-84.2299	10.1963	2360.79
-84.2304	10.1952	2344.89	-84.2299	10.1964	2341.12
-84.2304	10.1954	2344.41	-84.2299	10.1966	2330.41
-84.2304	10.1959	2368.18	-84.2299	10.1988	2336.59
-84.2304	10.1963	2360.79	-84.2299	10.1989	2336.47
-84.2304	10.1964	2330.41	-84.2299	10.1994	2340.11
-84.2304	10.1964	2360.79	-84.2299	10.2006	2452.61
-84.2304	10.1990	2330.41	-84.2298	10.1950	2344.52
-84.2304	10.2006	2452.61	-84.2298	10.1956	2343.99
-84.2303	10.1951	2344.89	-84.2298	10.1964	2341.12
-84.2303	10.1959	2368.18	-84.2298	10.1987	2331.41
-84.2303	10.1960	2368.18	-84.2298	10.1987	2331.52
-84.2303	10.1960	2368.23	-84.2298	10.1987	2335.04
-84.2303	10.1963	2360.79	-84.2298	10.1988	2334.94
-84.2303	10.1963	2360.96	-84.2298	10.1988	2335.04
-84.2303	10.1964	2360.79	-84.2298	10.1991	2337.18
-84.2303	10.1992	2340.11	-84.2298	10.1991	2337.49
-84.2303	10.1994	2340.11	-84.2298	10.1993	2337.49
-84.2303	10.1995	2340.11	-84.2298	10.1994	2340.11
-84.2303	10.2006	2452.61	-84.2298	10.2006	2452.61
-84.2302	10.1950	2344.89	-84.2297	10.1950	2344.52
-84.2302	10.1954	2344.41	-84.2297	10.1957	2343.99
-84.2302	10.1955	2343.82	-84.2297	10.1964	2341.12
-84.2302	10.1955	2344.41	-84.2297	10.1975	2330.41
-84.2302	10.1959	2368.23	-84.2297	10.1986	2330.26
-84.2302	10.1960	2368.23	-84.2297	10.1986	2330.41
-84.2302	10.1964	2360.79	-84.2297	10.1987	2331.41
-84.2302	10.1991	2330.41	-84.2297	10.1992	2337.49
-84.2302	10.1991	2340.11	-84.2297	10.2006	2452.61
-84.2302	10.1995	2340.11	-84.2296	10.1949	2344.52
-84.2302	10.2006	2452.61	-84.2296	10.1951	2344.25
-84.2301	10.1951	2344.89	-84.2296	10.1951	2344.52
-84.2301	10.1952	2344.70	-84.2296	10.1955	2343.30
-84.2301	10.1952	2344.89	-84.2296	10.1955	2343.43
-84.2301	10.1954	2344.41	-84.2296	10.1957	2343.99
-84.2301	10.1960	2368.23	-84.2296	10.1957	2344.25
-84.2301	10.1964	2360.79	-84.2296	10.1958	2343.99
-84.2301	10.1991	2340.11	-84.2296	10.1959	2343.99
-84.2301	10.1993	2340.11	-84.2296	10.1960	2343.99
-84.2301	10.1993	2340.22	-84.2296	10.1964	2341.12
-84.2301	10.1993	2340.52	-84.2296	10.1966	2341.12
-84.2301	10.1995	2340.11	-84.2296	10.1966	2341.69
-84.2301	10.2006	2452.61	-84.2296	10.1975	2334.10
-84.2301	10.2007	2452.13	-84.2296	10.1986	2330.01
-84.2301	10.2007	2452.61	-84.2296	10.1986	2330.51
-84.2300	10.1951	2344.89	-84.2296	10.1987	2330.01
-84.2300	10.1955	2344.41	-84.2296	10.1988	2333.82
-84.2300	10.1960	2368.23	-84.2296	10.1988	2334.20
-84.2300	10.1961	2368.23	-84.2296	10.1988	2334.35
-84.2300	10.1963	2360.79	-84.2296	10.1991	2337.49

-84.2296	10.2006	2452.61	-84.2293	10.1977	2334.38
-84.2295	10.1949	2344.52	-84.2293	10.1977	2334.99
-84.2295	10.1950	2344.52	-84.2293	10.1978	2333.02
-84.2295	10.1951	2344.52	-84.2293	10.1978	2333.16
-84.2295	10.1952	2344.52	-84.2293	10.1984	2338.55
-84.2295	10.1953	2343.43	-84.2293	10.1985	2338.55
-84.2295	10.1954	2343.43	-84.2293	10.1986	2338.55
-84.2295	10.1961	2339.89	-84.2293	10.1986	2338.55
-84.2295	10.1963	2339.89	-84.2293	10.1986	2338.72
-84.2295	10.1964	2339.89	-84.2293	10.2005	2452.61
-84.2295	10.1965	2341.12	-84.2292	10.1958	2343.99
-84.2295	10.1967	2339.18	-84.2292	10.1963	2339.34
-84.2295	10.1967	2339.41	-84.2292	10.1963	2339.92
-84.2295	10.1968	2339.18	-84.2292	10.1977	2334.99
-84.2295	10.1969	2339.18	-84.2292	10.1978	2333.16
-84.2295	10.1970	2337.86	-84.2292	10.1979	2337.68
-84.2295	10.1971	2336.98	-84.2292	10.1981	2336.41
-84.2295	10.1971	2337.86	-84.2292	10.1982	2332.85
-84.2295	10.1972	2337.86	-84.2292	10.1982	2333.17
-84.2295	10.1973	2337.86	-84.2292	10.1982	2335.34
-84.2295	10.1976	2334.10	-84.2292	10.1982	2335.45
-84.2295	10.1977	2329.99	-84.2292	10.1982	2336.41
-84.2295	10.1977	2330.22	-84.2292	10.1982	2336.41
-84.2295	10.1977	2330.40	-84.2292	10.1982	2336.63
-84.2295	10.1977	2330.41	-84.2292	10.1982	2336.75
-84.2295	10.1977	2330.48	-84.2292	10.1983	2335.45
-84.2295	10.1977	2330.49	-84.2292	10.1984	2335.45
-84.2295	10.1977	2330.62	-84.2291	10.1979	2336.77
-84.2295	10.1977	2330.74	-84.2291	10.1979	2337.68
-84.2295	10.1977	2330.92	-84.2291	10.1979	2337.80
-84.2295	10.1977	2330.93	-84.2291	10.1979	2337.82
-84.2295	10.1977	2333.52	-84.2291	10.1980	2336.41
-84.2295	10.1978	2333.34	-84.2291	10.1980	2336.77
-84.2295	10.1978	2333.34	-84.2291	10.2005	2452.61
-84.2295	10.1978	2333.52	-84.2290	10.1958	2341.76
-84.2295	10.1978	2333.72	-84.2290	10.1970	2337.28
-84.2295	10.1986	2333.95	-84.2290	10.1970	2337.44
-84.2295	10.1986	2334.65	-84.2290	10.1976	2338.08
-84.2295	10.1987	2334.65	-84.2290	10.1976	2338.34
-84.2295	10.1988	2333.82	-84.2290	10.1977	2338.34
-84.2295	10.1989	2333.82	-84.2290	10.1978	2336.77
-84.2295	10.1990	2333.82	-84.2289	10.1959	2341.76
-84.2295	10.2005	2452.61	-84.2289	10.1969	2337.44
-84.2294	10.1949	2344.52	-84.2289	10.1970	2337.44
-84.2294	10.1955	2343.43	-84.2289	10.1975	2338.34
-84.2294	10.1957	2343.99	-84.2289	10.1976	2338.34
-84.2294	10.1965	2339.89	-84.2289	10.1981	2342.68
-84.2294	10.1965	2340.41	-84.2289	10.1981	2342.70
-84.2294	10.1965	2340.45	-84.2289	10.1988	2351.24
-84.2294	10.1965	2340.45	-84.2289	10.1988	2351.54
-84.2294	10.1965	2340.46	-84.2289	10.1988	2352.87
-84.2294	10.1965	2340.47	-84.2289	10.1988	2353.77
-84.2294	10.1965	2340.48	-84.2289	10.1994	2349.21
-84.2294	10.1965	2340.50	-84.2289	10.1994	2362.10
-84.2294	10.1965	2340.53	-84.2289	10.1994	2362.78
-84.2294	10.1965	2340.70	-84.2289	10.1994	2363.35
-84.2294	10.1985	2334.65	-84.2289	10.1994	2364.81
-84.2294	10.2005	2452.61	-84.2289	10.1994	2369.39
-84.2293	10.1957	2343.99	-84.2289	10.1994	2370.15
-84.2293	10.1971	2336.96	-84.2288	10.1959	2341.76
-84.2293	10.1971	2337.19	-84.2288	10.1960	2341.76
-84.2293	10.1971	2337.55	-84.2288	10.1962	2341.76
-84.2293	10.1971	2337.56	-84.2288	10.1962	2342.26

-84.2288	10.1964	2341.76	-84.2276	10.1941	2471.05
-84.2288	10.1965	2340.56	-84.2276	10.1970	2412.22
-84.2288	10.1966	2340.56	-84.2276	10.1970	2412.46
-84.2288	10.1967	2340.56	-84.2276	10.1995	2471.22
-84.2288	10.1971	2337.44	-84.2275	10.1942	2471.05
-84.2288	10.1972	2337.44	-84.2275	10.1942	2471.41
-84.2288	10.1973	2338.34	-84.2275	10.1967	2412.16
-84.2288	10.1974	2338.34	-84.2275	10.1967	2412.49
-84.2288	10.1982	2346.94	-84.2275	10.1994	2471.22
-84.2288	10.1982	2346.94	-84.2275	10.1995	2471.22
-84.2288	10.1982	2346.95	-84.2274	10.1943	2471.41
-84.2288	10.1982	2347.05	-84.2274	10.1944	2471.41
-84.2288	10.1982	2347.18	-84.2274	10.1993	2471.22
-84.2288	10.1982	2347.23	-84.2273	10.1945	2471.41
-84.2288	10.2003	2471.55	-84.2273	10.1963	2414.82
-84.2287	10.1960	2341.76	-84.2273	10.1963	2414.93
-84.2287	10.1961	2341.76	-84.2273	10.1965	2414.33
-84.2287	10.1962	2341.76	-84.2273	10.1965	2414.43
-84.2287	10.1963	2341.76	-84.2273	10.1965	2414.53
-84.2287	10.1966	2340.65	-84.2273	10.1966	2411.44
-84.2287	10.1966	2340.82	-84.2273	10.1966	2412.54
-84.2287	10.1966	2340.83	-84.2273	10.1992	2454.94
-84.2287	10.1978	2338.54	-84.2273	10.1993	2454.94
-84.2287	10.1981	2352.42	-84.2272	10.1946	2471.41
-84.2287	10.1981	2352.42	-84.2272	10.1962	2414.82
-84.2287	10.1981	2355.02	-84.2272	10.1962	2414.93
-84.2287	10.1981	2355.41	-84.2272	10.1965	2414.33
-84.2287	10.2002	2471.55	-84.2272	10.1991	2454.94
-84.2286	10.1961	2341.76	-84.2271	10.1946	2471.41
-84.2286	10.2002	2471.55	-84.2271	10.1948	2471.41
-84.2285	10.1981	2361.45	-84.2271	10.1962	2420.89
-84.2285	10.1981	2361.89	-84.2271	10.1962	2420.90
-84.2285	10.2001	2471.55	-84.2271	10.1962	2420.91
-84.2284	10.1979	2367.78	-84.2271	10.1962	2421.02
-84.2284	10.1981	2367.08	-84.2271	10.1990	2454.94
-84.2284	10.1981	2367.53	-84.2271	10.1991	2454.94
-84.2284	10.2000	2471.55	-84.2270	10.1949	2470.29
-84.2283	10.1921	2541.76	-84.2270	10.1950	2470.29
-84.2283	10.1921	2541.86	-84.2270	10.1960	2432.99
-84.2283	10.1975	2381.12	-84.2270	10.1960	2433.70
-84.2283	10.1975	2381.27	-84.2270	10.1961	2429.79
-84.2283	10.1999	2471.55	-84.2270	10.1961	2430.11
-84.2282	10.1974	2385.14	-84.2270	10.1989	2454.94
-84.2282	10.1974	2385.32	-84.2269	10.1951	2470.29
-84.2282	10.1999	2471.55	-84.2269	10.1952	2470.29
-84.2281	10.1972	2392.76	-84.2269	10.1988	2454.94
-84.2281	10.1972	2393.40	-84.2268	10.1953	2470.29
-84.2281	10.1998	2471.22	-84.2268	10.1954	2470.29
-84.2281	10.1998	2471.55	-84.2268	10.1955	2470.25
-84.2280	10.1968	2384.23	-84.2268	10.1955	2470.29
-84.2280	10.1968	2408.31	-84.2268	10.1987	2454.94
-84.2280	10.1970	2384.23	-84.2267	10.1956	2470.29
-84.2280	10.1972	2391.82	-84.2267	10.1957	2470.29
-84.2280	10.1972	2391.98	-84.2267	10.1985	2455.20
-84.2280	10.1997	2471.22	-84.2267	10.1986	2455.20
-84.2279	10.1969	2408.31	-84.2267	10.1987	2454.94
-84.2279	10.1969	2408.55	-84.2267	10.1987	2455.20
-84.2279	10.1970	2402.62	-84.2266	10.1958	2470.29
-84.2279	10.1972	2396.83	-84.2266	10.1983	2455.20
-84.2279	10.1972	2397.07	-84.2266	10.1984	2455.20
-84.2279	10.1997	2471.22	-84.2265	10.1979	2465.37
-84.2278	10.1997	2471.22	-84.2265	10.1980	2455.20
-84.2277	10.1996	2471.22	-84.2265	10.1981	2455.20

-84.2265	10.1982	2455.20
-84.2264	10.1964	2465.92
-84.2264	10.1965	2465.92
-84.2264	10.1970	2465.92
-84.2264	10.1971	2465.37
-84.2264	10.1977	2465.37
-84.2263	10.1967	2465.92
-84.2263	10.1968	2465.92
-84.2263	10.1969	2465.92
-84.2264	10.1971	2465.92
-84.2264	10.1973	2465.37
-84.2264	10.1974	2465.37
-84.2264	10.1975	2465.37
-84.2264	10.1976	2465.37

Appendix C

Terrain correction programming for Bouguer Survey at Poás volcano, Costa Rica

---

C.1. Terrain correction code (MATLAB®)

```
% Function: terraincorrpoas
%
% Makes gravity terrain correction from Poas crater DEM
% Nico Fournier - Volcano Dynamics Group, The Open University, UK.
% Email: N.E.Fournier@open.ac.uk
% April 2003

%////////////////////// LOAD DATA (GRAVITY AND TOPOGRAPHY)//////////////////////////

% load gravity Bouguer stations --> G(x,y,z,gravity)
Gtot=load('D:\Poas\Gravity\PoasBOUGUER\BOUGUERheightcorrected\DATAheightc
orrected\poasbouguerstations.txt');
% select stations located at the bottom of the crater (i.e. delete base station at the
Mirador)
a=find(Gtot(:,2)>10.194);
Gdeg=Gtot(a,:);
G=[Gdeg(:,1).*cos(((Gdeg(:,2)/(2*pi))-floor(Gdeg(:,2)/(2*pi)))/360)*111300
Gdeg(:,2)*110600 Gdeg(:,3) Gdeg(:,4)];

% load Poas crater DEM grid (small) --> dem (x,y,z)
demdeg=load('D:\Poas\PoasDEM\gridcraterpoas.txt');
% convert degree --> cartesian
dem= [demdeg(:,1).*cos(((demdeg(:,2)/(2*pi))-floor(demdeg(:,2)/(2*pi)))/360)*111300
demdeg(:,2)*110600 demdeg(:,3)];
```

```
% load Poas DEM grid (large) --> DEM (x,y,z)
DEMdeg=load('D:\Poas\PoasDEM\gridfinalDEM.txt');
% convert degree --> cartesian
DEM= [DEMdeg(:,1).*cos(((DEMdeg(:,2)/(2*pi))-
floor(DEMdeg(:,2)/(2*pi)))/360)*111300 DEMdeg(:,2)*110600 DEMdeg(:,3)];


% ////////////////////// DEFINE MAX RADIUS TO USE FOR HAMMER ZONES//////////////

% defined with Function: defhammerradius
% Here are reported only the numbers to avoid unnecessary loops and, therefore,
processing time
radiusdem=482.4365;
radiusDEM=1293.0000;

% ////////////////////// DEFINE NEW COORDINATES FOR DEMs (RELATIVE TO
EACH GRAVITY STATION) ////

cylinders=[];
finalDEMpolar=[];

for n=1:length(G)
   n % keep track of the processing progress

   % studied gravity station (Bouguer survey)
   station=G(n,:);

   subroutineterrain; % Calls the subroutine "subroutineterrain"


   % reduce DEMs data for processing (keep only cylinders)

   a=find(demr<= radiusdem);
   cylinderdempolar=dempolar(a,:);

   a=find(DEMr>radiusdem & DEMr<=radiusDEM);
   cylinderDEMpolar=DEMpolar(a,:);

   % Merge both DEMs for Data processing (terrain correction) in polar coordinates for
each station
   finalDEMpolar=[cylinderdempolar
      cylinderDEMpolar];
   % attribute variable to each polar coordinate parameter (+ elevation difference) for
easier manipulation
   theta=finalDEMpolar(:,1);  % angle
   r=finalDEMpolar(:,2);      % radius
   dh=finalDEMpolar(:,3);     % dh = (DEM elevation) - (gravity station elevation)

   % ////////////////////////////////////// DATA PROCESSING//////////////////////////////////////////////////

   radiusindex=0:5:1295; % range of radius for the cylinders
```

```
angle=-pi:pi/16:pi;
gamma=6.672E-11;   % (m^3.kg^-1.s^-2)
rho=2400;          % substratum density chosen for the terrain correction (kg.m^-3)
meansectors=[];

for i=2:length(radiusindex)
   ri=find(r>radiusindex(i-1) & r<=radiusindex(i));
   R2=radiusindex(i);
   R1=radiusindex(i-1);
   zone=finalDEMpolar(ri,:);

   dgsector=[];
   numbsectors=1;
   for j=2:length(angle);
      thetaj=find(zone(:,1)>angle(j-1) & zone(:,1)<=angle(j));
      if ~isempty(thetaj) % checks that there are points in the analysed sector
         sector=zone(thetaj,:);
         h=mean(sector(:,3));
         DG=2*pi*numbsectors/32*gamma*rho*(R2-R1 + sqrt(R1^2+h^2) -
sqrt(R2^2+h^2)); % units: m.s^-2
         % Note: 1 microGals= 10^-8 m.s-2
         dgsector=[dgsector
            DG];
         % keep track of cylinders elevation for verification
         for k=1:length(sector(:,1))
            meansectors=[meansectors
            sector(k,1:2) h];
         end

         numbsectors=1;

      elseif isempty(thetaj) & j~=length(angle)
         numbsectors=numbsectors+1;
      elseif isempty(thetaj) & j==length(angle) % if last sector is empty of points --
>comes back to the last value
         numbsectors=numbsectors+1;
         DG=2*pi*numbsectors/32*gamma*rho*(R2-R1 + sqrt(R1^2+h^2) -
sqrt(R2^2+h^2));
         dgsector=[dgsector(1:length(dgsector)-1)
            DG];
      end
   end

   dgzone(i-1)=sum(dgsector); % sums all sectors for a zone

end



% ////////////////////////////////////
% keep track of all the zones corrections for each station
cylinders(:,n)=dgzone';
```

```
   % sums all the zones for a station
   dg(n)=sum(dgzone);

   % transform mean sectors elevation and coordinates from polar to cartesian (to be
able to plot it with DEM data)
   % DEM relative to station plot

[XDEM,YDEM,ZDEM]=pol2cart(finalDEMpolar(:,1),finalDEMpolar(:,2),finalDEMpo
lar(:,3));
   CARTDEM=[XDEM,YDEM,ZDEM];
   figure;
   plot3(XDEM,YDEM,ZDEM,'.');
   hold on;

   % mean sectors plot

[Xsector,Ysector,Zsector]=pol2cart(meansectors(:,1),meansectors(:,2),meansectors(:,3))
;
   CARTsectors=[Xsector,Ysector,Zsector];
   plot3(Xsector,Ysector,Zsector,'.r');
   hold off;
   rotate3d;

end

figure;
plot(radiusindex(2:260),cylinders,'.--');


% ////////////////// FINALIZE THE DATA PROCESSING: MAKE CORRECTION//////////

% Add terrain correction in m/s^2 at the end of the data matrix
G=[G dg'];
% Convert m/s^2 to mGal
%   1 Gal = 1E-2 m/s^2
%   --> 1 mGal = 1E-5 m/s^2
% and make correction
G=[G G(:,4)+G(:,5)*1E5];
% Finally normalize the gravity data to the station with lower elevation
G=[G G(:,6)-G(find(min(G(:,3))),6)];
csvwrite('D:\Poas\Gravity\PoasBOUGUER\Terraincorrection\terrcorrectedgravity2400',
G);


% ////////////////// INTERPOLATE AND PLOT THE TERRAIN CORRECTION/////////////

% interpolates and plots the terrain correction for the network;
x=G(:,1);
y=G(:,2);
z=G(:,5);
% Interpolates x data
```

```
xstep=(max(x)-min(x))/100;
e=[min(x):xstep:max(x)];

% Interpolates y data
ystep=(max(y)-min(y))/100;
n=[min(y):ystep:max(y)];

% Interpolates z data
[xi,yi,zi]=griddata(x,y,z,e,n','v4');

% plots grid data (xi,yi,zi)
colordef black
figure;
meshc(xi,yi,zi);
view(140,52);
colormap bone;
box;
hold on;
plot3(x,y,z,'.r');
hold off;
rotate3d;
colordef white


% //////// INTERPOLATE AND PLOT GRAVITY DATA CORRECTED AND NON-
CORRRECTED FOR TERRAIN EFFECT ////////////

% interpolates and plots the terrain correction for the network;
x=G(:,1);
y=G(:,2);
z=G(:,7);
% Interpolates x data
xstep=(max(x)-min(x))/100;
e=[min(x):xstep:max(x)];

% Interpolates y data
ystep=(max(y)-min(y))/100;
n=[min(y):ystep:max(y)];

% Interpolates z data
[xi,yi,zi]=griddata(x,y,z,e,n','v4');

% plots grid data (xi,yi,zi)
colordef black
figure;
meshc(xi,yi,zi);
view(140,52);
colormap bone;
box;
hold on;
plot3(x,y,z,'.r');
```

```
% plot the gravity data without terrain correction
x=G(:,1);
y=G(:,2);
z=G(:,4)-G(find(min(G(:,3))),4);
% Interpolates x data
xstep=(max(x)-min(x))/100;
e=[min(x):xstep:max(x)];

% Interpolates y data
ystep=(max(y)-min(y))/100;
n=[min(y):ystep:max(y)];

% Interpolates z data
[xi,yi,zi]=griddata(x,y,z,e,n','v4');

% plots grid data (xi,yi,zi)
meshc(xi,yi,zi);
view(140,52);
colormap bone;
box;
hold on;
plot3(x,y,z,'.r');

hold off;
rotate3d;
colordef white
```

C.2. Subroutine called from the main code (subroutineterrain.m) (MATLAB®)

```
% computes  the elevation difference between the station and the topo for both DEMs
% small crater DEM
demstation=[dem(:,1)-station(:,1) dem(:,2)-station(:,2) dem(:,3)-station(:,3)];
% larger DEM
DEMstation=[DEM(:,1)-station(:,1) DEM(:,2)-station(:,2) DEM(:,3)-station(:,3)];

% Change coordinate system from Cartesian to Polar
% with station coordinates beeing the origin

   % for large DEM
[DEMtheta DEMr
DEMdz]=cart2pol(DEMstation(:,1),DEMstation(:,2),DEMstation(:,3));
DEMpolar=[DEMtheta DEMr DEMdz]; % theta is the angle in radian, r the radius, dz
the elevation difference between station and topo points
   % for small DEM
[demtheta demr demdz]=cart2pol(demstation(:,1),demstation(:,2),demstation(:,3));
dempolar=[demtheta demr demdz];
 % theta is the angle in radian, r the radius, dz the elevation difference between station
and topo points
```

Appendix D

Continuous micro-gravity programming

D.1. g_logbasic (VISUAL BASIC®)

```
Option Explicit
Dim X As String
Dim StartTerminator As String, EndTerminator As String
Dim T As Long, I As Long
Dim Collect As String, Grav As String
Dim XStart As Integer, XLevel As String, XL As Single
Public X0 As Integer
Public XReset As String
Dim YStart As Integer, YLevel As String, YL As Single
Public Y0 As Integer
Public YReset As String
Public T0 As Single
Dim TStart As Integer, Temp As String, TC As Single
Public TReset As String
Dim pos1 As Long, pos2 As Long
Dim rawstring As String
Dim j As Long
'*****************************

'Dim the number of Samples displayed
Dim Samples As Double, g As Double
Dim FileWrite As String

Private Sub cmdStart_Click()
Me.Caption = "Logging....."
cmdStart.Enabled = False
cmdStop.Enabled = True

tmrMain.Enabled = True
```

```
MSComm1.CommPort = 1
MSComm1.InputLen = 0
MSComm1.RThreshold = 60
MSComm1.PortOpen = True
CreateFile
End Sub

Private Sub MSComm1_OnComm()
X = MSComm1.Input
End Sub

Private Sub cmdStop_Click()
cmdStop.Enabled = False
cmdStart.Enabled = True
Me.Caption = "Tu vas marcher BORDEL ??!!!!"
tmrMain.Enabled = False
MSComm1.PortOpen = False
End Sub

Private Sub tmrMain_Timer()
'Timer for Clock
Dim msg As String
msg = Time$
'frmLoad Clock (Start when cmdStart_Click)
If msg <> lblTime.Caption Then
  lblTime.Caption = Time$
End If


'*****************************
'Port Communication and String Filtering
'*****************************

StartTerminator = vbCr
On Error Resume Next
pos1 = InStr(X, StartTerminator)

EndTerminator = vbLf
On Error Resume Next
pos2 = InStr(pos1, X, EndTerminator)

If pos1 <> 0 Then
rawstring = Mid(X, pos1 + 3, 27)
End If

If InStr(1, rawstring, " ") = 1 Then
  I = 2
Else
  I = 1
End If
```

```
If pos1 <> 0 Then
  T = T + 1
  Collect = Mid(rawstring, I, 27)
  j = InStr(1, Collect, ",")
End If


If T >= 2 Then

'*****************************
'Get the different instrument parameters

  'Gravity
  On Error Resume Next
  Grav = Mid(Collect, 1, j - 1)
  lblGrav.Caption = Grav
  g = CDbl(Grav)
  lblSamples = Samples

  'Instrument XLevel
  On Error Resume Next
  XStart = InStr(6, Collect, ",")
  XLevel = Mid(Collect, XStart + 1, 6)

  'Instrument YLevel
  On Error Resume Next
  YStart = InStr(9, Collect, ",")
  YLevel = Mid(Collect, YStart + 1, 6)

  'Internal instrument Temperature
  On Error Resume Next
  TStart = InStr(16, Collect, ",")
  Temp = Mid(Collect, TStart + 1, 5)

  Samples = Samples + 1
  If Samples = 1000 Then
    CreateFile
    Samples = 0
  End If

  Open FileWrite For Append As #1
  Print #1, Day(Date) & " " & Month(Date) & " " & Year(Date) & " " & Hour(Time) &
" " & Minute(Time) & " " & Second(Time) & " " & Grav & " " & XLevel & " " &
YLevel & " " & Temp

  Close #1

  'Clears the buffer
  MSComm1.InBufferCount = 0
  MSComm1.InBufferSize = 0
  X = ""
End If
```

```
End Sub
Public Sub CreateFile()

'Initiate FileNo (Number of saved Files)

Dim FileName As String
Dim FileTest As String
Dim I As Integer
Dim DirSoft As String


DirSoft = "C:\Windows\Desktop\GlogData\" + CStr(Day(Date)) + "-"

'*****************************
FileName = DirSoft + Str(I) + ".txt"
FileTest = Dir(FileName)
While Dir(FileName) <> ""
  I = I + 1
  FileName = DirSoft + Str(I) + ".txt"
Wend
  FileWrite = DirSoft + Str(I) + ".txt"

Open FileWrite For Output As #1
'*****************************
Close #1

End Sub
```

D.2. g_log (VISUAL BASIC®)

```
g_log is an interface for Continuous measurements with Lacoste & Romberg D-meters
'It has been developped for Volcano monitoring
'Settings includes Sampling interval, Run Preferences, Communication Settings
'Not only g_log records the data in .txt file, it also proposes real-time graphs

'Nico Fournier, Volcano Dynamics Group, Dpt of Earth Sciences
'The Open University, UK
'email: n.e.fournier@open.ac.uk

Option Explicit

'*****************************
'Dim File Name to Save the Data

Dim FileWrite As String
Dim FileDate As String
Dim MaxSamples As Variant
Dim FileNumber As Double
'*****************************

'*****************************
'Dim variables for Timer

Dim sec As Long
Dim mn As Long
Dim hr As Long
Dim SamplingRate As Double
Dim totmin As Long
Dim remsec As Integer
Dim remmn As Integer
Dim a As Integer, b As Integer
'*****************************

'*****************************
'Dim variables for Run Options

Dim RunOption As Integer
Dim RunTime As Date
Dim StartTime As Date
Dim StopTime As Date
Dim StopDate As Date
Dim StopCollection As Integer
Dim Counter As Date
Dim CountStop As Date
'*****************************

'*****************************
```

```
'Dim variables for Port Communications and Data Sampling

Dim X As String
Dim pos1 As String, pos2 As String
Dim T As Integer
Public g As Single          'Gravity in milligals
Public gTCorrected As Single 'Tide Corrected Gravity in milligals
Dim StartTerminator As String, EndTerminator As String
Dim rawstring As String
Dim I As Integer, j As Integer

'Temperature and Level Checking
Dim Collect As String, Grav As String
Dim XStart As Integer, XLevel As String, XL As Single
Public X0 As Integer
Public XReset As String
Dim YStart As Integer, YLevel As String, YL As Single
Public Y0 As Integer
Public YReset As String
Public T0 As Single
Dim TStart As Integer, Temp As String, TC As Single
Public TReset As String
'*****************************

'Dim the number of Samples displayed
Dim S As Double

'*****************************
'Dim Z as if the zoom button has been activated
Public Z As Integer
'Dim Zoom as if the zoom button has been activated
Public Zoom As Integer
Dim AI As Integer
Public gMean As Double

'*****************************

'*****************************
'Dim variables for file saving
Dim DirSoft As String
Public DirTide As String
Public DirSettings As String
'Dim the array for Time setting
Dim GMT(0 To 24) As String
Dim igmt As Single
Dim TimeGMT As Date
'*****************************
'*****************************
'Dim Variables for Tide Correction
Public TideFile As String
Public TideFile2 As String
Public gTide As Double
```

```
Dim TideDate As Variant, TideTime As Variant, TideGrav As Variant, TimeTidebef As
Variant, TimeInterval
Dim Time1 As Variant, Time2 As Variant
Dim gTidebef As Double, gTideaft As Double
Dim LineString As String
Dim TimeDiff As Variant
Dim FirstStart As String
'*****************************
Private Sub FilterString()

End Sub

Sub FindTideCorrection()

Dim TideDay As String, TideMonth  As String
Dim TideDay2 As String, TideMonth2 As String
Dim Date2 As Date

'*************************************************************************
************
'Open the Tide Date file and find the Tide correction for the Present Computer Time
If Day(Date) < 10 Then
  TideDay = "0" + CStr(Day(Date))
Else
  TideDay = CStr(Day(Date))
End If

If Month(Date) < 10 Then
  TideMonth = "0" + CStr(Month(Date))
Else
  TideMonth = CStr(Month(Date))
End If
TideFile = frmTide.LocFile + TideDay + "-" + TideMonth + ".txt"

'*************************************************************************
************
'Open the Tide Date File for Day + 1 in case the measurement go over 23:55 GMT
Date2 = DateAdd("d", 1, Date)

If Day(Date2) < 10 Then
  TideDay2 = "0" + CStr(Day(Date2))
Else
  TideDay2 = CStr(Day(Date2))
End If

If Month(Date2) < 10 Then
  TideMonth2 = "0" + CStr(Month(Date2))
Else
  TideMonth2 = CStr(Month(Date2))
End If
TideFile2 = frmTide.LocFile + TideDay2 + "-" + TideMonth2 + ".txt"
```

```
'*****************************************************************************
'Open the Tide file
Open TideFile For Input As #2

Do While Not EOF(2)
  FilterString
  If Time1 = "" Then
    Time1 = TideTime
  Else
    Time2 = TideTime
    TimeInterval = Minute(Time2) - Minute(Time1)
    Time1 = ""
    Time2 = ""
  Exit Do
  End If
Loop
Close #2
Open TideFile For Input As #2

Do While Not EOF(2)

  'Get String for each line
  Line Input #2, LineString

  'Isolate Date in the string
  TideDate = Mid(LineString, 1, 8)
  On Error Resume Next
  TideDate = CDate(TideDate)

  'Isolate Time in the string
  On Error Resume Next
  TideTime = Mid(LineString, 9, 7)
  On Error Resume Next
  TideTime = CDate(TideTime)

  'Isolate Grav in the string
  On Error Resume Next
  TideGrav = Mid(LineString, 17, 5)
  On Error Resume Next
  TideGrav = CSng(TideGrav)

  'Get the Gravity correction for the present time
  TimeDiff = ((Hour(Time) - frmTide.jetlag) * 3600 + Minute(Time) * 60 +
Second(Time)) - (Hour(TideTime) * 3600 + Minute(TideTime) * 60 +
Second(TideTime))

  If TimeDiff = 0 Then
    gTide = TideGrav
    gTide = Int(gTide + 0.5)
    Close #2
    Exit Sub
  ElseIf TimeDiff < 0 Then
```

```
    gTideaft = TideGrav
    gTide = gTidebef + (gTideaft - gTidebef) / (TimeInterval * 60) * ((Minute(Time) -
Minute(TimeTidebef)) * 60 + Second(Time))
    gTide = Int(gTide + 0.5)
    Close #2
    Exit Sub
  End If

  gTidebef = TideGrav
  TimeTidebef = TideTime


Loop

'*********************************************************************
'If the time after the last Tide calculation of the File, it opens the next-day's file
Open TideFile For Input As #3

Do While Not EOF(3)
  FilterString
  If Time1 = "" Then
    Time1 = TideTime
  Else
    Time2 = TideTime
    TimeInterval = Minute(Time2) - Minute(Time1)
    Time1 = ""
    Time2 = ""
  Exit Do
  End If
Loop

Do While Not EOF(3)

  'Get String for each line
  Line Input #3, LineString

  'Isolate Date in the string
  TideDate = Mid(LineString, 1, 8)
  On Error Resume Next
  TideDate = CDate(TideDate)

  'Isolate Time in the string
  On Error Resume Next
  TideTime = Mid(LineString, 9, 7)
  On Error Resume Next
  TideTime = CDate(TideTime)

  'Isolate Grav in the string
  On Error Resume Next
  TideGrav = Mid(LineString, 17, 5)
  On Error Resume Next
  TideGrav = CSng(TideGrav)
```

```
  'Get the Gravity correction for the present time

  If TimeDiff = 0 Then
    gTide = TideGrav
    gTide = Int(gTide + 0.5)
    Close #3
    Exit Sub
  ElseIf Hour(TideTime) + Minute(TideTime) = 0 Then
    gTideaft = TideGrav
    gTide = gTidebef + (gTideaft - gTidebef) / (TimeInterval * 60) * ((Minute(Time) -
Minute(TimeTidebef)) * 60 + Second(Time))
    gTide = Int(gTide + 0.5)
    Close #3
    Exit Sub
  End If

  gTidebef = TideGrav
  TimeTidebef = TideTime

Loop

MsgBox "Tide Correction Not found. Check the Tide File"
cmdStop_Click
Close #2
Close #3

End Sub
'Fills the Combo Instrument in frmMain from the ...\Settings\Instrument.txt
Sub SetComboInstrument()

Dim InstrName As String, Temp As String
Open frmNewInstr.InstrFile For Input As #5
Do While Not EOF(5)
  Input #5, InstrName, Temp
  cboInstrument.AddItem InstrName
Loop
Close #5
End Sub

'Get the Instrument Temperature from the Combo Instrument in frmMain and
...\Settings\Instrument.txt
Sub GetTemperature(Name As String)
Dim InstrName As String, Temperature As String

Name = cboInstrument.Text
Open frmNewInstr.InstrFile For Input As #6
Do While Not EOF(6)
  Input #6, InstrName, Temperature
  If Name = InstrName Then
    T0 = CSng(Temperature)
    Close #6
```

```
    Exit Sub
  End If
Loop
Close #6

End Sub
'Create the Directory File if it doesn't exist already
'cf TestDir Project
Sub CreateNewDirectory(DirName As String)

  Dim NewLen As Integer
  Dim DirLen As Integer
  Dim MaxLen As Integer

  NewLen = 4
  MaxLen = Len(DirName)
  If Right$(DirName, 1) <> "\" Then
    DirName = DirName + "\"
    MaxLen = MaxLen + 1
  End If
  On Error GoTo DirError

MakeNext:
  DirLen = InStr(NewLen, DirName, "\")
  MkDir Left$(DirName, DirLen - 1)
  NewLen = DirLen + 1
  If NewLen >= MaxLen Then
    Exit Sub
  End If
  GoTo MakeNext
DirError:
  Resume Next
End Sub

Private Sub cmdNew_Click()
frmNewInstr.Show
End Sub

Public Sub cmdStart_Click()

'Set File Number to 1
I = 1

'Reset the Number of samples to be displayed
S = 0

'*****************************
'Check if an Instrument hass been selected
If cboInstrument.Text = "" Then
  MsgBox "Please select an Instrument"
  Exit Sub
End If
```

```
'*****************************
'Check Format of Run Options
'Option 2:
If RunOption = 2 And Not IsDate(txtRunTime.Text) Then
  MsgBox "Enter valid Run Time Format (hh:mm:ss)"
  txtRunTime.Text = ""
  Exit Sub
ElseIf RunOption = 2 And IsDate(txtRunTime.Text) Then
  RunTime = txtRunTime.Text
ElseIf RunOption = 3 And Not IsDate(txtStopTime.Text) Then
'Option 3 (StopTime)
  MsgBox "Enter valid Stop Time Format (hh:mm:ss)"
  txtStopTime.Text = ""
  Exit Sub
ElseIf RunOption = 3 And IsDate(txtStopTime.Text) Then
  StopTime = txtStopTime.Text

'*****************************

'Clear form and text boxes
frmLoad.lblInterval.Caption = ""
frmLoad.lblStartTime.Caption = ""
frmMain.Refresh

'Disables the cmdStart button
cmdStart.Enabled = False
cmdStop.Enabled = True
cmdStop.Default = True
'*****************************
End If
If FirstStart = "" Then
  DirTide = DirTide + "\TideData\"
  FirstStart = "No"
End If
If frmTide.chkTideSave.Enabled = True Then
  CreateNewDirectory DirTide
End If

'*****************************
'Start Statements for Timer Intervals

'Validate sampling rate
  'Seconds
  If txtsec.Text = "" Then
    txtsec.Text = 0
    sec = 0
  End If
  If IsNumeric(txtsec.Text) = False Then
    MsgBox "Enter valid Seconds number for Sampling Rate", 48
    Exit Sub
  End If
```

```
  If txtsec.Text > 60 Or txtsec.Text < 0 Then
    MsgBox "Seconds number must fall between 0 and 60", 48
    Exit Sub
  End If

  'Minutes
  If txtmin.Text = "" Then
    txtmin.Text = 0
    mn = 0

  End If
    If IsNumeric(txtmin.Text) = False Then
    MsgBox "Enter valid Minutes number for Sampling Rate", 48
    Exit Sub
  End If
  If txtmin.Text > 60 Or txtmin.Text < 0 Then
    MsgBox "Minutes number must fall between 0 and 60", 48
    Exit Sub
  End If

  'Hours
  If txthr.Text = "" Then
    txthr.Text = 0
    hr = 0
  End If
  If IsNumeric(txthr.Text) = False Then
    MsgBox "Enter valid Hours number for Sampling Rate", 48
    Exit Sub
  End If

  'Sampling Interval > 0 sec
  If (txtsec.Text + txtmin.Text + txthr.Text) = 0 Then
    MsgBox "Please enter a valid Sampling Interval"
    Exit Sub
  End If



'Assign Integer values to hours, minutes, seconds
If txtsec.Text = 60 Then
  txtmin.Text = txtmin.Text + 1
  txtsec.Text = 0
End If
If txtmin.Text = 60 Then
  txthr.Text = txtmin.Text + 1
  txtmin.Text = 0
End If
txtsec.Text = Int(txtsec.Text + 0.5)
txtmin.Text = Int(txtmin.Text + 0.5)
txthr.Text = Int(txthr.Text + 0.5)

sec = txtsec.Text 'Integer >= 0
```

```
mn = txtmin.Text  'Integer between 0 and 59
hr = txthr.Text   'Integer between 0 and 59
totmin = mn + hr * 60

SamplingRate = (sec + mn * 60 + hr * 3600) * 1000

If SamplingRate <= 30000 Then           'Sampling Rate <= 00:30
  a = 0
  tmrCollect.Interval = SamplingRate
ElseIf sec > 30 And totmin = 0 Then     ' 00:30 <Sampling Rate< 00:59
  a = 1
  remsec = 30
  tmrCollect.Interval = (sec - remsec) * 1000
ElseIf totmin > 0 And sec = 0 Then      'Sampling Rate = Minutes (mn:00)
  a = 2
  tmrCollect.Interval = 30 * 1000
  remmn = (totmin * 60) / 30 - 1   'remmn is the amount of 30 sec units in totmin
  remsec = 0
ElseIf totmin > 0 And sec > 30 Then     'Sampling Rate = mn:sec with sec > 00:30
  a = 3
  tmrCollect.Interval = 30 * 1000
  remmn = (totmin * 60) / 30 - 1    'remmn is the amount of 30 sec units in totmin
  remsec = 30
ElseIf totmin > 0 And sec <= 30 And sec <> 0 Then
  a = 4                             'Sampling Rate = mn:sec with 1<= sec <=30
  tmrCollect.Interval = 30 * 1000
  remmn = (totmin * 60) / 30 - 1    'remmn is the amount of 30 sec units in Sampling
Time
End If

'*****************************

'*****************************
'Show frmLoad (LoadForm.frm)
frmParam.Show
frmLoad.Show
frmLoad.imgOnOff = frmParam.imgOn
frmLoad.lblOnOff.Caption = "ON"
frmLoad.optionLock.Enabled = True
frmLoad.optionLock.Value = 0
StartTime = Time$

'*****************************
'Hide frmMain (MainForm.frm)
Me.Hide
'*****************************

'Call the CreateFile function
CreateFile

'*****************************
'Port Communication and String Filtering
```

```
'*****************************

'Set up for MSComm1
With MSComm1
  .InputMode = comInputModeText
  .InputLen = 0
  .RThreshold = 60
End With


'*****************************
'Enables tmrMain and tmrCollect
tmrMain.Enabled = True
tmrCollect.Enabled = True

'Gets the Temperature from the ...\Settings\Instrument.txt file
GetTemperature (cboInstrument.Text)

'*****************************


'*****************************
'Print Set Up for frmLoad (LoadForm.frm)
'*****************************
'Print Start Time
frmLoad.lblStartTime.Caption = Time$
'Print Stop Time
If txtRunTime.Text <> "" Then
frmLoad.lblStopTime.Caption = (StartTime + RunTime)
ElseIf txtStopTime.Text <> "" Then
  frmLoad.lblStopTime.Caption = txtStopTime.Text
Else
  frmLoad.lblStopTime.Caption = "When press Stop"
End If


'*****************************
'Print Collect Interval
frmLoad.lblInterval.Caption = (totmin * 60 + sec)
'*****************************


'*****************************
'Set StopTime and StopDate for Run Options
If RunOption = 2 Then
  StopTime = RunTime + Time$
  StopDate = Date
End If
'*****************************

End Sub
Public Sub CreateFile()
```

```
'Initiate FileNo (Number of saved Files)

Dim FileName As String
Dim FileTest As String
Dim I As Integer

'*****************************
FileName = DirSoft + Str(I) + ".txt"
FileTest = Dir(FileName)
While Dir(FileName) <> ""
  I = I + 1
  FileName = DirSoft + Str(I) + ".txt"
Wend
  FileWrite = DirSoft + Str(I) + ".txt"

Open FileWrite For Output As #1
'Write the Sampling details to the file
Print #1, "   Continuous micro-gravity measurement"
Print #1, "   ************************************"
Print #1, "   Instrument:  " & cboInstrument.Text
Print #1, "   Operator:  " & txtOperator.Text
Print #1, "   ------------------------"
Print #1, "   Date and Start at local time: " & lblDate & " at " & Time & "  (" &
cboGMT.Text & ")"
Print #1, "   -------------------------------------------------"
Print #1, ""
Print #1, "Grav = Gravity in milliGals"
Print #1, "Lev X and Lev Y = Instrument Levels X and Y"
Print #1, "Temp = Instrument Internal Temperature (degree Celsius)"
If frmTide.chkTideSave.Value = 1 And frmTide.chkTideSave.Enabled = True Then
  Print #1, "CorrGrav = Tide Corrected Gravity in milligals"
  Print #1, "File used for Tide correction: " + TideFile
  Print #1, ""
  Print #1, "Date", "Time (GMT)", "Grav  , Lev X, Leve Y, Temp, CorrGrav,   Tide
Correction (micro-Gals)"
Else
  Print #1, ""
  Print #1, "Date", "Time (GMT)", "Grav  , Lev X, Lev Y, Temp"
End If
Print #1, ""
'*****************************


End Sub
Public Sub cmdStop_Click()

frmLoad.cmdStart.Enabled = True
frmLoad.cmdExit.Default = True
frmLoad.cmdStop.Enabled = False
tmrMain.Enabled = False
tmrCollect.Enabled = False
```

```
Unload frmParam
Set frmParam = Nothing

Close #1

'*****************************
'Set up variable b for next run
b = 0
'*****************************

End Sub

Private Sub dtStopDate_Click()
StopDate = dtStopDate
End Sub

Private Sub Form_Load()
Dim FileDate As String

'*****************************
'Set lblDate and dt StopDate default values to Today's date
lblDate.Caption = Date
dtStopDate.Value = Date
'*****************************
'Set the combo with GMT Time setting
GMT(0) = "GMT -12"
GMT(1) = "GMT-11"
GMT(2) = "GMT-10"
GMT(3) = "GMT-9"
GMT(4) = "GMT-8"
GMT(5) = "GMT-7"
GMT(6) = "GMT-6"
GMT(7) = "GMT-5"
GMT(8) = "GMT-4"
GMT(9) = "GMT-3"
GMT(10) = "GMT-2"
GMT(11) = "GMT-1"
GMT(12) = "GMT"
GMT(13) = "GMT+1"
GMT(14) = "GMT+2"
GMT(15) = "GMT+3"
GMT(16) = "GMT+4"
GMT(17) = "GMT+5"
GMT(18) = "GMT+6"
GMT(18) = "GMT+7"
GMT(19) = "GMT+8"
GMT(20) = "GMT+9"
GMT(21) = "GMT+10"
GMT(22) = "GMT+11"
GMT(23) = "GMT+12"
GMT(24) = "GMT+13"
```

```
For igmt = 0 To 24
  cboGMT.AddItem (GMT(igmt))
Next igmt
cboGMT.ListIndex = 12
'*****************************
'Retrieve the software directory and create a Directory for the Data
DirSoft = CurDir()
If DirTide = "" Then
frmTide.DirLocation = CurDir()
DirTide = CurDir()
End If
FileDate = CStr(Day(Date)) + "-" + CStr(Month(Date)) + "-" + CStr(Year(Date))

'Creates the GLogSettings diretory if not existing
DirSettings = DirSoft + "\GLogSettings\"
CreateNewDirectory DirSettings
frmNewInstr.InstrFile = frmMain.DirSettings + "\Instruments.txt"
If Dir(frmNewInstr.InstrFile) <> "" Then
SetComboInstrument
End If

'Creates the GLogData diretory if not existing
DirSoft = DirSoft + "\GLogData\" + FileDate
CreateNewDirectory DirSoft


'Creates the TideData directory if not existing
If DirTide = "" Then
DirTide = DirTide + "\TideData\"
MsgBox DirTide
CreateNewDirectory DirTide
End If
'*****************************
'*****************************
'Set up variables a and b for the first run
a = 0
b = 0
'*****************************

'*****************************
'Set up default value for Run Options
RunOption = 1
Counter = "00:00:01"
'*****************************
'Set up default value for the amount of Samples per file
frmSaveFile.txtSaveFile = 1000

End Sub

Private Sub mnuCommSettings_Click()
Load frmCommSettings
frmCommSettings.Show
```

```
End Sub

Private Sub mnuExit_Click()
Dim cont As Integer
cont = MsgBox("Exit g_log ?", 32 + 4)
If cont = 6 Then
'Unload all the forms and end the application

  'Unload Options Windows
  Unload frmTide
  Set frmTide = Nothing
  Unload frmCommSettings
  Set frmCommSettings = Nothing
  Unload frmInstrument
  Set frmInstrument = Nothing
  Unload frmSaveFile
  Set frmSaveFile = Nothing

  'Unload Info Window
  Unload frmAbout
  Set frmAbout = Nothing

  'Unload Instrument Monitoring Window
  Unload frmParam
  Set frmParam = Nothing

  'Unload graphic Windows
  Unload frmChart
  Set frmChart = Nothing
  Unload frmZoom
  Set frmZoom = Nothing

  'Unload the Sampling Window
  Unload frmLoad
  Set frmLoad = Nothing

  'Unload the Main Window
  Unload Me
  Set frmMain = Nothing

End If
End Sub

Private Sub mnuAbout_Click()
Load frmAbout
frmAbout.Show
End Sub

Private Sub mnuFile_Click()
frmSaveFile.Show
Me.Enabled = False
End Sub
```

```
Private Sub mnuInstrument_Click()
frmInstrument.Show
Me.Enabled = False
End Sub

Private Sub mnuTide_Click()
frmTide.Show
Me.Enabled = False
End Sub

Private Sub MSComm1_OnComm()
X = MSComm1.Input
End Sub

Private Sub Option1_Click()

'Enables/Disables Run Options
txtRunTime.Enabled = False
txtRunTime.BackColor = &H8000000F

txtStopTime.Enabled = False
txtStopTime.BackColor = &H8000000F
dtStopDate.Enabled = False
RunOption = 1
StopCollection = 0
End Sub

Private Sub Option2_Click()

'Enables/Disables Run Options
RunOption = 2
txtRunTime.Enabled = True
txtRunTime.BackColor = &H80000009

txtStopTime.Enabled = False
txtStopTime.Text = ""
txtStopTime.BackColor = &H8000000F
dtStopDate.Enabled = False
RunOption = 2
StopCollection = 1

End Sub

Private Sub Option3_Click()

'Enables/Disables Run Options
RunOption = 3
txtStopTime.Enabled = True
txtStopTime.BackColor = &H80000009
dtStopDate.Enabled = True
```

```
txtRunTime.Enabled = False
txtRunTime.Text = ""
txtRunTime.BackColor = &H8000000F
RunOption = 3
StopCollection = 1

End Sub

Private Sub tmrCollect_Timer()

Dim Aveg As Double
Dim j As Double

'*****************************
'Timer filter core

'Time >= 1 minute
If remmn > 0 Then
  remmn = remmn - 1
  b = 0
  Exit Sub
End If
'Second step if Time >= 1 minute AND sec = 0
If a = 2 Then
  remmn = (totmin * 60) / 30 - 1
End If

'Second Step (remaining seconds)
If a = 3 And b = 0 Then
  remsec = 30
  tmrCollect.Interval = (sec - 30) * 1000
  b = 1
  Exit Sub
ElseIf a = 4 And b = 0 Then
  tmrCollect.Interval = sec * 1000
  b = 1
  Exit Sub
ElseIf a = 4 Then 'For Time > 1 minute
  tmrCollect.Interval = 30 * 1000  'Reset next tmr Event at 30 sec
  remmn = (totmin * 60) / 30 - 1   'Reset remmn to be blocked by the next tmr Event
'Sec between 31 and 59 seconds

ElseIf remsec > 0 Then
  remsec = remsec - 30
  tmrCollect.Interval = 30 * 1000
  Exit Sub
End If

'Second Step (remaining seconds)
If a = 1 Then   'For Time < 1 minute
  remsec = 30
  tmrCollect.Interval = (sec - remsec) * 1000
```

```
End If

If a = 3 Then
  remsec = 30
  tmrCollect.Interval = 30 * 1000
  remmn = (totmin * 60) / 30 - 1
End If

'*****************************


'***********************************
'***********************************
'EVENTS TRIGGERED BY THE TIMER


'*****************************
'Port Communication and String Filtering
'*****************************

StartTerminator = vbCr
On Error Resume Next
pos1 = InStr(X, StartTerminator)

EndTerminator = vbLf
On Error Resume Next
pos2 = InStr(pos1, X, EndTerminator)

If pos1 <> 0 Then
rawstring = Mid(X, pos1 + 3, 27)
End If

If InStr(1, rawstring, " ") = 1 Then
  I = 2
Else
  I = 1
End If

If pos1 <> 0 Then
  T = T + 1
  Collect = Mid(rawstring, I, 27)
  j = InStr(1, Collect, ",")
End If


If T >= 2 Then

'*****************************
'Get the different instrument parameters

  'Gravity
  On Error Resume Next
```

```
  Grav = Mid(Collect, 1, j - 1)


  frmLoad.lblGrav.Caption = Grav
  frmZoom.lblGrav.Caption = Grav

  'Instrument XLevel
  XStart = InStr(6, Collect, ",")
  XLevel = Mid(Collect, XStart + 1, 6)
  'Check eventual anomaly in the string and avoid bug
  If XLevel <> "" Then
    XL = CSng(XLevel)
  Else
    XL = 0
  End If
  If XReset <> "No" Then
    X0 = XL
    XReset = "No"
  End If
  frmParam.lblXLevel.Caption = XLevel
  'Check if the user has set up the XRange sensitivity and, if not, gives a default value
(10)
  If frmInstrument.txtXRange.Text = "" Then
    frmInstrument.txtXRange.Text = 5
  End If
  frmParam.lblXLevel0.Caption = "(" + CStr(X0) + " +/- " +
frmInstrument.txtXRange.Text + ")"
  'Check if the present XLevel is stable and if not, it shows a red button alarm
  If XL > (X0 - CLng(frmInstrument.txtXRange)) And XL < (X0 +
CLng(frmInstrument.txtXRange)) Then
    frmParam.imgXLevel.Picture = frmParam.imgOn.Picture
  Else
    frmParam.imgXLevel.Picture = frmParam.imgOff.Picture
  End If

  'Instrument YLevel
  YStart = InStr(9, Collect, ",")
  YLevel = Mid(Collect, YStart + 1, 6)
  'Check eventual anomaly in the string and avoid bug
  If YLevel <> "" Then
    YL = CSng(YLevel)
  Else
    YL = 0
  End If
  If YReset <> "No" Then
    Y0 = YL
    YReset = "No"
  End If
  frmParam.lblYLevel.Caption = YLevel
  'Check if the user has set up the YRange sensitivity and, if not, gives a default value
(10)
  If frmInstrument.txtYRange.Text = "" Then
```

```
    frmInstrument.txtYRange.Text = 5
  End If
  frmParam.lblYLevel0.Caption = "(" + CStr(Y0) + " +/- " +
frmInstrument.txtYRange.Text + ")"
  'Check if the present YLevel is stable and if not, it shows a red button alarm
  If YL > (Y0 - CLng(frmInstrument.txtYRange)) And YL < (Y0 +
CLng(frmInstrument.txtYRange)) Then
    frmParam.imgYLevel.Picture = frmParam.imgOn.Picture
  Else
    frmParam.imgYLevel.Picture = frmParam.imgOff.Picture
  End If


  'Internal instrument Temperature
  TStart = InStr(16, Collect, ",")
  Temp = Mid(Collect, TStart + 1, 5)
  If T0 = 0 Then
    T0 = 51#
  End If
  If frmInstrument.txtTRange.Text = "" Then
    frmInstrument.txtTRange.Text = 0.3
  End If
  'Check eventual anomaly in the string and avoid bug
  If Temp <> "" Then
    TC = CSng(Temp)
  Else
    TC = T0
  End If
  frmParam.lblTemp0.Caption = "(" + CStr(T0) + " +/- " +
frmInstrument.txtTRange.Text + ")"
  frmParam.lblTemp.Caption = Temp
  'Check if the user has set up the T0 and TRange sensitivity and, if not, gives a default
value (0.3)
  If TC > (T0 - CSng(frmInstrument.txtTRange.Text)) And TC < (T0 +
CSng(frmInstrument.txtTRange.Text)) Then
    frmParam.imgTemp.Picture = frmParam.imgOn.Picture
  Else
    frmParam.imgTemp.Picture = frmParam.imgOff.Picture
  End If


  'Data collect event + chart update


  g = CDbl(Grav)

  'Correct time and save the data AT GMT TIME
  Hour(TimeGMT) = Hour(Time) - (cboGMT.ListIndex - 12)
  TimeGMT = CDate(Hour(Time) - (cboGMT.ListIndex - 12) & ":" & Minute(Time) &
":" & Second(Time))
```

```
'Make the Tide Correction if wanted
If frmTide.chkTideSave.Value = 1 And frmTide.chkTideSave.Enabled = True Then
  FindTideCorrection
  gTCorrected = g + CDbl(gTide) / 1000
  Print #1, Date, TimeGMT, Collect, gTCorrected, gTide
End If
If frmTide.chkTide.Value = 1 Then
  FindTideCorrection
  gTCorrected = g + CDbl(gTide) / 1000
  frmZoom.lblTideCorr.Enabled = True
  frmZoom.lblGravCorr.Enabled = True
  frmZoom.chkg2.Enabled = True
  frmZoom.lblGravCorr.Caption = gTCorrected
Else
  gTCorrected = g
  Print #1, Date & " " & TimeGMT & " " & g & " " & XL & " " & YL & " " & TC
  frmZoom.lblTideCorr.Enabled = False
  frmZoom.lblGravCorr.Enabled = False
  frmZoom.chkg2.Enabled = False
End If
Close #1

S = S + 1
'If Number of Sample (S) reaches the max wanted per file (SamplesperFile)
'=> Creates a new file
MaxSamples = Int(frmSaveFile.txtSaveFile.Text + 0.5)
frmLoad.lblNSamples.Caption = CStr(S + FileNumber * MaxSamples)
frmLoad.lblFiles(0).Caption = S & " Sample(s)"
frmLoad.lblFiles(1).Caption = "+ " & FileNumber & " file(s) of"
frmLoad.lblFiles(2).Caption = MaxSamples & " sample(s)"
frmLoad.lblFiles(3).Caption = "for this run"
  If S = MaxSamples Then
  CreateFile
  'Update the number of file saved for the present run
  FileNumber = FileNumber + 1
  S = 0
  Close #1
End If
Open FileWrite For Append As #1

'Add point to the Chart (frmChart)
Call frmChart.AddPoint(g)

'Add point to the Zoom Chart (frmZoom)
Call frmLoad.AddPoint(g, gTCorrected)

'Clears the buffer
MSComm1.InBufferCount = 0
MSComm1.InBufferSize = 0
X = ""
```

```
End If

'***********************************
'***********************************

End Sub

Private Sub tmrGeneral_Timer()

'*****************************
'Set lblDate default values to Today's date if ever Measurements > 1 day.
lblDate.Caption = Date
'*****************************

'*****************************
'Timer for Clocks of frmMain
Dim clk As String
clk = Time$
'frmLoad Clock (Start when cmdStart_Click)
If clk <> txtClock Then
  txtClock = Time$
End If

End Sub

Private Sub tmrMain_Timer()

'*****************************
'Filters tmrCollect for Run Option (determine if Data Collection should go on or end)
If txtRunTime.Text <> "" Then
  RunTime = RunTime - Counter
End If
If txtStopTime.Text <> "" Then
  RunTime = StopTime - Time
  StopDate = dtStopDate
End If


If StopCollection = 1 And (StopDate - Date) = 0 And (Hour(RunTime) +
Minute(RunTime) + Second(RunTime)) = 0 Then
  MsgBox "End Data Collection at   " & Time
  Call frmLoad.cmdStop_Click
  Exit Sub
End If
'*****************************

'*****************************
'Timer for Clocks of frmLoad
Dim msg As String
msg = Time$
'frmLoad Clock (Start when cmdStart_Click)
```

```
If msg <> frmLoad.lblClock.Caption Then
  frmLoad.lblClock.Caption = Time$
  frmZoom.lblClock.Caption = Time$
End If

End Sub
```

D.3. Automated Earth Tides correction (MATLAB®)

```
% Function: corrtide
% Makes tides correction for continous gravity monitoring
% It uses files generated by TideCalc for the tide correction
% Nico Fournier. Volcano Dynamics Group, The Open University, United Kingdom.
December 2002.

% Example of input files
% Gravity data: hr min sec gravity(mGal)
A=load('D:\Desktopbackup\gravregisgmt.txt');
% Tide data 5 min intervals: hr min gravity(microGal)
B=load('D:\Desktopbackup\tidedataregis.txt');

for i=1:length(A(:,1))
  gravtime(i) = A(i,1)*3600 + A(i,2)*60 + A(i,3);

  for j=1:length(B(:,1))
    tidetime(j)=B(j,1)*3600 + B(j,2)*60;
    [i length(A)]

    if tidetime(j) == gravtime(i)
      tidecorrection= (B(j,3)/1000);
      newgrav(i,:)=[A(i,1) A(i,2) A(i,3) gravtime(i) tidecorrection (A(i,4)-
tidecorrection)];
      break
    end

    if tidetime(j) > gravtime(i)

      if j==1
      else
        tidecorrection = (B(j-1,3)+ (gravtime(i)-tidetime(j-1))*(B(j,3)-B(j-
1,3))/(5*60))/1000;
        newgrav(i,:)=[A(i,1) A(i,2) A(i,3) gravtime(i) tidecorrection (A(i,4)-
tidecorrection)];
      end
      break
    end


  end

end
grav=[(A(:,1))*3600 + A(:,2)*60 + A(:,3) A(:,4)];
tide=[B(:,1)*3600+B(:,2)*60 B(:,3)/1000];

% Tides
figure;
```

```
plot(tide(:,1),tide(:,2))
hold on;
plot(newgrav(:,4),newgrav(:,5),'r')
hold off;

% Gravity raw and tides corrected
figure;
plot(newgrav(:,4),newgrav(:,6));
hold on;
plot(grav(:,1),grav(:,2),'r');
hold off;
```

D.4. Power spectrum analysis (MATLAB®)

```
% function: powerspec
%
% Compute the power spectrum of a set of gravity data (G)
% with G(:,1) = time in seconds
% and G(:,2) = gravity data
%
% Nico Fournier (The Open University, UK), Emily Brodsky (U.C.L.A, USA)
% Email: N.E.Fournier@open.ac.uk
% March 2003



Y=fft(G(:,2));
Y(1)=[];
n=length(Y);
power=abs(Y(1:n/2)).^2;
nyquist=1/2;
freq=(1:n/2)/(n/2)*nyquist;
period=1./freq;

plot(period,power,'.-');
index=find(power==max(power));
hold on;
plot(period(index),power(index),'ok');
mainPeriodStr=num2str(period(index));
text(period(index)+5,power(index),['Period = ',mainPeriodStr],'EraseMode','none');
hold off;
```

D.5. Response function (MATLAB®)

```
% Fonction: SeismoOU
%
% 1.Gets simultaneous Seismic data and Gravity data
% (from the experiment at the OU the 8-8-2002)
%
% 2.Makes a power spectrum of the seismic 3 components and of the gravity data.
%
% 3.It finally makes the response fonction of the gravity meter to the Z vertical axis of
the seismometer
%
% Nico Fournier (The Open University, UK), Emily Brodsky (U.C.L.A, USA) - 22-08-
2002.

%load gravity data
load D:\Responsefun\Guralpdata\GraviOU\8-8-2002\bothseism\3.txt;
load D:\Responsefun\Guralpdata\GraviOU\8-8-2002\bothseism\4.txt;
```

```
load D:\Responsefun\Guralpdata\GraviOU\8-8-2002\bothseism\5.txt;
load D:\Responsefun\Guralpdata\GraviOU\8-8-2002\bothseism\6.txt;
load D:\Responsefun\Guralpdata\GraviOU\8-8-2002\bothseism\7.txt;
load D:\Responsefun\Guralpdata\GraviOU\8-8-2002\bothseism\8.txt;
load D:\Responsefun\Guralpdata\GraviOU\8-8-2002\bothseism\9.txt;
load D:\Responsefun\Guralpdata\GraviOU\8-8-2002\bothseism\10.txt;
G=[X3
  X4
  X5
  X6
  X7
  X8
  X9
  X10];
% interpolate missing gravity data
h=G(:,1);
m=G(:,2);
s=G(:,3);
t=(h-h(1))*3600+(m-m(1))*60+s-s(1);
dt=t(2:length(t))-t(1:length(t)-1);
% I is the vector of missing data index (8th point, 23th point...)
I=find(dt~=1);

% loops to assign interpolated values
% assume dt for gravity =1
% and all skipped points have dt=2 (only 1 point missed)
q=G(:,4);
n=1;
for J=1:I(1);
  q2(n)=q(n);
  n=n+1;
end
q2(n)=(q(I(1))+q(I(1)+1))/2;
n=n+1;

for K=1:length(I)-1
        for J=I(K)+1:I(K+1)
    q2(n)=q(J);
    n=n+1;
  end
  q2(n)=(q(I(K+1))+q(I(K+1)+1))/2;
  n=n+1;
end

for J=I(length(I))+1:length(q);
  q2(n)=q(J);
  n=n+1;
end



%load sesmic data
```

```
%load Z files (y is the data column)
[yz1,idz1,spsz1,istz1]=readgcffile('D:\Responsefun\Guralpdata\6108z0\20020808_1300
z.gcf');
[yz2,idz2,spsz2,istz2]=readgcffile('D:\Responsefun\Guralpdata\6108z0\20020808_1400
z.gcf');
[yz3,idz3,spsz3,istz3]=readgcffile('D:\Responsefun\Guralpdata\6108z0\20020808_1500
z.gcf');
Z =[yz1
  yz2
  yz3];
%load N files
[yn1,idn1,spsn1,istn1]=readgcffile('D:\Responsefun\Guralpdata\6108n0\20020808_130
0n.gcf');
[yn2,idn2,spsn2,istn2]=readgcffile('D:\Responsefun\Guralpdata\6108n0\20020808_140
0n.gcf');
[yn3,idn3,spsn3,istn3]=readgcffile('D:\Responsefun\Guralpdata\6108n0\20020808_150
0n.gcf');
N =[yn1
  yn2
  yn3];
%load N files
[ye1,ide1,spse1,iste1]=readgcffile('D:\Responsefun\Guralpdata\6108e0\20020808_1300
e.gcf');
[ye2,ide2,spse2,iste2]=readgcffile('D:\Responsefun\Guralpdata\6108e0\20020808_1400
e.gcf');
[ye3,ide3,spse3,iste3]=readgcffile('D:\Responsefun\Guralpdata\6108e0\20020808_1500
e.gcf');
E =[ye1
  ye2
  ye3];


%Adjust seismic data to gravity dat length and sampling rate
N2=N(14300:length(N));
E2=E(14300:length(E));
Z2=Z(14200:length(Z));

n=1;


for i=1:100:length(E2) % length (E2) = length (Z2)= length (N2)
E3(n)=E2(i);
Z3(n)=Z2(i);
N3(n)=N2(i);
n=n+1;
end

% !!!! need to find the missing 5 seconds in gravity data.

% temporary way of making the file at the same length
E4=E3(6:length(E3))';
N4=N3(6:length(N3))';
```

```
Z4=Z3(6:length(Z3))';

q2=q2';

dt = 1;

% fft for N
n=fft(N4);
% power
N=length(N4);
mn=n.*conj(n)/(N*N);
% put back in dt
mn=mn.*dt.*dt;
%frequency
fn=(0:N-1)'/(dt*N);
%power
mn=sqrt(mn(1:N/2));
fn=fn(1:N/2);

% fft fo Z
z=fft(Z4);
% power
N=length(Z4);
mz=z.*conj(z)/(N*N);
% put back in dt
mz=mz.*dt.*dt;
%frequency
fz=(0:N-1)'/(dt*N);
%power
mz=sqrt(mz(1:N/2));
fz=fz(1:N/2);

% fft for E
e=fft(E4);
% power
N=length(E4);
me=e.*conj(e)/(N*N);
% put back in dt
me=me.*dt.*dt;
%frequency
fe=(0:N-1)'/(dt*N);
%power
me=sqrt(me(1:N/2));
fe=fe(1:N/2);

% fft for g (gravity)
g=fft(q2);
% power
N=length(q2);
mg=g.*conj(g)/(N*N);
% put back in dt
mg=mg.*dt.*dt;
```

```
%frequency
fg=(0:N-1)'/(dt*N);
%power
mg=sqrt(mg(1:N/2));
fg=fg(1:N/2);


subplot(2,2,1)
loglog(fn(1:N/2),mn(1:N/2)')
Title('N component')
subplot(2,2,2)
loglog(fe(1:N/2),me(1:N/2)')
Title('E component')
subplot(2,2,3)
loglog(fz(1:N/2),mz(1:N/2)')
Title('Z component')
subplot(2,2,4)
loglog(fg(1:N/2),mg(1:N/2)')
Title('G gravity')

%power spectrum
figure;
subplot(2,1,1);
loglog(fz,mg./mz)
Title('(Power spectrum gravity over vertical seimic)');
Xlabel('Frequency');
subplot(2,1,2);
plot(fz,mg./mz)
Title('(Power spectrum gravity over vertical seimic)');
Xlabel('Frequency');


%plot
figure
t=[1:length(E4)]*dt-dt;
plot(t,E4,t,N4,t,Z4);
```